

Copyright
by
Rachit Agarwal
2013

**The Dissertation Committee for Rachit Agarwal Certifies that this is the approved
version of the following dissertation:**

**Effect of Shape on Cell Internalization of Polymeric Hydrogel
Nanoparticles**

Committee:

Krishnendu Roy, Supervisor

S.V. Sreenivasan

Li Shi

Laura J. Suggs

Robert O. Williams III

**Effect of Shape on Cell Internalization of Polymeric Hydrogel
Nanoparticles**

by

Rachit Agarwal, B.Tech.; M.Tech.

Dissertation

Presented to the Faculty of the Graduate School of

The University of Texas at Austin

in Partial Fulfillment

of the Requirements

for the Degree of

Doctor of Philosophy

The University of Texas at Austin

May 2013

Dedication

To my parents

Acknowledgements

I would like to express my gratitude to number of people without whom this dissertation work would not have been possible. Firstly, I would like to thank my advisor, Dr. Krishnendu Roy for all his help. It is hard to put words to all that he has done for me.

He has been an excellent mentor during all my Phd. work. In all the discussions I had with him, he has always patiently listened to my ideas and concerns, promoted the correct approaches and rightly pointed out the shortcomings and alternatives. He has always emphasized on getting the basics right and has offered exceptional advices and resources in order to develop proper concepts. He has treated me like his colleague that has allowed me to easily approach him with any problems or unconventional ideas. He instilled me with knowledge, hopes, dreams and values. He always managed to take time out from his busy schedule and meet me on a regular basis whenever I needed his advice. He supported me during the times of my illness, encouraged me during failures and heartily congratulated me for my achievements. Dr. Roy has always shown belief in my potential. He has also helped in my professional development by letting me write grants and papers and have insightful discussions about methods of academic writing and expression of ideas. I couldn't have finished my Phd. without his constant support.

I would also like thank my collaborators, Dr. Li Shi and Dr. S.V. Sreenivasan whom I had the chance to meet atleast once every week. Dr. Shi has provided valuable feedback and discussion about my research and has always been supportive of the work. He has always provided constructive criticisms and pushed me to strive for more. He also

had patience to sit through my rough paper drafts and polish them for publications. Dr Sreenivasan has also provided valuable research and life advices. I have learned a lot about handling pressure situations and focusing on research that result in real life impact.

I would also like to thank my other committee members, Dr. Laura Suggs and Dr. Robert Williams. They took time out of their busy schedule to be on my dissertation committee, brought fresh perspective to my research and provided feedback and positive criticisms about my research. I also owe a thanks to all department faculties I interacted with about research guidance and all my teachers who taught me basics of biomedical and nanotechnology.

I would also like to thank facilities of Institute of Cellular and Molecular Biology (ICMB) (especially Dwight, Angela and Julie), Center for Nano and Molecular Science (CNM), Pickle Research Campus and Molecular Imprints (especially Tina Stoddard and John Graves). These facilities provided me with all the instruments and training without which this project would not have been possible.

I would like to thank my project mates, Vikramjit and Patrick for their collaborative work in various areas of my research project and being cooperative enough to come late night and weekends for the experiments. A special thanks goes to all my labmates, Irina, Tracy, Jardin, Ankur, Asha, Michelle, Prinda, Eileen, Nathalie and Jian. I would also like to thank my undergrads, Zachary and Mansi for the all the hard work they did in this project and I learned a lot about teaching because of them. I also owe thanks to all my friends (just too big a list to write here) for recharging me with lots of fun and good times.

Finally I would like to thank my family for their unconditional support in all my endeavors. I feel very privileged that I was given all the love and support that I needed to follow my passion. My father is my source of inspiration and it was him who introduced me to Biomedical Engineering. I have learned to work hard and at the same time efficiently from him. My mother taught me to be grounded and check and analyze all possibilities in a given situation. Both my elder brothers and sister-in-law gave me immense love and took care of all my needs. This Phd. and in fact all that I have achieved in my life would not have been possible without their support.

Effect of Shape on Cell Internalization of Polymeric Hydrogel Nanoparticles

Rachit Agarwal, PhD.

The University of Texas at Austin, 2013

Supervisor: Krishnendu Roy

Recent progress in drug discovery has enabled us to target specific intracellular molecules to achieve therapeutic effects. These next generation therapeutics are often biologics which cannot enter cells by mere diffusion. Therefore it is imperative that drug carriers are efficiently internalized by cells before releasing their cargo. Nanoscale polymeric carriers are particularly suitable for such intra-cellular delivery. Although size and surface-charge has been the most studied parameters for nanocarriers, it is now well appreciated that particle shape also plays a critical role in their transport across physiological barriers. Hence there is increasing interest in fabricating shape-specific polymeric nano and microparticles for efficient delivery of drugs and imaging agents. Nanoimprint lithography methods, such as Jet-and-flash imprint lithography (J-FIL), provide versatile top-down processes to fabricate shape-specific, biocompatible nanoscale hydrogels that can deliver therapeutic and diagnostic molecules in response to disease-specific cues. However, the key challenges in top-down fabrication of such nanocarriers are scalable imprinting with biological and biocompatible materials, ease of particle-surface modification using both aqueous and organic chemistry as well as simple yet biocompatible harvesting. Here we report that a biopolymer-based sacrificial release layer in combination with improved nanocarrier-material formulation can address these challenges. The sacrificial layer improves scalability and ease of imprint-surface

modification due to its switchable solubility through simple ion exchange between monovalent and divalent cations. This process enables large-scale bio-nanoimprinting and efficient, one-step harvesting of hydrogel nanoparticles in both water- and organic-based imprint solutions. We also show that when shape is decoupled from volume, charge and composition, mammalian cells preferentially internalize disc-shaped nanohydrogels of higher aspect ratios over nanorods. Interestingly, unlike nanospheres, larger-sized hydrogel nanodiscs and nanorods are internalized more efficiently. Uptake kinetics, efficiency and internalization mechanisms are all shape-dependent and cell-type specific. Although macropinocytosis is used by all cells, epithelial cells uniquely internalize nanodiscs using caveolae pathway. On the other hand, endothelial cells use clathrin-mediated uptake along with macropinocytosis for all shapes and show significantly higher uptake efficiency compared to epithelial cells. We also study the effect of shape and surface properties for their tissue uptake and penetration using spheroids as a 3D tumor model and show that hydrophobic particles show no difference in penetration inside such models even after 125 fold reduction in volume. These results provide a fundamental understanding of how cell and tissue behavior is influenced by nanoscale shape and surface properties and are critical for designing improved nanocarriers and predicting nanomaterial toxicity.

Table of Contents

List of Tables	xiv
List of Figures	xv
Chapter 1: Specific Aims and Overview	1
1.1 Introduction.....	1
1.2 Specific Aims.....	3
1.2.1 Specific Aim 1: To fabricate, optimize and characterize nanocarriers of precise size and geometry (shape and aspect ratio) using a high throughput, top-down nano-manufacturing process.	3
1.2.2 Specific Aim 2: To evaluate the effects of nanoparticle size, shape and material composition on <i>in vitro</i> cellular uptake in various cell lines.....	3
1.2.3 Specific Aim 3: To study the effects of nanoparticle size, shape and material on <i>in vitro</i> tumor models (Spheroids)	4
1.3 Dissertation Summary.....	4
1.4 References.....	5
Chapter 2: Background and Significance	7
2.1: Drug Delivery and Nanoparticles	7
2.2 Uptake Pathways: How Cells Internalize NPs and How to Study Them	10
2.3 Size: Is Smaller Better?.....	15
2.4 Charge: Cationic, Anionic or Neutral?	20
2.5 Elasticity: Does it Matter How Hard or Soft the NP is?	24
2.6 Surface Composition: What the Cell “Sees”	26
2.7 Shape: Spheres, Rods and Discs have Unique Internalization Properties	30
2.8 Combination of Parameters in a Multivariate Space: A Perspective.....	35
2.9 References.....	37
Chapter 3: Scalable Imprinting of Shape-specific Polymeric Nanocarriers	49
3.1 Introduction.....	49
3.2 Materials and Methods.....	52
3.2.1 Materials and Reagents	52

3.2.2 Imprinting Solution	53
3.2.3 Release Layer	53
3.2.4 PAA Release Layer	53
3.2.5 Imprinting Parameters	54
3.2.6 Release and Imaging of Nanoparticles	54
3.2.7 In vitro Cytotoxicity	55
3.2.8 Doxorubicin release kinetics	55
3.2.9 Encapsulation of fluorescent molecules	55
3.3 Results and Discussion	56
3.3.1 Imprint with a PVA Release Layer	56
3.3.2 Release Layer Optimization	58
3.3.3 Imprint with a PAA Release Layer	59
3.3.4 In vitro Cytotoxicity	65
3.3.5 Doxorubicin Release Kinetics	66
3.3.6 Encapsulation of fluorescent molecules	68
3.4 Conclusions	69
3.5 References	70
Chapter 4: Effect of Shape of Nanoparticles on Uptake by Cells	73
4.1 Introduction	73
4.2 Materials and Methods	75
4.2.1 Materials and Reagents	75
4.2.1 Nanoimprinting	75
4.2.2 Release and Characterization of Nanoparticles	76
4.2.3 Cell Culture	77
4.2.4 Cytotoxicity Assay	78
4.2.5 Thermo-Gravimetric Analysis	78
4.2.6 Confocal Microscopy	78
4.2.7 Flow Cytometry	79
4.2.8 Inverted Culture Studies	79
4.2.9 Pharmacological Inhibition Studies	80

4.3 Results and Discussion	81
4.3.1 Particle Characterization	81
4.3.2 Cytotoxicity Assay	83
4.3.2 Thermo-Gravimetric Analyzer	84
4.3.3 Confocal Microscopy	85
4.3.4 Flow Cytometry	86
4.3.5 Inverted Culture Studies	91
4.3.6 Pharmacological Inhibition Studies	94
4.3.7 Confocal Microscopy with RPE cells	97
4.4 Conclusions	99
4.5 References	100
Chapter 5: Effect of Shape of Nanoparticles on Uptake and Penetration in Spheroids	104
5.1 Introduction	104
5.2 Materials and Methods	106
5.2.1 Spheroid Synthesis (Poly-HEMA)	106
5.2.2 Spheroid Synthesis (Agarose Gel)	106
5.2.3 SEM of Spheroids	107
5.2.4 2-Photon Microscopy	107
5.2.5 Image Analysis	108
5.2.6 Flow Cytometry Analysis	108
5.3 Results	109
5.3.1 Spheroid Formation	109
5.3.2 2-Photon Microscopy	112
5.3.3: Flow Cytometry	115
5.4 Conclusions	116
5.5 References	117
Chapter 6: Conclusions and Future Work	119
6.1 Research Summary	119
6.2 Conclusions and future directions	119

6.2.1: Fabrication of Particles	119
6.2.2: Cellular Uptake Studies	121
Glossary	123
Abbreviations	123
References	125
Vita	140

List of Tables

Table 2.1: Uptake pathways involved in internalization of non-targeted nanoparticles and tools that can be used to study these pathways.	15
Table 2.2: Nanoparticle Parameters and its effect on <i>in vivo</i> circulation and cellular uptake.....	34
Table 3.1: Release Layer Optimization	59
Table 3.2: Contact angle (in degrees) measurement results	64
Table 4.1: DLS and Zeta potential characterization of particles after incubation in 10% serum:	83

List of Figures

Figure 2.1: Schematic representation of different uptake pathways potentially utilized by mammalian cells to take up foreign NPs and the intra-cellular fate of internalized NPs as a function of physical parameters such as size, shape and charge. Proton Sponge Effect is a strategy used for endosomal escape of nanoparticles based on surface properties of NPs. Particles are designed to carry secondary or tertiary amines on the surface such that they can buffer the pH of endosomes. This results in proton influx through the endosomal proton pumps, followed by chloride ion transport that eventually leads to osmotic swelling and bursting of vesicles, thus releasing the particles in the cytoplasm.12

Figure 2.2: Schematic representation of barriers to particle delivery in vivo. A. Representation of systemic circulation of blood and major organs involved in nanoparticle voyage. Smallest capillaries are 5 μm in diameter and kidney clears anything below 10 nm thereby defining the upper and lower bound on particle dimensions. B. Particle clearance by liver. Kupffer cells present in blood vessels of liver efficiently clear particles greater than 500nm from the blood. C. Particle clearance by Spleen. Arteries release blood in the red pulp region of spleen where it re-enters the circulation through splenic venous sinuses via slits between endothelial cells that are about 200 nm wide and hence traps and clears particles with larger dimensions. D. Enhanced Permeation and Retention (EPR) effect. Vasculature in tumor regions has leaky endothelial cell linings which can allow NPs to pass through and accumulate in tumor.17

Figure 2.3: Schematic representation of effect of nanoparticle charge on its fate in vivo.23

Figure 3.1: Representative SEM and Fluorescence Microscopy images of PEG imprints on a PVA release layer with the use of a water-based imprint solution. a) SEM image of imprint at low magnification, b) and, c) Fluorescence microscopy images of the imprint region at excitation wavelength of 488 nm and emission at 520 nm. d), e), f) - Zoomed in SEM images of the imprints highlighting different regions of defective and good imprints.58

Figure 3.2: Imprints over PAA using a DMSO based imprint solution (a) Cross-sectional SEM images of 100 nm diameter x 80 nm height cylindrical particles (b) Top SEM images of 800 nm x 100 nm x 100 nm cuboidal particles (c) Fluorescence images of FITC containing 100 nm diameter x 80 nm height cylindrical particles (d) Fluorescence images of Doxorubicin containing 325 nm diameter x 100 nm height cylindrical particles taken 2 hours after being released in water.60

Figure 3.3: (a) Optical photograph of a wafer showing more than 325 successful automated repeatable imprints of a dense 5 mm x 5 mm template with 100-nm-diameter and 80-nm-height imprint features. (b) Cross-sectional SEM of 800 nm x 100 nm x 100 nm cuboids with sub 10 nm residual layer thickness.....62

Figure 3.4: Reversible tuning of the solubility of PAA in water by exchanging between Ca^{2+} and Na^+ ions.63

Figure 3.5: (a) SEM and (b) fluorescence microscopy images of 220 nm diameter and 125 nm height cylindrical, FITC-loaded particles imprinted over Ca^{2+} treated PAA layer using a water-based PEGDA resist. Imprints were released from the imprint substrate into water and subsequently drop casted on a different clean silicon wafer substrate for SEM imaging.64

Figure 3.6: SEMs of (a) 100 nm diameter x 80 nm height cylindrical imprinted PEGDA particles in DMSO after imprinting and etching, (b) after incubation in 0.1M CaCl_2 water solution for 5 minutes, (c) after washing twice with deionized water for 5 minutes each time, (d) after washing with 0.1M NaOH water solution.....66

Figure 3.7: Fluorescence images of Doxorubicin containing 325 nm diameter x 100 nm height cylindrical particles taken after 72 hours of dialysis in water.	67
Figure 3.8: Kinetics of release of Doxorubicin from imprinted nanoparticles (325nm diameter x 100nm height) fabricated with 55% PEGDA resist in DMSO	68
Figure 3.9: Fluorescence images of 220 nm diameter x 100 nm height cylindrical particles encapsulating A. Texas Red, B. Texas Red conjugated to 10KDa Dextran, C. Rhodamine Acrylate and D. Alexa Fluor 647. .	69
Figure. 4.1: Nanoparticle Characterization – Specific Shapes, Uniform Fluorescence and Equivalent Surface Charge: SEM micrograph of A) 80nm diameter x 70nm height discs, B) 220nm diameter x 100nm height discs, C) 325nm diameter x 100nm height discs, D) 400nm x 100nm x 100nm rods, E) 800nm x 100nm x 100nm rods. Fluorescence images of F) 800nm x 100nm x 100nm rods, G) 325nm diameter x 100nm height discs. H) Zeta potential plot for all particles.....	82
Figure 4.2: Particle characterization in presence of serum shows no aggregation of particles: A) Fluorescence Microscopy images of 220nm diameter x 100nm height particles at excitation wavelength of 488nm and emission at 520nm, B) SEM image of 400nm x 100nm x 100nm particles after incubation in 10% serum.	83
Figure. 4.3: In vitro cytotoxicity assay show particles are non-toxic. Cytotoxicity assay for HeLa, HEK 293 and HUVEC cells done with 400 nm x 100 nm x 100nm particles.....	84

Figure. 4.4: Correlation of fluorescence signal with mass of nanoparticle. Plot showing correlation between fluorescence units and mass of particles.85

Figure. 4.5: Confocal Microscopy of particle uptake by HeLa cells. Confocal cross-section images of HeLa cells showing internalization of shape-specific particles A) 80nm diameter x 70nm height discs, B) 220nm diameter x 100nm height discs, C) 325nm diameter x 100nm height discs, D) 400nm x 100nm x 100nm rods, E) 800nm x 100nm x 100nm rods. 86

Figure. 4.6: Cellular uptake kinetics of different shape-specific nanoparticles in various cell lines. A) HeLa cells, B) HEK 293 cells, C) HUVEC cells, D) BMDCs. In figure A-D, red lines are for discs (hollow for 325x100nm disc, dashed for 220x100nm disc and solid for 80x70nm disc) and blue lines for rods (dashed for 400x100x100nm rods and solid for 800x100x100nm rods). Error bars are standard deviation with n=3 for each data point. E-F) Normalized median particle uptake per cell (indicates relative number of particles internalized by cells when normalized to 80x70nm disc) at the maximum internalization time point (72 hours for HeLa and BMDC, 48 hours for HEKs and 24 hours for endothelial cells)89

Figure. 4.7: Flow cytometry kinetic plots for uptake of polystyrene beads in 4 cell lines. Effect of size of nanoparticles on uptake kinetics in A) HeLa cells, B) HEK 293 cells, C) HUVEC cells, D) BMDCs. In figure a-d, dashed green line for 200nm polystyrene spherical particles and solid green line for 100nm polystyrene spherical particles. Error bars are standard deviation with n=3 for each data point.90

Figure. 4.8: Cellular uptake kinetics of different shape-specific nanoparticles in various cell lines. A) HeLa cells, B) HEK 293 cells, C) HUVEC cells, D) BMDCs. In figure A-D, red lines are for discs (hollow for 325x100nm disc, dashed for 220x100nm disc and solid for 80x70nm disc) and blue lines for rods (dashed for 400x100x100nm rods and solid for 800x100x100nm rods). Error bars are standard deviation with n=3 for each data point.....91

Figure. 4.9: Inverted Culture Uptake studies: Shape still matters. A) Experimental setup for uptake studies in inverted conditions B) Inverted cellular uptake of spherical polystyrene beads after 24 hours in HEK 293. Inverted cellular uptake of shape specific nanoparticles after 24 hours in C) HEK 293 cells, D) HUVEC cells. In figure b, hollow green bars are for 200nm diameter spherical polystyrene bead and solid green bars are for 100nm diameter spherical polystyrene bead. In figure c-d, red bars are for discs (hollow red bars for 325nm x 100nm disc, dashed red bars for 220nm x 100nm disc and solid red bars for 80nm x 70nm disc) and blue bars for rods (dashed blue bars for 400nm x 100nm x 100nm and solid blue bars for 800nm x 100nm x 100nm). Error bars are standard deviation with n=3 for each data point.93

Figure 4.10: Effect of serum concentration on uptake of 220 nm x 100 nm disc shaped nanoparticles by HEK 293 cells after 24 hours. Plot showing effect of serum concentration on uptake of nanoparticle by HEK 293 after 24 hour of incubation.94

Figure. 4.11: Effect of pharmacological inhibitors on uptake of various shape-specific nanoparticles A) Inhibitors used (with function and concentration) for the uptake experiments. B-C) Change in normalized median fluorescence uptake due to presence of inhibitors in HEK 293 and HUVEC cells. Error bars are standard deviation with n=5 for each data point. Red bars are for discs (solid for 80nm diameter discs, dashed for 220nm diameter and hollow for 325nm diameter) and blue lines for rods (dashed for 400x100x100nm rods and solid for 800x100x100nm rods).
96

Figure. 4.12: Effect of Pharmacological Inhibitors on uptake of spherical polystyrene nanoparticles. Change in normalized median fluorescence uptake due to presence of inhibitors in HEK 293 Cells. Solid green bars are for 100nm diameter polystyrene beads, dashed green bars are for 200nm diameter polystyrene beads and hollow green bars are for 500nm diameter polystyrene beads. Error bars are standard deviation with n=5 for each data point.....97

Figure. 4.13: Confocal Microscopy of particle uptake and localization by clathrin labeled RPE cells. Confocal Images of RPE cell lines incubated with shape-specific particles to test the co-localization of particles with clathrin pits. A) 80nm diameter x 70nm height discs, B) 220nm diameter x 100nm height discs, C) 325nm diameter x 100nm height discs, D) 400nm x 100nm x 100nm rods, E) 800nm x 100nm x 100nm rods. 98

Figure. 4.14: Summary of cell-uptake mechanisms: Illustrative image showing differences in mechanisms and relative efficiencies for cell uptake of shape-specific nanoparticles in A) Epithelial and B) Endothelial cells.	99
Figure 5.1: Light microscopy images of Spheroids cultured over PolyHEMA under static conditions a) HeLa spheroid on day one b) HeLa spheroid on day four.....	109
Figure 5.2: Light microscopy images of HEK spheroids cultured over 2% agarose gel under A) static conditions for 72 hours and B) rotatory shaker for 72 hours at 240rpm.	109
Figure 5.3: Growth Kinetics of spheroids showing change in diameter of spheroids grown in A) static conditions and B) rotatory shaker at 240rpm....	110
Figure 5.4: Growth Kinetics of spheroids showing percent change in volume of spheroids grown in A) static conditions and B) on rotatory shaker at 240rpm.	111
Figure 5.5: Scanning Electron Microscopy images of HEK spheroid cultured over 2% agarose gel on rotatory shaker for 72 hours at 240rpm.	112
Figure 5.6: 2-Photon microscopy images of spheroids at 200 um deep from the top edge of the spheroids incubated with A) 200 nm polystyrene beads and B) 500 nm polystyrene beads.....	113
Figure 5.7: Graph showing comparison of normalized pixel intensity associated with spheroid per slice with different diameter polystyrene beads.....	113

Figure 5.8: Picture showing spheroid optical sections at 120 μm depth and an area selection circle used to compute the radial intensity distribution for polystyrene beads of diameters A) 100 nm, B) 200 nm and C) 500 nm.114

Figure 5.9: Normalized radial intensity distribution of polystyrene nanoparticles as a function of distance from the center of the spheroid.114

Figure 5.10: Normalized radial intensity distribution of Disc-shaped nanoparticles as a function of distance from the center of the spheroid.....115

Figure 5.11: Graph showing comparison of particle association with spheroid after 48 hours of incubation with different size polystyrene beads analyzed using flow cytometry.116

Chapter 1: Specific Aims and Overview

1.1 INTRODUCTION

Developments of effective and toxic drugs against diseases such as cancer have created the need to efficiently deliver their therapeutic doses to target tissues and simultaneously minimizing their presence in healthy tissues (Ma and Adjei, 2009). Nanoparticles (NPs) offer solutions for delivery of bioagents for various imaging and therapeutic purposes (Davis et al., 2008; Ferrari, 2005; Hamidi et al., 2008; Panyam and Labhasetwar, 2003; Peppas, 2004). Hence it becomes paramount that these particles are optimally designed to deliver the cargo efficiently to their target. Various particle parameters play a key role in determining delivery efficiency. It has been previously shown that particle size and material are important for successful delivery of drugs to cells *in vitro* as well as *in vivo* but recently the effect of shape of particles is also being unraveled to play a major role (Chithrani and Chan, 2007; Decuzzi et al., 2009; Geng et al., 2007; Gratton et al., 2007; Mitragotri, 2009). Most of the natural structures that flow in our body are non-spherical including red blood cells, viruses and bacteria and these acts as an inspiration to study the effect of shape in their biodistribution and retention in body. Theoretical studies have predicted that particle size and shape play an important role in margination dynamics of particles in blood vessels (Decuzzi et al., 2009). Hence to understand the effect of shape and size of nanoparticle, varied shape and size nanoparticles were fabricated using UV nanoimprint lithography (NIL). Tests were performed on various mammalian cell lines to see the effect of geometry in internalization.

In order to optimize nanoparticle properties for further testing in animals, the particles were examined in spheroids, which served as *in vitro* tumor models and are known to closely resemble the architecture, biological properties, and physiological characteristics of human tumor tissue (Friedrich et al., 2009). Spheroids not only allow us to test nanoparticle uptake and drug efficacy by cells cultured in 3D environment but also allow opportunity to test the drug and particle penetration inside tissue matrix. Most nanoparticles injected *in vivo* only accumulate near the peripheral regions of the solid tumor and are unable to penetrate deep inside the tumor tissue due to the dense collagen matrix and high interstitial pressure that lies within. Further, the permeability of the vessels may not be the same throughout a tumor and may lead to uneven distribution of the particles within the tumor tissue. As diffusion is the primary mode of operation for distribution of the particles inside a tumor, various strategies have been investigated to increase the diffusion of particles in order to overcome interstitial tissue barriers. Kim *et al.* varied the charge on gold nanoparticles to show that anionic nanoparticles penetrate deeper into *in vitro* models of tumors as compared to cationic particles (Kim et al., 2010). In another strategy, Wong *et al.* shrunk the size of nanoparticles from 100nm to 10nm upon their entrance into the tumor matrix in order to increase the diffusion and penetration of particles in the interstitial tissue (Wong et al., 2011). Similarly, Park *et al.* showed that cylindrical gold nanoparticles diffuse more in solid tumors compared to spherical gold nanoparticles after intra-tumor injections (J. Park et al., 2010).

We hypothesized that shape and size must be optimized in a multivariate design space in order to develop effective nanocarriers with efficient transport properties across different biological barriers that can eventually be used for delivery of contrast agents and therapeutics to treat various diseases. Specifically, we proposed the following specific aims:

1.2 SPECIFIC AIMS

1.2.1 Specific Aim 1: To fabricate, optimize and characterize nanocarriers of precise size and geometry (shape and aspect ratio) using a high throughput, top-down nanomanufacturing process.

Specifically, we used use Jet and Flash Imprint Lithography (J-FIL) to synthesize highly monodisperse polyethylene glycol (PEG)-based nano-hydrogels of various shapes, and sizes. Top-down nanomanufacturing is the only way to fabricate monodisperse nanoparticles of precise sizes and non-spherical geometry and to impart multiple functionalities e.g. elasticity and triggered degradation on shape-specific particles. However, the limitation of top down fabrication is that it is essentially a wafer-based batch process which results in limited number of nanoparticles. In addition, these nanoimprinting processes, originally developed for electronics application, needed to be optimized for biological materials and drugs, especially for encapsulation of drugs. Hence, in this aim, process was optimized to produce wafer-scale imprints in a continuous process to get large quantities of particles.

1.2.2 Specific Aim 2: To evaluate the effects of nanoparticle size, shape and material composition on *in vitro* cellular uptake in various cell lines.

Cellular uptake efficacy of fluorescent NPs of various shape and size was evaluated through a series of *in vitro* cell culture studies using confocal microscopy and flow cytometry to verify intracellular particle localization and cell uptake efficiency. The idea is to find which particle size and shape would work best in vitro for equal amounts of model drug dose. Also it would be fascinating to study the kinetics of uptake and whether there is some shape dependent uptake kinetics. We used a variety of relevant cells such as epithelial, endothelial and immune cells.

1.2.3 Specific Aim 3: To study the effects of nanoparticle size, shape and material on *in vitro* tumor models (Spheroids)

In this aim we tested the effect of size and shape of nanoparticles on 3D culture models (spheroids). Spheroids were formed using HEK 293 cell lines and various size and shape particles were tested for their association and penetration inside spheroids. The purpose of this aim is to analyze and quantify the effects of geometry on particle uptake and penetration within the tumor mass using spheroids as *in vitro* tumor models. We hypothesize that certain shape can enhance penetration of particles of similar volumes compared to spherical counterparts.

1.3 DISSERTATION SUMMARY

Chapter 2 provides the previous work and background necessary to understand what has been known in the literature and the approaches taken by different researchers to treat diseases using nanoparticles. This chapter also highlights the need for use of top down fabrication to synthesize and study shape-specific polymeric nanoparticles for drug delivery applications. Chapter 3 describes our approach to make polymeric nanoparticles of precise shape and size using top-down fabrication (Jet and Imprint Flash Lithography) and optimization of the process to achieve high scale throughput of nanoparticles. This section also talks about strategies to encapsulate various drugs and imaging biomolecules. Chapter 4 establishes the effect of size and shape on uptake by mammalian cells and shows that shape matters and the effects are cell line specific. Chapter 5 demonstrates the effect of particle size and shape on *in vitro* tumor model uptake and penetration. Finally chapter 6 concludes the dissertation and provides insight on future work.

1.4 REFERENCES

- Chithrani, B. D., and Chan, W. C. (2007). Elucidating the mechanism of cellular uptake and removal of protein-coated gold nanoparticles of different sizes and shapes. *Nano Lett* 7, 1542-1550.
- Davis, M. E., Chen, Z., and Shin, D. M. (2008). Nanoparticle therapeutics: an emerging treatment modality for cancer. *Nat Rev Drug Discov* 7, 771-782.
- Decuzzi, P., Pasqualini, R., Arap, W., and Ferrari, M. (2009). Intravascular delivery of particulate systems: does geometry really matter? *Pharm Res* 26, 235-243.
- Ferrari, M. (2005). Cancer nanotechnology: opportunities and challenges. *Nat Rev Cancer* 5, 161-171.
- Friedrich, J., Seidel, C., Ebner, R., and Kunz-Schughart, L. A. (2009). Spheroid-based drug screen: considerations and practical approach. *Nat Protoc* 4, 309-324.
- Geng, Y., Dalhaimer, P., Cai, S., Tsai, R., Tewari, M., Minko, T., and Discher, D. E. (2007). Shape effects of filaments versus spherical particles in flow and drug delivery. *Nat Nanotechnol* 2, 249-255.
- Gratton, S. E., Pohlhaus, P. D., Lee, J., Guo, J., Cho, M. J., and Desimone, J. M. (2007). Nanofabricated particles for engineered drug therapies: a preliminary biodistribution study of PRINT nanoparticles. *J Control Release* 121, 10-18.
- Hamidi, M., Azadi, A., and Rafiei, P. (2008). Hydrogel nanoparticles in drug delivery. *Advanced Drug Delivery Reviews* 60, 1638-1649.
- J. Park, A. Estrada, J. A. Schwartz, P. Diagaradjane, S. Krishnan, A. K. Dunn, and Tunnell, J. W. (2010). Intra-Organ Biodistribution of Gold Nanoparticles Using Intrinsic Two-Photon-Induced Photoluminescence. *Lasers in Surgery and Medicine* 42, 630-639.
- Kim, B., Han, G., Toley, B. J., Kim, C. K., Rotello, V. M., and Forbes, N. S. (2010). Tuning payload delivery in tumour cylindroids using gold nanoparticles. *Nat Nanotechnol* 5, 465-472.
- Ma, W. W., and Adjei, A. A. (2009). Novel agents on the horizon for cancer therapy. *CA Cancer J Clin* 59, 111-137.
- Mitragotri, S. (2009). In drug delivery, shape does matter. *Pharm Res* 26, 232-234.
- Panyam, J., and Labhasetwar, V. (2003). Biodegradable nanoparticles for drug and gene delivery to cells and tissue. *Advanced Drug Delivery Reviews* 55, 329-347.

- Peppas, N. A. (2004). Intelligent therapeutics: biomimetic systems and nanotechnology in drug delivery. *Advanced Drug Delivery Reviews* 56, 1529-1531.
- Wong, C., Stylianopoulos, T., Cui, J., Martin, J., Chauhan, V. P., Jiang, W., Popovic, Z., Jain, R. K., Bawendi, M. G., and Fukumura, D. (2011). Multistage nanoparticle delivery system for deep penetration into tumor tissue. *Proc Natl Acad Sci U S A* 108, 2426-2431.

Chapter 2: Background and Significance

2.1: DRUG DELIVERY AND NANOPARTICLES

With advancements in the field of drug discovery, biologists and chemists are rapidly creating a large array of drugs that can potentially be highly effective against complex diseases (Korfee et al., 2004). However, these advancements have not translated into clinical success primarily due to our inability to efficiently deliver drugs, contrast agents and biologics to target cells while sparing other cells and tissues of the body. The new wave of drugs and vaccines that have emerged over the past decade are often biologics (e.g. DNA, siRNA, oligonucleotides, aptamers, peptides and proteins) that interfere with key intracellular processes and can only act when delivered inside specific cellular compartments (e.g. cytoplasm, mitochondria, lysosomes, nucleus, etc.). Since many of these biologics are charged and have high molecular weights, they cannot freely diffuse across the cell membrane and need active uptake processes for internalization. Such drugs are also sensitive to the extra-cellular environment and are easily rendered ineffective by enzymes. Further their presence in healthy tissues can cause unwarranted damage and limits effective dosing in patients. Therefore to fully utilize the potential of these next generation of therapeutics, it is paramount that delivery be maximized to target sites and to specific intracellular locations while at the same time minimizing side-effects.

Nanoparticles or nanocarriers (henceforth referred to as NPs) have emerged as a possible solution for the delivery of imaging and therapeutic cargo (Davis et al., 2008; Ferrari, 2005; Hamidi et al., 2008; Panyam and Labhasetwar, 2003; Peppas, 2004; Schafer et al., 1992). Use of NPs for delivery offers various advantages. Biologics can be adsorbed, dissolved or dispersed throughout the matrix or can be covalently attached and hence are protected from the harsh external environment experienced (immune clearance

and enzymatic degradation) during their voyage to target site. It allows delivery of both hydrophilic and hydrophobic molecules which could not be directly injected in the blood stream. Various bulk and surface characteristics of NPs can be modified and controlled to suit applications without compromising the efficacy of payload and impart “stealth” properties to bypass the immune system. NPs could allow long shelf life, controlled release of payload and ease of administration through various routes to diseased cells. They also offer the potential to target specific uptake pathways in cells and hence can deliver drugs to specific subcellular organelles. However, along with such advantages, there are also concerns about toxicity associated with injected nanomaterials (Lison et al., 2008; Nel et al., 2006; Teeguarden et al., 2007). Specifically, non-degradable particles above 10 nm in size cannot not be cleared from the body and raises concerns about their long term toxicity. Ballou *et al.* were able to image quantum dots after more than 4 months of administration in mice (Ballou et al., 2004). Long term studies about the fate of such non-degradable particles needs attention. Interested readers are encouraged to read reviews for metal NPs for biomedical applications (Dykman and Khlebtsov, 2012; Liao et al., 2006). The focus of this review is the use of polymer based degradable NPs for biomedical applications, especially those related to therapeutics delivery.

Polymeric nanocarriers are particularly interesting because their properties and design parameters can be easily customized and availability of a large pool of polymeric materials allow for customized applications. Although NP-based therapeutic delivery has been studied for several decades, our knowledge on the fundamental biology of cell-particle interactions, particle uptake in various cells as well as particle transport is alarmingly lacking. Most studies in NP design has relied on imperical testing of the end-effects (e.g. cell function, biodistribution or protein expression readouts) without identifying how key properties of a particle effect their interaction with cells and their

transport across biological barriers. Although particle properties and design parameters can significantly effect NP interactions with cells and with all cellular and physiological barriers, of particular interest for intracellular therapeutics delivery is how particle-properties effect cell-uptake, organelle-targeting and intracellular transport of NPs.

The majority of NP uptake and optimization studies in the literature, including our own, are in *in vitro* 2-dimensional culture in either serum free medium or 10% serum containing media, none of which is indicative of the *in vivo* environment. Further, the body's immune system and flow dynamics plays an important role and changes the pharmacodynamics and kinetics of NPs *in vivo*. Few studies have been done in appropriate flow and shear rate conditions present near the cells and showed that results can be significantly different when compared to static *in vitro* conditions (Bhowmick et al., 2012; Han et al., 2012). Studies that do report *in vivo* performance of NPs primarily report tissue accumulation. There are not many studies in the literature reporting cellular uptake efficiencies and mechanisms of internalization of particles *in vivo*. Instead the term tissue uptake used in the literature mostly signifies tissue accumulation. Tissues consist of many types of mixed cells (epithelial, macrophages, dendritic cells, neutrophils, other lymphocytes, red blood cells, endothelial cells) at target sites such as tumors. Often it is unclear as to which cell type the NPs affect and how that influences the therapeutic outcome.

Another major limitation to our current understanding of NP uptake by cells is the lack of multivariate analysis on how various geometric, mechanical and surface parameters of particles affect their interaction with cells. Some of these parameters like shape, elasticity, surface compositions are only being individually studied for the past few years. Further complicating the process is the fact that different cell types of the body, both normal and diseased, would likely interact with these NP parameters

differently. Thus the optimal design space of NPs for efficient *in vitro* and *in vivo* delivery must consist of multiple NP parameters as well as target cell parameters, and the inter-dependence of these parameters should be studied.

In this chapter we will focus on these aforementioned issues, specifically discussing the various uptake pathways in cells and how particle design parameters affect intracellular delivery both *in vitro* and *in vivo*.

2.2 UPTAKE PATHWAYS: HOW CELLS INTERNALIZE NPs AND HOW TO STUDY THEM

In order to design effective NPs for therapeutic delivery it is imperative that we understand how cells internalize nanomaterials and how NP parameters affect these cell-uptake pathways. Physiologically, cells internalize a variety of molecules of varying molecular weights, charges and compositions. The mechanism for such uptake varies from cell-to-cell. Thus it is critical to understand both the fundamental biology of each uptake pathway as well as their mechanism of interactions with NPs.

The plasma membrane acts as a physical barrier for biomolecules and particles for entry into and out of cells. To facilitate exchange with external environment and cellular signaling, cells have evolved several specific mechanisms which can be potentially exploited for NP internalization. These mechanisms are collectively known as endocytosis and can be broadly divided into 5 types: Clathrin mediated uptake, Caveolae mediated uptake, clathrin and caveolae independent uptake, macropinocytosis and phagocytosis (Figure 2.1). Clathrin mediated uptake is the most studied pathway and uses many adaptor and accessory proteins like (AP)2 adaptor-protein complex. These proteins initiate clathrin polymerization at the plasma membrane which results in vesicle formation. These vesicles are finally constricted and cleaved resulting in internalization of external materials (Doherty and McMahon, 2009). Many cell-surface proteins like the

transferrin receptor, epidermal growth factor receptor (EGFR), low-density lipoprotein receptor are specifically internalized by this pathway (Parton and Simons, 2007). Caveolae mediated uptake is characterized by the presence of caveolin and appear as smooth flask shaped pits on the cholesterol-enriched microdomains of plasma membrane. This pathway is involved in trafficking of cholesterol, cholera toxin and glycosylphosphatidylinositol (GPI)-anchored proteins etc. (Parton and Simons, 2007). Caveolae pathway has also been associated with transcytosis of serum albumin especially in endothelial cells. Another uptake mechanism that has recently been found and is not well characterized is clathrin and caveolae independent uptake (Doherty and McMahon, 2009). This pathway neither involves use of clathrin nor caveolae and has been shown to be utilized for uptake of cytokine receptors, growth hormones etc. Macropinocytosis and phagocytosis involves large membrane deformation and engulfment of surrounding medium and particles (Ivanov, 2008). Rac and actin proteins are involved in these large protrusions. Although macropinocytosis is present in all cells, phagocytosis is limited to only specialized cells such as macrophages and dendritic cells. Macropinocytosis is also shown to be associated with uptake of surrounding apoptotic cell debris (Henson et al., 2001; Hoffmann et al., 2001).

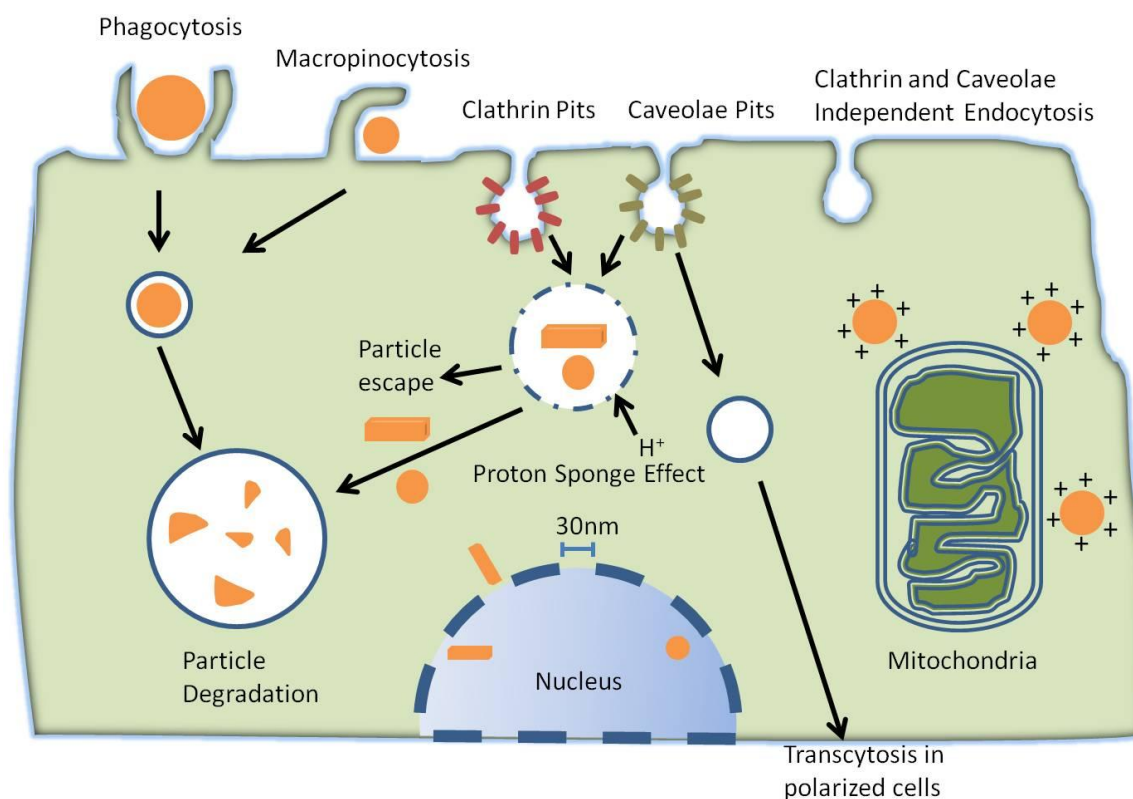


Figure 2.1: Schematic representation of different uptake pathways potentially utilized by mammalian cells to take up foreign NPs and the intra-cellular fate of internalized NPs as a function of physical parameters such as size, shape and charge. Proton Sponge Effect is a strategy used for endosomal escape of nanoparticles based on surface properties of NPs. Particles are designed to carry secondary or tertiary amines on the surface such that they can buffer the pH of endosomes. This results in proton influx through the endosomal proton pumps, followed by chloride ion transport that eventually leads to osmotic swelling and bursting of vesicles, thus releasing the particles in the cytoplasm.

There are 4 major methods to study these pathways and their involvement in uptake of particles and materials. The most commonly used method is to perform uptake studies in the presence of pharmacological inhibitors and look for a specific decrease in internalization efficiencies. Although many commonly used inhibitors are not very specific to their targets, they can provide large quantitative information and are widely

used in the literature (Ivanov, 2008). It should also be noted that inhibition of one pathway may lead to enhancement of another pathway (Chen et al., 2011). Another method is co-localization with tagged proteins that are known to be endocytosed using specific mechanisms. This usually involves administration of test material/particle with labeled proteins like transferrin or folate receptors and then performing confocal microscopy to see co-localization (Huth et al., 2006). This method is slow and only gives qualitative information. Furthermore, the presence of tagged proteins can potentially compete with NPs and saturate the uptake pathways involved thereby affecting the uptake. The 2 methods described can be combined by first comparing the inhibition of known tagged proteins using pharmacological inhibitors to characterize the response of cells in presence of such inhibitors followed by inhibition of test molecules/NPs with same cell type, concentration of inhibitors and time to provide more conclusive results as shown by Georgieva *et al.* (Georgieva et al., 2011). Another method that has recently been reported involves silencing of pathway-specific proteins in cells of interest using siRNA and then performing uptake studies with those cells (Bhattacharya et al., 2012). For instance Rac can be knocked out to evaluate the role of macropinocytosis and phagocytosis in uptake. This approach is very specific (if the correct target protein is known) and can be used for quantification as well. However efficient silencing using siRNA is difficult and in most cases only partial. Finally, the use of labeled cell lines that are stably/transiently tagged with fluorescent markers on proteins involved in uptake, e.g. clathrin or caveolae, can also be used to study these pathways (Mettlen et al., 2010; Mundy et al., 2012). This method provides qualitative information about the pathways that are being used and is very specific to the mechanism involved. However only a small number of stable cell lines have been reported to date and it is often difficult to obtain high transient transfection efficiencies of proteins tagged with fluorescent markers. It is

difficult to distinguish between macropinocytosis and phagocytosis based on just one simple technique. Phagocytosis is receptor mediated, used to engulf large particles only by specialized cells and the resulting phagosome is very tightly packed around the particles. In contrast, macropinocytosis is non-specific, can have varied size macropinosome and is characterized by presence of fluid in macropinosome. To distinguish between the 2 pathways, uptake studies can be performed in presence of aggregated IgG and a neutralizing CD18 mAb which will compete for specific receptors used in phagocytosis and inhibit uptake by this pathway where macropinocytosis should remain unaffected (Sandgren et al., 2010).

Although significant advances have been made in our understanding of endocytic pathway biology, much less is known about how NP properties, e.g. size, shape, charge, surface compositions, and mechanical properties affect each of these pathways. It is expected that the interaction of the cell membrane with NPs and subsequent signaling events leading to activation of specific internalization pathways would depend on all these parameters. It is difficult to study pathway specific *interactions in vivo*, so most efforts to date has focused on studying NP-cell interactions *in vitro* using the methods discussed above. However, much more effort needs to be invested to thoroughly correlate NP properties to cell-uptake mechanisms. Table 2.1 summarizes the uptake pathways and ways to study them.

Table 2.1: Uptake pathways involved in internalization of non-targeted nanoparticles and tools that can be used to study these pathways.

Pathway	Particle Size limitations	Intracellular fate	Study tools (Most specific)
Clathrin	<120nm	Lysosomes	Chlorpromazine inhibition, Clathrin knockdown, EGFR co-localization
Caveolae	<100nm	Lysosomes, transcytosis in polar cells	Filipin Inhibition, Co-localization with GPI-anchored proteins, Caveolae Knockdown
Clathrin and Caveolae independent	<50nm	Lysosomes, cytoplasm	Multiple pathways involved, Cholesterol inhibition
Macropinocytosis	<1 μ m	Lysosomes, Recycled back to plasma membrane (Cell type dependent)	Inhibition with Cystochalsin D and Amiloride, Knockdown of Rac protein
Phagocytosis	<5 μ m	Phagosomes	Inhibition with Cystochalsin D and Amiloride, Knockdown of Rac protein

2.3 SIZE: IS SMALLER BETTER?

Size is the most researched NP parameter for uptake and *in vivo* delivery. Size generally signifies volume of the particle, but since almost of the studies reported uses spherical NPs, it is commonly represented in terms of diameter. Recent advances in particle fabrication techniques have allowed us to produce non-spherical particles, enabling evaluation of their size effects on cellular internalization (Acharya et al., 2010; Agarwal et al., 2012; Canelas et al., 2009; Glangchai et al., 2008; Rolland et al., 2005; Tasciotti et al., 2008). However, very few studies have looked at the interplay of size and shape. This will be further discussed in later sections.

In the context of intracellular delivery, it is well established that in *in vitro* conditions, uptake efficiencies of NPs increases as the size decreases (up to 50 nm). Osaki *et al.* showed that 50 nm polysaccharide coated quantum dots outperform similar particles below that size range (Osaki et al., 2004). Chithrani *et al.* also showed, with spherical gold NPs in epithelial cells, that 50 nm diameter particles were internalized at a higher efficiency (number of particles per cell) compared to other sizes between 10 and 100 nm (Chithrani et al., 2006a). Lu *et al.* reported that 50 nm silicon mesoporous particles were able to deliver more particles in terms of weight in cells as compared to smaller and larger sized particles (Lu et al., 2009). He *et al.* showed that for polymeric NPs between size ranges of 100-500 nm, non-phagocytic cells internalize smaller sized particles more efficiently (He et al., 2010). From these results it is evident that the optimal size range for spherical NP uptake *in vitro* for non-phagocytic cells is between 50 and 100 nm. Further, with respect to size effects on intra-cellular transport, it has been shown that NPs greater than 50 nm in diameter tend to be excluded out of the nucleus (Oh et al., 2011; Rudolph et al., 2003).

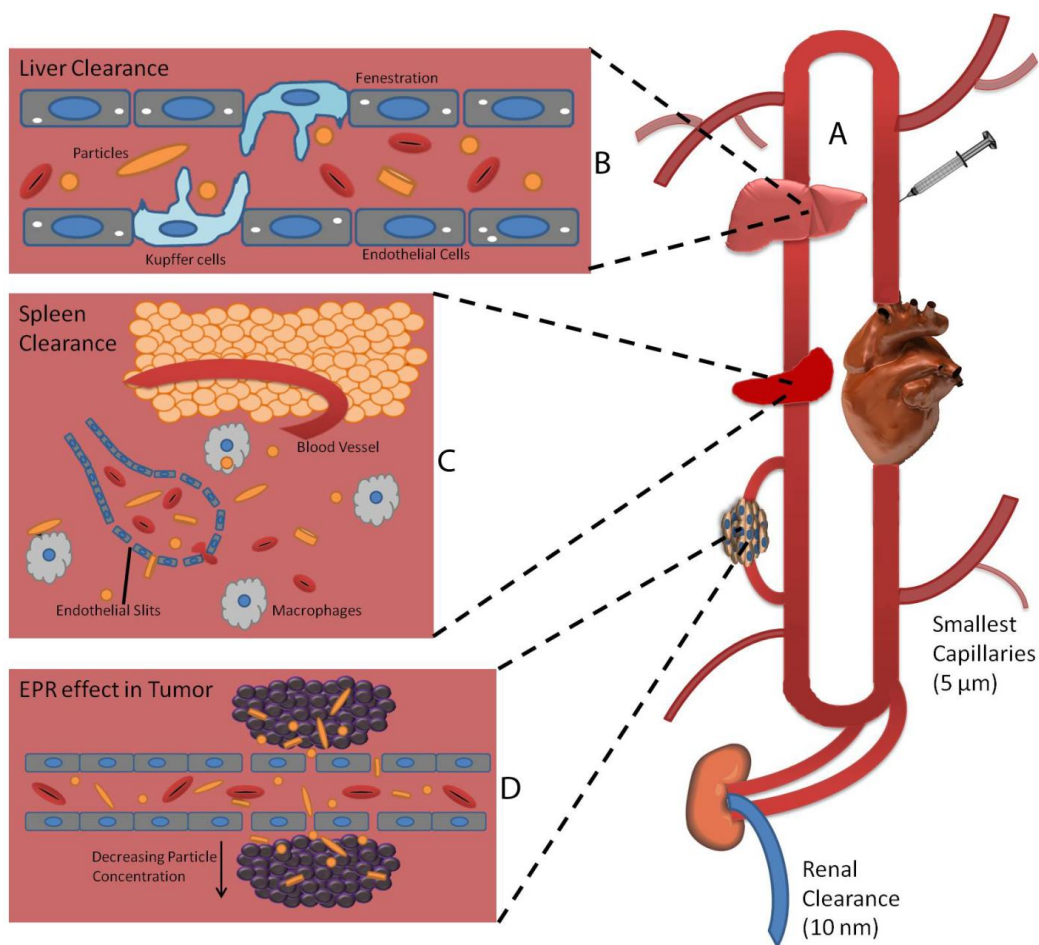


Figure 2.2: Schematic representation of barriers to particle delivery in vivo. A. Representation of systemic circulation of blood and major organs involved in nanoparticle voyage. Smallest capillaries are 5 μm in diameter and kidney clears anything below 10 nm thereby defining the upper and lower bound on particle dimensions. B. Particle clearance by liver. Kupffer cells present in blood vessels of liver efficiently clear particles greater than 500nm from the blood. C. Particle clearance by Spleen. Arteries release blood in the red pulp region of spleen where it re-enters the circulation through splenic venous sinuses via slits between endothelial cells that are about 200 nm wide and hence traps and clears particles with larger dimensions. D. Enhanced Permeation and Retention (EPR) effect. Vasculature in tumor regions has leaky endothelial cell linings which can allow NPs to pass through and accumulate in tumor.

For spherical particles, the clathrin-mediated pathway can internalize particles up to about 120 nm in diameter (Conner and Schmid, 2003) while caveolae mediated pits are about 50-100nm in diameter (Conner and Schmid, 2003; Mayor and Pagano, 2007). Clathrin and caveolae independent pathways can be up to 40-50nm in diameter (Edidin, 2001). Macropinocytosis uses larger invagination of the cell-membrane and can take up particles up to 1 μm while phagocytosis can internalize particles up to 5 μm in diameter (Conner and Schmid, 2003; Korn and Weisman, 1967; Schafer et al., 1992). However these size limitations are not very definitive and there are several reports in the literature that suggest involvement of one or multiple pathway for all particle size ranges (Chen et al., 2011; Rejman et al., 2005; Rejman et al., 2006; Rejman et al., 2004b). For instance, it was shown that latex beads less than 200nm in diameter utilized the clathrin-mediated pathway while the mechanism shifted to caveolae-mediated uptake for 500nm diameter particles (Rejman et al., 2004b). More definitive studies directly comparing particles of various material compositions and evaluating how the fundamental biological interactions of cell-membranes (adhesion, membrane engulfing and endocytosis etc.) vary with particle size are needed. In this context surface-charge, surface compositions and groups, ligands etc. would also have significant interplay with size.

The consideration of intracellular delivery *in vivo* must take into account the transport properties of NPs in the circulation and into various normal and diseased tissues following delivery. It is only after tissue penetration and accumulation that cell-uptake is relevant (except for endothelial and immune cell targeting). The lower limit on diameter of spherical NPs that can be injected into the blood stream is defined by renal clearance. Kidney glomerular walls allow particles less than 10 nm diameter to pass through and hence any particle in and around that range can be quickly cleared from the body (Figure 2.2A) (Choi et al., 2007). The upper limit on diameter is defined by the size of smallest

blood capillaries (Figure 2.2A). These are about as 5 μm in diameter and hence particles larger than 2-3 μm can clog these vessels (Ilium et al., 1982). Different target sites also impose size limitations. For cancer applications, the newly formed vasculature in tumor regions have leaky endothelial fenestrations, a phenomenon also known as Enhanced Permeation and Retention (EPR) effect, which can allow NPs to pass through and accumulate in local tissues (tumor) (Jain and Stylianopoulos, 2010) at a higher rate than normal vasculatures (enhanced permeation) (Figure 2.2D). These particles remain retained in tumor tissues as afferent lymphatic vessels are poorly developed resulting in poor drainage (enhanced retention). The exact size of such pores varies with the type of tumor and with various stages of tumor development. Pore sizes in several tumor models have been found to be around 380 to 780 nm (Hobbs et al., 1998; Unezaki et al., 1996; Yuan et al., 1995), thereby limiting the particle size between 10 to 500 nm for efficient targeting by passive diffusion.

When NPs are administered *in vivo*, smaller sized particles (less than 200 nm) have been found to have longer circulation times (i.e. reduced clearance and hence better targeting to tissues other than the lungs, liver and spleen). Larger particles (above 200-300 nm), on the other hand, get cleared rapidly by the liver and spleen (Figure 2.2B and 2.2C) and often get “filtered” out by the lungs (Longmire et al., 2008; Shuvaev et al., 2011). The anatomy of the spleen is such that arteries release blood in the red pulp region and the blood re-enters the circulation through splenic venous sinuses via slits between endothelial cells. If spherical particles are rigid and larger than inter-endothelial slits (approximated to be about 200nm wide) then they could get trapped and filtered out and are eventually taken up by red-pulp macrophages (Moghimi, 1995). Hence for long term and tumor delivery of therapeutics, the ideal particle size range is between 10-200nm (Jain and Stylianopoulos, 2010) while for delivery to liver, spleen and immune cells, 200

nm - 1 μ m particles provide maximal efficiencies when delivered intra-vascularly. Perrault *et al.* showed that among particles in the size range of 20 nm to 100 nm, 60 nm particles gave the maximum accumulation in tumor over 24 hours (Perrault et al., 2009). However another challenge is to ensure that NPs are distributed uniformly in target sites. Tissues like tumors are dense and hence particles cannot freely diffuse through the extra-cellular matrix. Researchers found that as the size of NP decreases, more isotropic delivery to tissues is obtained. Among all the particles used by Perrault *et al.*, 20 nm diameter particles were found farthest away from blood vessels in tumor and hence most isotropically distributed (Perrault et al., 2009).

All these studies establish size as a clear design criterion for targeting NPs to various sites. However one aspect that has been mostly neglected in the literature is the intra-cellular uptake dependence of particles *in vivo*. Although a lot of studies have been done *in vitro*, the environment *in vivo* is significantly different. The presence of factors such as interstitial fluid flow, blood flow, high protein concentration, dense extra cellular matrix affecting diffusion and varying and highly mixed populations of cells (immune, endothelial, epithelial, fibroblasts etc.) as well as the state of cells (proliferating to necrotic) can result, either independently or as a combinatorial effect, in different uptake efficiencies and kinetics and can have marked impact on the efficacy of payloads reaching intra-cellular targets.

2.4 CHARGE: CATIONIC, ANIONIC OR NEUTRAL?

Mammalian cell membranes are slightly negatively charged due to the presence of sulfated proteoglycans (Belting, 2003). Hence for *in vitro* experiments cationic NPs outperform their anionic counterparts due to favorable electrostatic interactions

(Albanese et al., 2012; Thorek and Tsourkas, 2008). He *et al.* showed that non-phagocytic cells preferred positively or neutrally charged chitosan based NPs over negatively charged NPs (He et al., 2010). For macrophage uptake, increasing surface charge (negative or positive) resulted in an increase in uptake of 100-500nm diameter spherical particles. Positively charged particles were internalized more efficiently as compared to negatively charged particles in all cell lines. Arvizo *et al.* showed that positively charged particles electrostatically interact with the cell membrane to depolarize it while neutral and negatively charged particles have negligible effects (Arvizo et al., 2010). They also showed that this electrostatic interaction results in increased Ca^{2+} influx and hence inhibiting cell proliferation. Interestingly, malignant cells were found to be resistant to such mechanisms. Wang *et al.* studied the effects of charged particles on phospholipid membranes and showed that polymeric cationic NPs of 20 nm diameter increases the local fluidity of the membrane whereas anionic NPs caused local gelation (Wang et al., 2008).

Charge has been shown to influence the uptake mechanisms as well as intra-cellular fate of NPs. It was shown that dendrimers that carry negative charge utilize the caveolae-mediated pathway for uptake while neutral and positively charged dendrimers were internalized by neither clathrin nor caveolae pathways in an epithelial cell line (Perumal et al., 2008). Poly Lactic Acid (PLA) particles were found to have different intra-cellular fate depending on the NP charge (Harush-Frenkel et al., 2008). Although both anionic and cationic particles were up taken by clathrin-mediated endocytosis and negatively charged particles were localized inside lysosomes, a large amount of cationic particles were found to be exocytosed. Intra-cellularly, mitochondria can be targeted by making the surface of NPs more cationic which disrupts the electrochemical potential of the mitochondrial membrane allowing the particles to diffuse through (Callahan and

Kopecek, 2006). Given all these results, it can be concluded that at least *in vitro*, positively charged particles can interact and get internalized in cells more efficiently than neutral and negatively charged particles *in vitro*. Majority of positively charged particles utilize clathrin and macropinocytosis while negatively charged particles tend to utilize caveolae mediated pathway (Harush-Frenkel et al., 2007; Harush-Frenkel et al., 2008; Sahay et al., 2010a; Sahay et al., 2010b; Zhang and Monteiro-Riviere, 2009). However there are exceptions to this and due to the lack of studies it is not conclusive whether charge alone can influence one uptake pathway over others.

In vivo, the effect of charge is difficult to understand because of protein adsorption. Most serum proteins in our body are negatively charged at physiological pH and salt concentrations and they rapidly interact and bind to positively charged particles which are then recognized by immune cells and get cleared from the body (Figure 2.3) (Peer et al., 2007). The extent of this would depend on the amount of cationic charge and the local tissue microenvironment following *in vivo* delivery. Campbell *et al.* showed that there was no significant difference in accumulation of cationic and neutrally charged particles (150 nm diameter) in peri-vascular regions of multiple tumor models, however, tumor vascular endothelial cells showed significantly enhanced accumulation of cationic particles when compared to neutral charged particles of same size (Campbell et al., 2002). A mathematical model was proposed by Stylianopoulos *et al.* that proposed that electrostatic attraction of positively charged nanoparticles compete with hydrodynamic and steric forces for transvascular flux and above a certain surface charge density of nanoparticles becomes dominant and can lead to enhanced accumulation in tumors (Stylianopoulos et al., 2013). However for tumors such as brain and pancreatic tumors, pore sizes are very small and steric force might be too high for electrostatic interaction to overcome and hence different particle formulations are needed depending on different

type of tumors (Stylianopoulos et al., 2013). Cedervall *et al.* studied the protein corona that is formed on the surface of NPs in high protein concentrations (Cedervall et al., 2007b). They proposed that proteins compete for space on NP surface and though initially abundant proteins in serum will bind to NPs, over time these proteins will be replaced by high affinity proteins even if they are at lower concentrations (Vroman effect). This protein corona outside the NP surface ultimately decides the fate of a particle inside the body (Lynch and Dawson, 2008; Lynch et al., 2009). Blood residence time is thus lowest for positively charged particles as they are tagged by immunoglobulins, coagulation factors and other proteins for rapid clearance by the reticulo-endothelial system (RES). Positively charged NPs, especially with exposed surface groups like primary amines can also damage platelets and cause hemolysis (Domański et al., 2004; Malik et al., 2000). Neutral and slightly negatively charged particles are able to circulate in the blood for long time (Albanese et al., 2012).

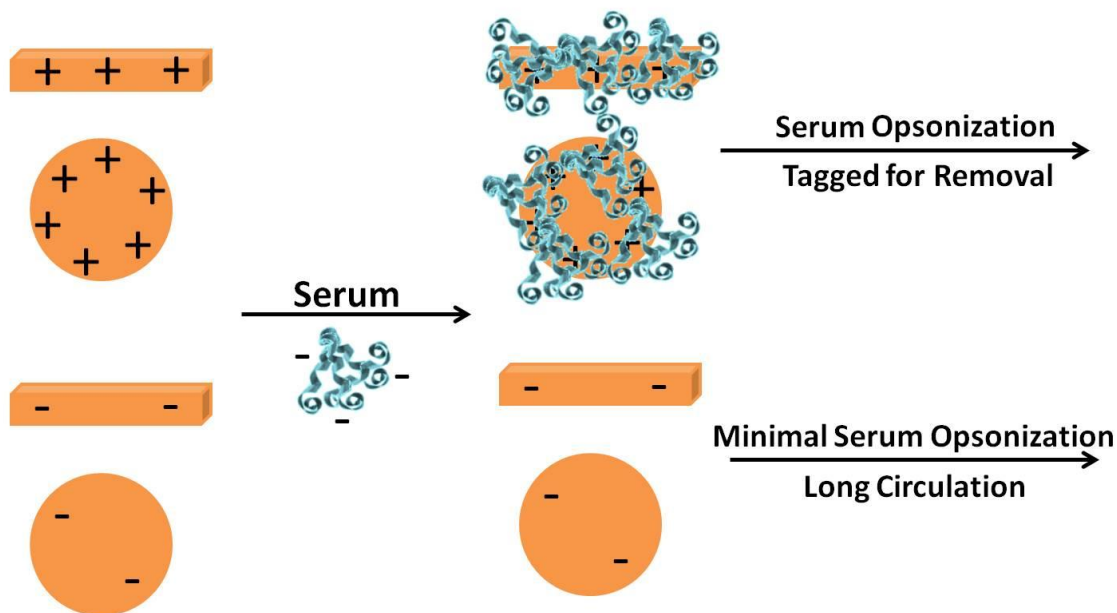


Figure 2.3: Schematic representation of effect of nanoparticle charge on its fate in vivo.

From all this it can be concluded that effective charge of the particle once it is injected into the blood stream is either neutral or slightly negative. Not much is known about effect of charge on uptake by cells *in vivo*. Kim *et al.* used cylindroids as *in vitro* tumor models to see the effect charge has on 6 nm particle penetration inside tissue matrix (Kim et al., 2010). They showed that cationic NPs are taken up by proliferating cells and do not penetrate deep into the matrix while anionic particles diffuse quickly into the deep tissue matrix. Despite our understanding of charge based interactions of cell surface and NPs *in vitro*, a significant knowledge gap exists on definitively establishing the magnitude and type of charge that would allow for efficient *in vivo* intracellular delivery. These values are likely to be different for different target tissues and could even be different under various disease conditions that alter immune-clearance. Further, the interplay between particle shape and charge has not been studied and adds another critical dimension to this complex problem.

2.5 ELASTICITY: DOES IT MATTER HOW HARD OR SOFT THE NP IS?

Elasticity is another parameter that has recently been established as an important design criterion in NPs for cellular uptake and drug delivery applications. It is well proven that the elasticity of the substrate on which cells are grown has profound effect on cell proliferation and expression (Discher et al., 2005). Studies with NPs have now also shown that cells can “feel” the stiffness of NPs (Banquy et al., 2009; Yi et al., 2011). Elasticity could have profound effect at the nanoscale. Yi *et al.* did molecular simulations to show that stiffer particles can be wrapped around by cell membranes at lower energy cost as compared to softer particles whereas softer particles can be partially wrapped around at much less energy input compared to stiffer particles (Yi et al., 2011). Banquy *et*

al. showed that elasticity influences cell uptake by utilizing different uptake mechanisms. They used hydrogel particles of different elasticities (18kPa to 211kPa) and showed that soft NPs uses macropinocytosis while harder NPs are primarily internalized through clathrin dependent mechanisms (Banquy et al., 2009). NPs with intermediate elasticities were found to utilize several uptake mechanisms.

Elasticity has also been shown to have profound effect in circulation times in blood. The best known example is red blood cells that are known to circulate in blood for months. RBCs are highly elastic cells and can squeeze through capillaries that are much smaller than the dimensions of the cells (Petros and DeSimone, 2010). Presence of inhibitory receptors such as CD47 on RBC's surface also inhibits their uptake and clearance by macrophages (Oldenborg et al., 2002). Inspired by these characteristics of RBCs, Merkel *et al.* fabricated particles of different elasticity in the shape of RBCs and showed that by decreasing the modulus of particles by 8 times resulted in increase in blood residence time by about 30 times (Merkel et al., 2011). They further showed that when low modulus particles of different sizes were injected in blood, larger particles (6.4 μm) were able to circulate in blood longer compared to their smaller counterparts (780 nm) (Merkel et al., 2012). This was attributed to the fact that smaller particles are taken up by immune cells and hence cleared rapidly compared to larger particles which are too large to be up taken. Geng *et al.* showed that filomicelles, that are highly deformable can circulate in rodent blood for up to a week while once they were crosslinked and formed rigid structures like carbon nanotubes, they were cleared rapidly from the system (Geng et al., 2007).

From these results, it is clear that increasing elasticity increases blood residence time and avoids clearance by immune system. However, there is not much information about the cell uptake of these particles by cancerous and diseased cells *in vivo*. Whether

elastic particles would be more efficient in delivering drug across the cell membrane once they reach the target site still needs to be answered.

2.6 SURFACE COMPOSITION: WHAT THE CELL “SEES”

Some of the required characteristics of materials for polymeric particles are for it to be biocompatible, degradable and the degradation product should be non-toxic. Hydrophobic NPs tend to be internalized faster as compared to hydrophilic NPs *in vitro*. Computational studies on interactions of NPs with cell like membranes have shown that hydrophobic particles can penetrate into the bilayer membrane while hydrophilic particles remain adsorbed on the surface (Li et al., 2008). Particles with different surface chemistries have been shown to utilize different uptake mechanisms. Brandenberger *et al.* used 15 nm uncoated and PEG-coated gold NPs and showed that PEG-coated NPs utilize caveolae- and clathrin-mediated pathways more than uncoated particles which also utilized macropinocytosis (Brandenberger et al., 2010). Higher amounts of PEG coated NPs were measured free within the cytoplasm compared to uncoated particles. This was attributed to possibly endocytosis independent uptake mechanism but no evidence was shown. Similarly several strategies have been proposed for endosomal escape of nanoparticles based on surface properties of NPs. The most widely used strategy is the so-called “proton sponge” effect (Figure 2.1). Particles are designed to carry secondary or tertiary amines on the surface such that they can buffer the pH of endosomes. This results in proton influx through the endosomal proton pumps, followed by chloride ion transport that eventually leads to osmotic swelling and bursting of vesicles, thus releasing the particles in the cytoplasm (Figure 2.1) (Lin and Engbersen, 2008). Conjugation of peptides that can create pores in endosomal membrane also been proposed (Jenssen et al., 2006). Evans *et al.* studied the mechanism of PEI coated 100-200nm spherical particles

and showed that endocytosis involved interaction of particles with plasma membrane, induction of tubular invagination followed by intra-cellular clustering of particles (Evans et al., 2011). However no clear studies are available about how different bulk materials effects internalization and uptake mechanism as it has been difficult to have same size, shape and charge for different materials.

In vivo, NPs with hydrophobic surfaces are cleared efficiently by liver, spleen and lungs (Brannon-Peppas and Blanchette, 2004) while hydrophilic surfaces show less clearance (Gaur et al., 2000). When NPs come in contact with blood, they get coated with plasma proteins and lipids. Thus it is not the bulk material of the particle that is interacting with cells but the protein corona surrounding it (Lynch and Dawson, 2008). Lesniak *et al.* showed that the formation of protein corona on the surface of NPs decreases the adhesion to cell membrane and hence subsequent internalization (Lesniak et al., 2013). However the specific properties of an NP surface can determine what types of proteins will be adsorbed and hence provide another design parameter to selectively adsorb proteins of interest on the surface. The corona formed by proteins is expected to be very dynamic as initially abundant serum proteins will bind and will then be replaced by proteins present at low concentrations but higher affinity (Cedervall et al., 2007a). Hence this corona would also be different in different tissues and even intracellular locations depending on the type of proteins and their concentrations in that location. Particles are shown to bind apolipoproteins in serum which has many receptors on cells. This is particularly significant as apolipoprotein E is a protein involved in brain trafficking (Kim et al., 2007; Michaelis et al., 2006) and hence can be used to transport NPs across brain endothelium. Such strategies can open interesting directions for therapeutics delivery by controlling types of protein adsorption based on materials.

Another such strategy was shown using nab®-paclitaxel which is a paclitaxel bound to the serum protein albumin (Hawkins et al., 2008). Nab®-paclitaxel showed enhance accumulation in tumor regions as albumin transport pathways were used to shuttle drugs. The gp60 albumin receptor is also known to transcytose albumin across endothelial cells and can be used to extravasate out of blood vessels (Desai et al., 2006). This strategy was also used to deliver particles systemically through the intratracheal route, further indicating a role of transcytosis across alveolar epithelial and endothelial cells (Kim and Malik, 2003). Particle size can also play an important role in reducing the adsorption of large proteins as smaller sized particles have very high radius of curvature (Klein, 2007).

PEG and polysaccharides such as dextran are also used as coatings on the NP surface to reduce protein absorption (Yoo et al., 2010). Addition of PEG (PEGylation) makes the particle surface inert, hydrophilic, avoids immune clearance and increases the blood circulation time. Mosqueira *et al.* showed that longer PEG chain lengths (20kDa over 5kDa) and high surface density (30% w/w over 10% w/w of total polymer) result in increase in blood half-life of NPs (Mosqueira et al., 2001). However stealth features of PEG on the surface of nanoparticles also results in lower uptake by target cells. To address this problem, strategies are now proposed that would allow surface to be PEGylated when traveling through blood and then shedding of PEG layer at the target site using surrounding cues such as pH (Masson et al., 2004; Shin et al., 2003) and enzymes (Hatakeyama et al., 2007; Zhu et al., 2012) to facilitate uptake. Although recently it has also been shown that the immune system can make antibodies against PEG which can clear the particles rapidly and can cause safety concerns (Ishida and Kiwada, 2008; Ishida et al., 2007; Wang et al., 2007).

The complement system (part of the innate immune system) is another barrier that NPs need to overcome for long circulation. Complement proteins can recognize molecular patterns on foreign objects like bacteria, viruses and NPs and “mark” them for clearance which is then cleared by RES. Hamad *et al.* showed that various surface coatings can trigger different complement pathway which is also dependent on configuration and density of the coating on the particles (Hamad et al., 2010). It was shown that even PEG coating can activate complement and that extent of PEG coating can influence which complement pathway would be activated. Mushroom configuration (low density of PEG on the surface) resulted in C1q-dependent activation while brush configuration (high density of PEG on the surface) triggered the lectin pathway. The amount of complement activation was lower when PEG chains were in brush configuration. The complement system consists of many protein and enzyme complexes which can recognize specific surface features. C1q binds to charge clusters and hydrophobic domains (Kang et al., 2009). Carbohydrates and sugar are recognized by lectins through hydroxyl groups while ficolins binds to acetyl functional groups (Thomsen et al., 2011; Wallis et al., 2010). One of the best strategies to avoid recognition by the complement system has been to bind factor H on the surface of particle. Factor H is a regulatory protein that is recognized as a self-marker and hence does not cause activation (Schneider et al., 2009). Functionalizing molecules like peptide motifs, glycosaminoglycans or heparin that can bind factor H can increase the circulation time of NPs (Clark et al., 2006). Similarly functionalizing particles with CD47 (another marker of self) can reduce macrophage uptake (Tsai and Discher, 2008). However again there is not much information on effect of surface on uptake of particles *in vivo* and the mechanism by which they are taken up. It is intuitive that addition of ligands to NP surface will greatly influence their interaction with specific cells and can also alter the

individual effects of size, shape or elasticity. The effects of ligand-attachment are further discussed in later sections.

2.7 SHAPE: SPHERES, RODS AND DISCS HAVE UNIQUE INTERNALIZATION PROPERTIES

NP Shape has only recently begun to be used as a design criterion and has gained significant interest in past decade (Caldorera-Moore et al., 2010; Champion et al., 2007; Liu et al., 2012; Peiris et al., 2012; Simone et al., 2008; Tao et al.; Toy et al., 2011). The idea that pathogens have evolutionarily conserved shapes and target or accumulate in specific cells and tissues, as well as in intracellular compartments, has inspired the use of NP-shape as a potential parameter for therapeutics delivery. Traditionally it has been difficult to synthesize and control the shape of polymeric NPs as most self-assembly based synthesis methods result in spherical or near-spherical NP shapes, primarily due to thermodynamic forces. Further, due to limitations on the fabrication techniques, it is difficult to decouple shape-effects from other parameters (size, charge, surface chemistries etc.). However, recent advancements in the field of top-down fabrication have made it possible to fabricate NPs with precise and pre-defined sizes and shapes while maintain their surface compositions and charge (Acharya et al., 2010; Agarwal et al., 2012; Canelas et al., 2009; Glangchai et al., 2008; Rolland et al., 2005; Tasciotti et al., 2008). Although studies on the effect of shape on NP transport across biological barriers are just emerging, significant insights has been gathered in the past few years.

For *in vitro* cell uptake studies, Chithrani *et al.* used sub 100 nm gold particles of spherical and rod shaped geometry and found that cells were able to internalize spheres more efficiently than rods (Chithrani et al., 2006a). However, since Cetyl Trimethyl Ammonium Bromide (CTAB) was used for synthesis of nanorods and not nanospheres,

even after extensive washing, the presence of different surface chemistry for different shapes could not be ruled out. Huang *et al.* used mesoporous silicon NPs in the range 100 to 500 nm dimensions and showed that high aspect ratio nanorods are up taken more efficiently compared to smaller aspect ratio rods which in turn outperformed nanospheres (Huang et al., 2010). In this study, different molar ratios of CTAB were used and also the size (volume) of the 3 types of particles used was not comparable which could have been a significant factor in differences observed in uptake efficiencies. Gratton *et al.* showed with polymeric NPs that for particles in the range of 100 nm to 500 nm, long aspect ratio rods outperform more symmetric cylindrical particles (Gratton et al., 2008). Champion *et al.* synthesized micron scale polymeric particles and showed that the local shape in contact with cell membrane is determinant of uptake of particles by macrophages (Champion and Mitragotri, 2006). Recently, Barua *et al.* showed that when shape specific hydrophobic polystyrene nanoparticles are coated with specific antibodies, then rod shaped particles are more efficiently up taken by target cells as compared to spherical particles (Barua et al., 2013).

In another strategy, it was shown that particles can be fabricated such that they can change shape over time or after receiving an external stimuli (Lee et al., 2012). Yoo *et al.* showed that particle shape can be controlled temporally and that elliptical disc shaped particles are not internalized by macrophages but when the same particles change shape to spherical under the influence of external stimuli, such particles are rapidly taken up (Yoo and Mitragotri, 2010). Such temporal control over the shape of particles can be used to address different shape requirements for long circulation and targeted uptake *in vivo*. For instance, to avoid macrophage uptake *in vivo* the particles can be elliptically shaped and then change shape such that it become optimal for uptake by target cells once they accumulate in target sites (Yoo et al., 2011a; Yoo et al., 2011b). Such a strategy can

allow particles to utilize the best flow dynamics and RES avoidance shape for the initial time point and then transform over time such that they become favorable for uptake by target cells. From these *in vitro* studies, trend seems to be in the pattern that rod shaped NPs have better uptake efficiencies compared to spherical NPs in the size range of 100 nm to 1 μm . While in the range of sub 100 nm, though there have been very few studies, spheres outperform rods.

Again, for *in vivo* intracellular delivery the combination of extracellular transport (i.e. circulation, extravasation and tissue penetration) and cell-uptake needs to be studied. Shape has been shown to be an important factor in flow margination, avoidance of immune system and tissue accumulation. Theoretical studies predict that due to asymmetry, non-spherical particles experience torque and hence tumble during flow, thereby exploring and marginating towards vessel sides and into new capillaries (Decuzzi et al., 2005; Shah et al., 2011). This also could allow particles to accumulate more in tumor and diseased sites through vessel wall fenestrations. Tao *et al.* used theoretical modeling to show that discs has the highest probability to adhere to side walls of vessels in flow followed by rods, ellipsoids and spheres (Tao et al.). Van de ven *et al.* used top down fabrication to synthesize mesoporous silicon microparticles in range of 600 nm to 3 μm and showed that non-spherical particles, especially discs, accumulate near cancerous tissues (van de Ven et al., 2012). Geng *et al.* showed that filomicelles (cylindrically shaped soft polymeric micelles) as long as 8 μm in length can persist in circulation for more than a week in rodents while their spherical counterparts of similar volume get cleared within 48 hours (Geng et al., 2007). Red blood cells (RBCs) have also drawn attention due to their flexible discoidal shape and ability to circulate in blood for up to months. Researchers have mimicked RBCs using polymeric particles and shown a increase in blood residence time (Doshi et al., 2009; Merkel et al., 2011). Shape can also

play an important role in penetration through the matrix once NPs reaches the target tissues. Chauhan *et al.* showed that PEG-coated sub 100 nm silica nanorods penetrate further away from blood vessels through tumor matrix as compared to nanospheres (Chauhan et al., 2011). However somewhat contradictorily, it was recently shown that effect of shape on extravasation using the EPR effect is dependent on the type of tumors where in some tumors more nanorods were found while in others, nanospheres dominated (Smith et al., 2012). It was also shown that the EPR effect was absent in some tumors and the particles were not able to accumulate in tumor regions despite being nanosized. These recent results underscore the importance of cell type as “context” and shows that a set of universal design specification is unlikely for all *in vivo* applications.

In spite of these reports it is not clear what geometry is best for uptake and how and why are there differences seen between different shapes. No clear answer is known as to which shape utilizes which uptake pathways, which is likely to differ between cell types. Very few studies have focused on trying to find uptake pathways involved with different shapes and all shapes studied have been shown to utilize multiple pathways (Gratton et al., 2008). Yang *et al.* used computer simulations to see how NPs of different shapes interacted with cell membranes (Yang and Ma, 2010). They concluded that initial orientation, contact area and volume are important factors involved in uptake. Direct translocation of particles through the lipid bilayer was simulated whereas many active processes like endocytosis, pinocytosis and phagocytosis that have been shown to play an important role in cellular uptake were not considered. Further there is little work done on uptake of particles *in vivo* by target cells (as opposed to tissue accumulation). Mao *et al.* reported gene transfection efficiencies of DNA based micelles in liver of rats and showed that nanoworm-shaped particles were about 1600 times more efficient than spherical micelles (Jiang et al., 2012). Since DNA transfection needs uptake of particles by the

cells and translocation of cargo to nucleus, hence this gives some indication of *in vivo* uptake of NPs. A possible explanation of different uptake efficiencies for different shape can be the presence of multivalent interactions of non-spherical particles with cell membrane and hence stronger adhesion and more sites for the uptake process to “trigger” as compared to spherical particles where theoretically there is only a point contact. Work needs to be done to understand the mechanisms behind internalization of varied shaped particles.

Table 2.2: Nanoparticle Parameters and its effect on *in vivo* circulation and cellular uptake

Parameter	Long circulation	Cell internalization	Delivery to immune cells
Size	50-200nm	50-100nm	~1 μ m
Shape	Rods or long aspect ratio. At least One dimension less than 200nm	Unclear	Spherical shaped
Charge	Neutral to anionic	Positively charged	Positively charged
Elasticity	Highly elastic particle	Unknown	Rigid particles
Material	Hydrophilic, PEGylation	Hydrophobic	Hydrophobic

Research on shapes has mainly concentrated on spheres, rods and discs. More shapes should to be explored in order to discover shape effects and enhance our understanding about how shape can be exploited for different applications. Another consideration that is necessary in all these experiments is to decouple the effect of shape

with size. Comparisons can only be made between 2 different shapes when volume (or dimensions or surface area) is kept constant.

2.8 COMBINATION OF PARAMETERS IN A MULTIVARIATE SPACE: A PERSPECTIVE

Combining the best parameters to make NPs is not straightforward. Changing one parameter can significantly influence particle behavior and requirements for other parameters. NPs cannot have any of their dimensions less than 10 nm to avoid rapid renal clearance and should have at least one dimension less than 200-300 nm to pass through spleen. As we have seen with shape studies that some shapes can allow long circulation even with micron-sized particles, so there needs to be more work done to determine upper limit on all dimensions. For long circulation, neutral or slightly negatively charged particles are considered best, but if these are combined with selective protein adsorption strategies like apolipoproteins E then charge may not be that important. This could potentially be an important area of research if we can understand how serum proteins would interact with NP surface materials and develop strategies to program self-attachment of serum proteins to guide the particles. This could also significantly reduce the cost of particle modification with expensive biomolecules like antibodies and recombinant proteins and instead use body's inherent proteins. Similarly, low modulus elastic particles can allow larger particles to flow through the blood for longer times as they can squeeze through spleen barrier and can avoid uptake by macrophages. However low elasticity and larger size can also affect the uptake by target cells and may not be beneficial. Studies need to be conducted to determine the optimum size and elasticity values. Another question that needs answer is how soft the particles can be. Would decreasing elasticity always correspond to increasing circulation time for fixed size and shape? The answer to this is limited by the synthesis processes as it has been difficult to

synthesize and handle soft particles. However with developments in top-down approach to fabricate NPs, it might be feasible to fabricate softer particles.

As described above, shape is an important parameter that has shown credible room for optimization. Shape can be coupled with multiple ligand targeting as it provides larger surface area and contact with surrounding. Only few shapes like spheres, rods and discs have been studied till now and there is a need to explore newer shapes. These studies need to be coupled and guided by theoretical modeling to better understand, predict and design various shapes for desired application. However all these studies need to be coupled with uptake mechanisms both *in vitro* as well uptake efficiencies *in vivo*. The uptake *in vitro* does not correspond to *in vivo* uptake due to presence of many external factors *in vivo*. Cells used *in vitro* are modified cell lines that are cultured in 2-dimension cultures and does not necessarily behave like cells *in vivo* that are organized in 3-dimensional matrix. Recently spheroids have been proposed as *in vitro* tumor models and are known to closely resemble the architecture, biological properties, and physiological characteristics of human tumor tissue (Friedrich et al., 2009). More studies should be performed on such systems as not only the results obtained will be a close representative of results *in vivo* but also allow studies such as tissue penetration of NPs. Studies should also be done in high serum concentration to mimic the protein milieu present in the body. To evaluate the uptake efficiencies *in vivo*, tumors can be isolated and dissociated into individual cells to facilitate analysis like confocal microscopy and flow cytometry to determine intracellular spatial location and quantitative evaluation.

There is also a need to quantify and model the internalization kinetics so that rather than the widely used hit by trial methods, rationale design can guide NP synthesis. Ideally we should be able to define the criteria mathematically in a multivariate space. For example:

Amount of NP delivery to cell X in tissue Y after time $t = f(x, y, t, \text{Size}) + f(x, y, t, \text{Shape}) + f(x, y, t, \text{elasticity}) + f(x, y, t, \text{charge}) + f(x, y, t, \text{material}) + f(x, y, t, \text{combination effects})$.

This is of course an extremely complicated process and often decoupling of the variables in real life experiments is near impossible. Nevertheless, approaches towards this goal are warranted and would provide new insights and directions in NP research.

2.9 REFERENCES

- Acharya, G., Shin, C. S., McDermott, M., Mishra, H., Park, H., Kwon, I. C., and Park, K. (2010). The hydrogel template method for fabrication of homogeneous nano/microparticles. *J Control Release* *141*, 314-319.
- Agarwal, R., Singh, V., Journey, P., Shi, L., Sreenivasan, S. V., and Roy, K. (2012). Scalable Imprinting of Shape-Specific Polymeric Nanocarriers Using a Release Layer of Switchable Water Solubility. *ACS Nano* *6*, 2524-2531.
- Albanese, A., Tang, P. S., and Chan, W. C. (2012). The effect of nanoparticle size, shape, and surface chemistry on biological systems. *Annu Rev Biomed Eng* *14*, 1-16.
- Arvizo, R. R., Miranda, O. R., Thompson, M. A., Pabelick, C. M., Bhattacharya, R., Robertson, J. D., Rotello, V. M., Prakash, Y. S., and Mukherjee, P. (2010). Effect of nanoparticle surface charge at the plasma membrane and beyond. *Nano Lett* *10*, 2543-2548.
- Ballou, B., Lagerholm, B. C., Ernst, L. A., Bruchez, M. P., and Waggoner, A. S. (2004). Noninvasive imaging of quantum dots in mice. *Bioconjug Chem* *15*, 79-86.
- Banquy, X., Suarez, F., Argaw, A., Rabanel, J.-M., Grutter, P., Bouchard, J.-F., Hildgen, P., and Giasson, S. (2009). Effect of mechanical properties of hydrogel nanoparticles on macrophage cell uptake. *Soft Matter* *5*, 3984-3991.
- Barua, S., Yoo, J. W., Kolhar, P., Wakankar, A., Gokarn, Y. R., and Mitragotri, S. (2013). Particle shape enhances specificity of antibody-displaying nanoparticles. *Proc Natl Acad Sci U S A*.
- Belting, M. (2003). Heparan sulfate proteoglycan as a plasma membrane carrier. *Trends Biochem Sci* *28*, 145-151.

- Bhattacharya, S., Roxbury, D., Gong, X., Mukhopadhyay, D., and Jagota, A. (2012). DNA conjugated SWCNTs enter endothelial cells via Rac1 mediated macropinocytosis. *Nano Lett* *12*, 1826-1830.
- Bhowmick, T., Berk, E., Cui, X., Muzykantov, V. R., and Muro, S. (2012). Effect of flow on endothelial endocytosis of nanocarriers targeted to ICAM-1. *J Control Release* *157*, 485-492.
- Brandenberger, C., Muhlfeld, C., Ali, Z., Lenz, A. G., Schmid, O., Parak, W. J., Gehr, P., and Rothen-Rutishauser, B. (2010). Quantitative evaluation of cellular uptake and trafficking of plain and polyethylene glycol-coated gold nanoparticles. *Small* *6*, 1669-1678.
- Brannon-Peppas, L., and Blanchette, J. O. (2004). Nanoparticle and targeted systems for cancer therapy. *Adv Drug Deliv Rev* *56*, 1649-1659.
- Caldorera-Moore, M., Guimard, N., Shi, L., and Roy, K. (2010). Designer nanoparticles: incorporating size, shape and triggered release into nanoscale drug carriers. *Expert Opin Drug Deliv* *7*, 479-495.
- Callahan, J., and Kopecek, J. (2006). Semitelechelic HPMA copolymers functionalized with triphenylphosphonium as drug carriers for membrane transduction and mitochondrial localization. *Biomacromolecules* *7*, 2347-2356.
- Campbell, R. B., Fukumura, D., Brown, E. B., Mazzola, L. M., Izumi, Y., Jain, R. K., Torchilin, V. P., and Munn, L. L. (2002). Cationic charge determines the distribution of liposomes between the vascular and extravascular compartments of tumors. *Cancer Res* *62*, 6831-6836.
- Canelas, D. A., Herlihy, K. P., and DeSimone, J. M. (2009). Top-down particle fabrication: control of size and shape for diagnostic imaging and drug delivery. *Wiley Interdiscip Rev Nanomed Nanobiotechnol* *1*, 391-404.
- Cedervall, T., Lynch, I., Foy, M., Berggård, T., Donnelly, S. C., Cagney, G., Linse, S., and Dawson, K. A. (2007a). Detailed Identification of Plasma Proteins Adsorbed on Copolymer Nanoparticles. *Angewandte Chemie International Edition* *46*, 5754-5756.
- Cedervall, T., Lynch, I., Lindman, S., Berggard, T., Thulin, E., Nilsson, H., Dawson, K. A., and Linse, S. (2007b). Understanding the nanoparticle-protein corona using methods to quantify exchange rates and affinities of proteins for nanoparticles. *Proc Natl Acad Sci U S A* *104*, 2050-2055.
- Champion, J. A., Katare, Y. K., and Mitragotri, S. (2007). Particle shape: a new design parameter for micro- and nanoscale drug delivery carriers. *J Control Release* *121*, 3-9.
- Champion, J. A., and Mitragotri, S. (2006). Role of target geometry in phagocytosis. *Proc Natl Acad Sci U S A* *103*, 4930-4934.

- Chauhan, V. P., Popovic, Z., Chen, O., Cui, J., Fukumura, D., Bawendi, M. G., and Jain, R. K. (2011). Fluorescent nanorods and nanospheres for real-time in vivo probing of nanoparticle shape-dependent tumor penetration. *Angew Chem Int Ed Engl* *50*, 11417-11420.
- Chen, Y., Wang, S., Lu, X., Zhang, H., Fu, Y., and Luo, Y. (2011). Cholesterol sequestration by nystatin enhances the uptake and activity of endostatin in endothelium via regulating distinct endocytic pathways. *Blood* *117*, 6392-6403.
- Chithrani, B. D., Ghazani, A. A., and Chan, W. C. (2006). Determining the size and shape dependence of gold nanoparticle uptake into mammalian cells. *Nano Lett* *6*, 662-668.
- Choi, H. S., Liu, W., Misra, P., Tanaka, E., Zimmer, J. P., Itty Ipe, B., Bawendi, M. G., and Frangioni, J. V. (2007). Renal clearance of quantum dots. *Nat Biotechnol* *25*, 1165-1170.
- Clark, S. J., Higman, V. A., Mulloy, B., Perkins, S. J., Lea, S. M., Sim, R. B., and Day, A. J. (2006). His-384 allotypic variant of factor H associated with age-related macular degeneration has different heparin binding properties from the non-disease-associated form. *J Biol Chem* *281*, 24713-24720.
- Conner, S. D., and Schmid, S. L. (2003). Regulated portals of entry into the cell. *Nature* *422*, 37-44.
- Davis, M. E., Chen, Z., and Shin, D. M. (2008). Nanoparticle therapeutics: an emerging treatment modality for cancer. *Nat Rev Drug Discov* *7*, 771-782.
- Decuzzi, P., Lee, S., Bhushan, B., and Ferrari, M. (2005). A theoretical model for the margination of particles within blood vessels. *Ann Biomed Eng* *33*, 179-190.
- Desai, N., Trieu, V., Yao, Z., Louie, L., Ci, S., Yang, A., Tao, C., De, T., Beals, B., Dykes, D., *et al.* (2006). Increased antitumor activity, intratumor paclitaxel concentrations, and endothelial cell transport of cremophor-free, albumin-bound paclitaxel, ABI-007, compared with cremophor-based paclitaxel. *Clin Cancer Res* *12*, 1317-1324.
- Discher, D. E., Janmey, P., and Wang, Y. L. (2005). Tissue cells feel and respond to the stiffness of their substrate. *Science* *310*, 1139-1143.
- Doherty, G. J., and McMahon, H. T. (2009). Mechanisms of endocytosis. *Annu Rev Biochem* *78*, 857-902.
- Domański, D. M., Klajnert, B., and Bryszewska, M. (2004). Influence of PAMAM dendrimers on human red blood cells. *Bioelectrochemistry* *63*, 189-191.
- Doshi, N., Zahr, A. S., Bhaskar, S., Lahann, J., and Mitragotri, S. (2009). Red blood cell-mimicking synthetic biomaterial particles. *Proc Natl Acad Sci U S A* *106*, 21495-21499.

- Dykman, L., and Khlebtsov, N. (2012). Gold nanoparticles in biomedical applications: recent advances and perspectives. *Chem Soc Rev* *41*, 2256-2282.
- Eddidin, M. (2001). Shrinking patches and slippery rafts: scales of domains in the plasma membrane. *Trends Cell Biol* *11*, 492-496.
- Evans, C. W., Fitzgerald, M., Clemons, T. D., House, M. J., Padman, B. S., Shaw, J. A., Saunders, M., Harvey, A. R., Zdyrko, B., Luzinov, I., *et al.* (2011). Multimodal analysis of PEI-mediated endocytosis of nanoparticles in neural cells. *ACS Nano* *5*, 8640-8648.
- Ferrari, M. (2005). Cancer nanotechnology: opportunities and challenges. *Nat Rev Cancer* *5*, 161-171.
- Friedrich, J., Seidel, C., Ebner, R., and Kunz-Schughart, L. A. (2009). Spheroid-based drug screen: considerations and practical approach. *Nat Protoc* *4*, 309-324.
- Gaur, U., Sahoo, S. K., De, T. K., Ghosh, P. C., Maitra, A., and Ghosh, P. K. (2000). Biodistribution of fluoresceinated dextran using novel nanoparticles evading reticuloendothelial system. *Int J Pharm* *202*, 1-10.
- Geng, Y., Dalhaimer, P., Cai, S., Tsai, R., Tewari, M., Minko, T., and Discher, D. E. (2007). Shape effects of filaments versus spherical particles in flow and drug delivery. *Nat Nanotechnol* *2*, 249-255.
- Georgieva, J. V., Kalicharan, D., Couraud, P. O., Romero, I. A., Weksler, B., Hoekstra, D., and Zuhorn, I. S. (2011). Surface characteristics of nanoparticles determine their intracellular fate in and processing by human blood-brain barrier endothelial cells in vitro. *Mol Ther* *19*, 318-325.
- Glangchai, L. C., Caldorera-Moore, M., Shi, L., and Roy, K. (2008). Nanoimprint lithography based fabrication of shape-specific, enzymatically-triggered smart nanoparticles. *J Control Release* *125*, 263-272.
- Gratton, S. E., Ropp, P. A., Pohlhaus, P. D., Luft, J. C., Madden, V. J., Napier, M. E., and DeSimone, J. M. (2008). The effect of particle design on cellular internalization pathways. *Proc Natl Acad Sci U S A* *105*, 11613-11618.
- Hamad, I., Al-Hanbali, O., Hunter, A. C., Rutt, K. J., Andresen, T. L., and Moghimi, S. M. (2010). Distinct polymer architecture mediates switching of complement activation pathways at the nanosphere-serum interface: implications for stealth nanoparticle engineering. *ACS Nano* *4*, 6629-6638.
- Hamidi, M., Azadi, A., and Rafiei, P. (2008). Hydrogel nanoparticles in drug delivery. *Advanced Drug Delivery Reviews* *60*, 1638-1649.
- Han, J., Zern, B. J., Shuvaev, V. V., Davies, P. F., Muro, S., and Muzykantov, V. (2012). Acute and chronic shear stress differently regulate endothelial internalization of nanocarriers targeted to platelet-endothelial cell adhesion molecule-1. *ACS Nano* *6*, 8824-8836.

- Harush-Frenkel, O., Debotton, N., Benita, S., and Altschuler, Y. (2007). Targeting of nanoparticles to the clathrin-mediated endocytic pathway. *Biochem Biophys Res Commun* 353, 26-32.
- Harush-Frenkel, O., Rozentur, E., Benita, S., and Altschuler, Y. (2008). Surface charge of nanoparticles determines their endocytic and transcytotic pathway in polarized MDCK cells. *Biomacromolecules* 9, 435-443.
- Hatakeyama, H., Akita, H., Kogure, K., Oishi, M., Nagasaki, Y., Kihira, Y., Ueno, M., Kobayashi, H., Kikuchi, H., and Harashima, H. (2007). Development of a novel systemic gene delivery system for cancer therapy with a tumor-specific cleavable PEG-lipid. *Gene Ther* 14, 68-77.
- Hawkins, M. J., Soon-Shiong, P., and Desai, N. (2008). Protein nanoparticles as drug carriers in clinical medicine. *Adv Drug Deliv Rev* 60, 876-885.
- He, C., Hu, Y., Yin, L., Tang, C., and Yin, C. (2010). Effects of particle size and surface charge on cellular uptake and biodistribution of polymeric nanoparticles. *Biomaterials* 31, 3657-3666.
- Henson, P. M., Bratton, D. L., and Fadok, V. A. (2001). Apoptotic cell removal. *Curr Biol* 11, R795-805.
- Hobbs, S. K., Monsky, W. L., Yuan, F., Roberts, W. G., Griffith, L., Torchilin, V. P., and Jain, R. K. (1998). Regulation of transport pathways in tumor vessels: role of tumor type and microenvironment. *Proc Natl Acad Sci U S A* 95, 4607-4612.
- Hoffmann, P. R., deCathelineau, A. M., Ogden, C. A., Leverrier, Y., Bratton, D. L., Daleke, D. L., Ridley, A. J., Fadok, V. A., and Henson, P. M. (2001). Phosphatidylserine (PS) induces PS receptor-mediated macropinocytosis and promotes clearance of apoptotic cells. *J Cell Biol* 155, 649-659.
- Huang, X., Teng, X., Chen, D., Tang, F., and He, J. (2010). The effect of the shape of mesoporous silica nanoparticles on cellular uptake and cell function. *Biomaterials* 31, 438-448.
- Huth, U. S., Schubert, R., and Peschka-Suss, R. (2006). Investigating the uptake and intracellular fate of pH-sensitive liposomes by flow cytometry and spectral bio-imaging. *J Control Release* 110, 490-504.
- Ilium, L., Davis, S. S., Wilson, C. G., Thomas, N. W., Frier, M., and Hardy, J. G. (1982). Blood clearance and organ deposition of intravenously administered colloidal particles. The effects of particle size, nature and shape. *International Journal of Pharmaceutics* 12, 135-146.
- Ishida, T., and Kiwada, H. (2008). Accelerated blood clearance (ABC) phenomenon upon repeated injection of PEGylated liposomes. *Int J Pharm* 354, 56-62.

- Ishida, T., Wang, X., Shimizu, T., Nawata, K., and Kiwada, H. (2007). PEGylated liposomes elicit an anti-PEG IgM response in a T cell-independent manner. *J Control Release* *122*, 349-355.
- Ivanov, A. I. (2008). Pharmacological inhibition of endocytic pathways: is it specific enough to be useful? *Methods Mol Biol* *440*, 15-33.
- Jain, R. K., and Stylianopoulos, T. (2010). Delivering nanomedicine to solid tumors. *Nat Rev Clin Oncol* *7*, 653-664.
- Jenssen, H., Hamill, P., and Hancock, R. E. (2006). Peptide antimicrobial agents. *Clin Microbiol Rev* *19*, 491-511.
- Jiang, X., Qu, W., Pan, D., Ren, Y., Williford, J. M., Cui, H., Luijten, E., and Mao, H. Q. (2012). Plasmid-Templated Shape Control of Condensed DNA-Block Copolymer Nanoparticles. *Adv Mater*.
- Kang, Y. H., Tan, L. A., Carroll, M. V., Gentle, M. E., and Sim, R. B. (2009). Target pattern recognition by complement proteins of the classical and alternative pathways. *Adv Exp Med Biol* *653*, 117-128.
- Kim, B., Han, G., Toley, B. J., Kim, C. K., Rotello, V. M., and Forbes, N. S. (2010). Tuning payload delivery in tumour cylindroids using gold nanoparticles. *Nat Nanotechnol* *5*, 465-472.
- Kim, H. R., Andrieux, K., Gil, S., Taverna, M., Chacun, H., Desmaële, D., Taran, F., Georgin, D., and Couvreur, P. (2007). Translocation of Poly(ethylene glycol-co-hexadecyl)cyanoacrylate Nanoparticles into Rat Brain Endothelial Cells: Role of Apolipoproteins in Receptor-Mediated Endocytosis. *Biomacromolecules* *8*, 793-799.
- Kim, K. J., and Malik, A. B. (2003). Protein transport across the lung epithelial barrier. *Am J Physiol Lung Cell Mol Physiol* *284*, L247-259.
- Klein, J. (2007). Probing the interactions of proteins and nanoparticles. *Proc Natl Acad Sci U S A* *104*, 2029-2030.
- Korfee, S., Gauler, T., Hepp, R., Pottgen, C., and Eberhardt, W. (2004). New targeted treatments in lung cancer--overview of clinical trials. *Lung Cancer* *45 Suppl 2*, S199-208.
- Korn, E. D., and Weisman, R. A. (1967). Phagocytosis of latex beads by *Acanthamoeba*. II. Electron microscopic study of the initial events. *J Cell Biol* *34*, 219-227.
- Lee, K. J., Yoon, J., Rahmani, S., Hwang, S., Bhaskar, S., Mitragotri, S., and Lahann, J. (2012). Spontaneous shape reconfigurations in multicompartamental microcylinders. *Proc Natl Acad Sci U S A* *109*, 16057-16062.

- Lesniak, A., Salvati, A., Santos-Martinez, M. J., Radomski, M. W., Dawson, K. A., and Aberg, C. (2013). Nanoparticle adhesion to the cell membrane and its effect on nanoparticle uptake efficiency. *J Am Chem Soc* *135*, 1438-1444.
- Li, Y., Chen, X., and Gu, N. (2008). Computational investigation of interaction between nanoparticles and membranes: hydrophobic/hydrophilic effect. *J Phys Chem B* *112*, 16647-16653.
- Liao, H., Nehl, C. L., and Hafner, J. H. (2006). Biomedical applications of plasmon resonant metal nanoparticles. *Nanomedicine (Lond)* *1*, 201-208.
- Lin, C., and Engbersen, J. F. (2008). Effect of chemical functionalities in poly(amido amine)s for non-viral gene transfection. *J Control Release* *132*, 267-272.
- Lison, D., Thomassen, L. C., Rabolli, V., Gonzalez, L., Napierska, D., Seo, J. W., Kirsch-Volders, M., Hoet, P., Kirschhock, C. E., and Martens, J. A. (2008). Nominal and effective dosimetry of silica nanoparticles in cytotoxicity assays. *Toxicol Sci* *104*, 155-162.
- Liu, Y., Tan, J., Thomas, A., Ou-Yang, D., and Muzykantov, V. R. (2012). The shape of things to come: importance of design in nanotechnology for drug delivery. *Ther Deliv* *3*, 181-194.
- Longmire, M., Choyke, P. L., and Kobayashi, H. (2008). Clearance properties of nano-sized particles and molecules as imaging agents: considerations and caveats. *Nanomedicine (Lond)* *3*, 703-717.
- Lu, F., Wu, S. H., Hung, Y., and Mou, C. Y. (2009). Size effect on cell uptake in well-suspended, uniform mesoporous silica nanoparticles. *Small* *5*, 1408-1413.
- Lynch, I., and Dawson, K. A. (2008). Protein-nanoparticle interactions. *Nano Today* *3*, 40-47.
- Lynch, I., Salvati, A., and Dawson, K. A. (2009). Protein-nanoparticle interactions: What does the cell see? *Nat Nanotechnol* *4*, 546-547.
- Malik, N., Wiwattanapatapee, R., Klopsch, R., Lorenz, K., Frey, H., Weener, J. W., Meijer, E. W., Paulus, W., and Duncan, R. (2000). Dendrimers:: Relationship between structure and biocompatibility in vitro, and preliminary studies on the biodistribution of 125I-labelled polyamidoamine dendrimers in vivo. *Journal of Controlled Release* *65*, 133-148.
- Masson, C., Garinot, M., Mignet, N., Wetzter, B., Mailhe, P., Scherman, D., and Bessodes, M. (2004). pH-sensitive PEG lipids containing orthoester linkers: new potential tools for nonviral gene delivery. *J Control Release* *99*, 423-434.
- Mayor, S., and Pagano, R. E. (2007). Pathways of clathrin-independent endocytosis. *Nat Rev Mol Cell Biol* *8*, 603-612.

- Merkel, T. J., Chen, K., Jones, S. W., Pandya, A. A., Tian, S., Napier, M. E., Zamboni, W. E., and Desimone, J. M. (2012). The effect of particle size on the biodistribution of low-modulus hydrogel PRINT particles. *J Control Release*.
- Merkel, T. J., Jones, S. W., Herlihy, K. P., Kersey, F. R., Shields, A. R., Napier, M., Luft, J. C., Wu, H., Zamboni, W. C., Wang, A. Z., *et al.* (2011). Using mechanobiological mimicry of red blood cells to extend circulation times of hydrogel microparticles. *Proc Natl Acad Sci U S A* *108*, 586-591.
- Mettlen, M., Loerke, D., Yarar, D., Danuser, G., and Schmid, S. L. (2010). Cargo- and adaptor-specific mechanisms regulate clathrin-mediated endocytosis. *J Cell Biol* *188*, 919-933.
- Michaelis, K., Hoffmann, M. M., Dreis, S., Herbert, E., Alyautdin, R. N., Michaelis, M., Kreuter, J., and Langer, K. (2006). Covalent linkage of apolipoprotein e to albumin nanoparticles strongly enhances drug transport into the brain. *J Pharmacol Exp Ther* *317*, 1246-1253.
- Moghimi, S. M. (1995). Mechanisms of splenic clearance of blood cells and particles: towards development of new splenotropic agents. *Advanced Drug Delivery Reviews* *17*, 103-115.
- Mosqueira, V. C., Legrand, P., Morgat, J. L., Vert, M., Mysiakine, E., Gref, R., Devissaguet, J. P., and Barratt, G. (2001). Biodistribution of long-circulating PEG-grafted nanocapsules in mice: effects of PEG chain length and density. *Pharm Res* *18*, 1411-1419.
- Mundy, D. I., Li, W. P., Luby-Phelps, K., and Anderson, R. G. (2012). Caveolin targeting to late endosome/lysosomal membranes is induced by perturbations of lysosomal pH and cholesterol content. *Mol Biol Cell* *23*, 864-880.
- Nel, A., Xia, T., Madler, L., and Li, N. (2006). Toxic potential of materials at the nanolevel. *Science* *311*, 622-627.
- Oh, E., Delehanty, J. B., Sapsford, K. E., Susumu, K., Goswami, R., Blanco-Canosa, J. B., Dawson, P. E., Granek, J., Shoff, M., Zhang, Q., *et al.* (2011). Cellular uptake and fate of PEGylated gold nanoparticles is dependent on both cell-penetration peptides and particle size. *ACS Nano* *5*, 6434-6448.
- Oldenborg, P. A., Gresham, H. D., Chen, Y., Izui, S., and Lindberg, F. P. (2002). Lethal autoimmune hemolytic anemia in CD47-deficient nonobese diabetic (NOD) mice. *Blood* *99*, 3500-3504.
- Osaki, F., Kanamori, T., Sando, S., Sera, T., and Aoyama, Y. (2004). A quantum dot conjugated sugar ball and its cellular uptake. On the size effects of endocytosis in the subviral region. *J Am Chem Soc* *126*, 6520-6521.
- Panyam, J., and Labhasetwar, V. (2003). Biodegradable nanoparticles for drug and gene delivery to cells and tissue. *Advanced Drug Delivery Reviews* *55*, 329-347.

- Parton, R. G., and Simons, K. (2007). The multiple faces of caveolae. *Nat Rev Mol Cell Biol* 8, 185-194.
- Peer, D., Karp, J. M., Hong, S., Farokhzad, O. C., Margalit, R., and Langer, R. (2007). Nanocarriers as an emerging platform for cancer therapy. *Nat Nano* 2, 751-760.
- Peiris, P. M., Bauer, L., Toy, R., Tran, E., Pansky, J., Doolittle, E., Schmidt, E., Hayden, E., Mayer, A., Keri, R. A., *et al.* (2012). Enhanced delivery of chemotherapy to tumors using a multicomponent nanochain with radio-frequency-tunable drug release. *ACS Nano* 6, 4157-4168.
- Peppas, N. A. (2004). Intelligent therapeutics: biomimetic systems and nanotechnology in drug delivery. *Advanced Drug Delivery Reviews* 56, 1529-1531.
- Perrault, S. D., Walkey, C., Jennings, T., Fischer, H. C., and Chan, W. C. (2009). Mediating tumor targeting efficiency of nanoparticles through design. *Nano Lett* 9, 1909-1915.
- Perumal, O. P., Inapagolla, R., Kannan, S., and Kannan, R. M. (2008). The effect of surface functionality on cellular trafficking of dendrimers. *Biomaterials* 29, 3469-3476.
- Petros, R. A., and DeSimone, J. M. (2010). Strategies in the design of nanoparticles for therapeutic applications. *Nat Rev Drug Discov* 9, 615-627.
- Rejman, J., Bragonzi, A., and Conese, M. (2005). Role of clathrin- and caveolae-mediated endocytosis in gene transfer mediated by lipo- and polyplexes. *Mol Ther* 12, 468-474.
- Rejman, J., Conese, M., and Hoekstra, D. (2006). Gene transfer by means of lipo- and polyplexes: role of clathrin and caveolae-mediated endocytosis. *J Liposome Res* 16, 237-247.
- Rejman, J., Oberle, V., Zuhorn, I. S., and Hoekstra, D. (2004). Size-dependent internalization of particles via the pathways of clathrin- and caveolae-mediated endocytosis. *Biochem J* 377, 159-169.
- Rolland, J. P., Maynor, B. W., Euliss, L. E., Exner, A. E., Denison, G. M., and DeSimone, J. M. (2005). Direct fabrication and harvesting of monodisperse, shape-specific nanobiomaterials. *J Am Chem Soc* 127, 10096-10100.
- Rudolph, C., Plank, C., Lausier, J., Schillinger, U., Muller, R. H., and Rosenecker, J. (2003). Oligomers of the arginine-rich motif of the HIV-1 TAT protein are capable of transferring plasmid DNA into cells. *J Biol Chem* 278, 11411-11418.
- Sahay, G., Alakhova, D. Y., and Kabanov, A. V. (2010a). Endocytosis of nanomedicines. *J Control Release* 145, 182-195.

- Sahay, G., Kim, J. O., Kabanov, A. V., and Bronich, T. K. (2010b). The exploitation of differential endocytic pathways in normal and tumor cells in the selective targeting of nanoparticulate chemotherapeutic agents. *Biomaterials* *31*, 923-933.
- Sandgren, K. J., Wilkinson, J., Miranda-Saksena, M., McInerney, G. M., Byth-Wilson, K., Robinson, P. J., and Cunningham, A. L. (2010). A differential role for macropinocytosis in mediating entry of the two forms of vaccinia virus into dendritic cells. *PLoS Pathog* *6*, e1000866.
- Schafer, V., von Briesen, H., Andreesen, R., Steffan, A. M., Royer, C., Troster, S., Kreuter, J., and Rubsamen-Waigmann, H. (1992). Phagocytosis of nanoparticles by human immunodeficiency virus (HIV)-infected macrophages: a possibility for antiviral drug targeting. *Pharm Res* *9*, 541-546.
- Schneider, M. C., Prosser, B. E., Caesar, J. J., Kugelberg, E., Li, S., Zhang, Q., Quoraishi, S., Lovett, J. E., Deane, J. E., Sim, R. B., *et al.* (2009). *Neisseria meningitidis* recruits factor H using protein mimicry of host carbohydrates. *Nature* *458*, 890-893.
- Shah, S., Liu, Y., Hu, W., and Gao, J. (2011). Modeling particle shape-dependent dynamics in nanomedicine. *J Nanosci Nanotechnol* *11*, 919-928.
- Shin, J., Shum, P., and Thompson, D. H. (2003). Acid-triggered release via dePEGylation of DOPE liposomes containing acid-labile vinyl ether PEG-lipids. *J Control Release* *91*, 187-200.
- Shuvaev, V. V., Tliba, S., Pick, J., Arguiri, E., Christofidou-Solomidou, M., Albelda, S. M., and Muzykantov, V. R. (2011). Modulation of endothelial targeting by size of antibody-antioxidant enzyme conjugates. *J Control Release* *149*, 236-241.
- Simone, E. A., Dziubla, T. D., and Muzykantov, V. R. (2008). Polymeric carriers: role of geometry in drug delivery. *Expert Opin Drug Deliv* *5*, 1283-1300.
- Smith, B. R., Kempen, P., Bouley, D., Xu, A., Liu, Z., Melosh, N., Dai, H., Sinclair, R., and Gambhir, S. S. (2012). Shape matters: intravital microscopy reveals surprising geometrical dependence for nanoparticles in tumor models of extravasation. *Nano Lett* *12*, 3369-3377.
- Stylianopoulos, T., Soteriou, K., Fukumura, D., and Jain, R. K. (2013). Cationic nanoparticles have superior transvascular flux into solid tumors: insights from a mathematical model. *Ann Biomed Eng* *41*, 68-77.
- Tao, L., Hu, W., Liu, Y., Huang, G., Sumer, B. D., and Gao, J. Shape-specific polymeric nanomedicine: emerging opportunities and challenges. *Exp Biol Med (Maywood)* *236*, 20-29.
- Tasciotti, E., Liu, X., Bhavane, R., Plant, K., Leonard, A. D., Price, B. K., Cheng, M. M., Decuzzi, P., Tour, J. M., Robertson, F., and Ferrari, M. (2008). Mesoporous

- silicon particles as a multistage delivery system for imaging and therapeutic applications. *Nat Nanotechnol* 3, 151-157.
- Teeguarden, J. G., Hinderliter, P. M., Orr, G., Thrall, B. D., and Pounds, J. G. (2007). Particokinetics in vitro: dosimetry considerations for in vitro nanoparticle toxicity assessments. *Toxicol Sci* 95, 300-312.
- Thomsen, T., Schlosser, A., Holmskov, U., and Sorensen, G. L. (2011). Ficolins and FIBCD1: soluble and membrane bound pattern recognition molecules with acetyl group selectivity. *Mol Immunol* 48, 369-381.
- Thorek, D. L., and Tsourkas, A. (2008). Size, charge and concentration dependent uptake of iron oxide particles by non-phagocytic cells. *Biomaterials* 29, 3583-3590.
- Toy, R., Hayden, E., Shoup, C., Baskaran, H., and Karathanasis, E. (2011). The effects of particle size, density and shape on margination of nanoparticles in microcirculation. *Nanotechnology* 22, 115101.
- Tsai, R. K., and Discher, D. E. (2008). Inhibition of "self" engulfment through deactivation of myosin-II at the phagocytic synapse between human cells. *J Cell Biol* 180, 989-1003.
- Unezaki, S., Maruyama, K., Hosoda, J.-I., Nagae, I., Koyanagi, Y., Nakata, M., Ishida, O., Iwatsuru, M., and Tsuchiya, S. (1996). Direct measurement of the extravasation of polyethyleneglycol-coated liposomes into solid tumor tissue by in vivo fluorescence microscopy. *International Journal of Pharmaceutics* 144, 11-17.
- van de Ven, A. L., Kim, P., Haley, O., Fakhoury, J. R., Adriani, G., Schmulen, J., Moloney, P., Hussain, F., Ferrari, M., Liu, X., *et al.* (2012). Rapid tumorotropic accumulation of systemically injected plateloid particles and their biodistribution. *J Control Release* 158, 148-155.
- Wallis, R., Mitchell, D. A., Schmid, R., Schwaeble, W. J., and Keeble, A. H. (2010). Paths reunited: Initiation of the classical and lectin pathways of complement activation. *Immunobiology* 215, 1-11.
- Wang, B., Zhang, L., Bae, S. C., and Granick, S. (2008). Nanoparticle-induced surface reconstruction of phospholipid membranes. *Proc Natl Acad Sci U S A* 105, 18171-18175.
- Wang, X., Ishida, T., and Kiwada, H. (2007). Anti-PEG IgM elicited by injection of liposomes is involved in the enhanced blood clearance of a subsequent dose of PEGylated liposomes. *J Control Release* 119, 236-244.
- Yang, K., and Ma, Y. Q. (2010). Computer simulation of the translocation of nanoparticles with different shapes across a lipid bilayer. *Nat Nanotechnol* 5, 579-583.

- Yi, X., Shi, X., and Gao, H. (2011). Cellular uptake of elastic nanoparticles. *Phys Rev Lett* *107*, 098101.
- Yoo, J. W., Chambers, E., and Mitragotri, S. (2010). Factors that control the circulation time of nanoparticles in blood: challenges, solutions and future prospects. *Curr Pharm Des* *16*, 2298-2307.
- Yoo, J. W., Doshi, N., and Mitragotri, S. (2011a). Adaptive micro and nanoparticles: temporal control over carrier properties to facilitate drug delivery. *Adv Drug Deliv Rev* *63*, 1247-1256.
- Yoo, J. W., Irvine, D. J., Discher, D. E., and Mitragotri, S. (2011b). Bio-inspired, bioengineered and biomimetic drug delivery carriers. *Nat Rev Drug Discov* *10*, 521-535.
- Yoo, J. W., and Mitragotri, S. (2010). Polymer particles that switch shape in response to a stimulus. *Proc Natl Acad Sci U S A* *107*, 11205-11210.
- Yuan, F., Dellian, M., Fukumura, D., Leunig, M., Berk, D. A., Torchilin, V. P., and Jain, R. K. (1995). Vascular permeability in a human tumor xenograft: molecular size dependence and cutoff size. *Cancer Res* *55*, 3752-3756.
- Zhang, L. W., and Monteiro-Riviere, N. A. (2009). Mechanisms of quantum dot nanoparticle cellular uptake. *Toxicol Sci* *110*, 138-155.
- Zhu, L., Kate, P., and Torchilin, V. P. (2012). Matrix metalloprotease 2-responsive multifunctional liposomal nanocarrier for enhanced tumor targeting. *ACS Nano* *6*, 3491-3498.

Chapter 3: Scalable Imprinting of Shape-specific Polymeric Nanocarriers

3.1 INTRODUCTION

In recent years, nanoparticles have been widely investigated for delivering various biomolecules and drugs for both diagnostic and therapeutic purposes (Davis et al., 2008; Ferrari, 2005; Hamidi et al., 2008; Panyam and Labhasetwar, 2003; Peppas, 2004). Due to their small size, nanoparticles could deliver drugs and imaging agents intracellularly and also penetrate through the narrow gaps between the endothelial cells of blood vessels at tumor sites (Enhanced Permeation and Retention, (EPR) effect), thereby allowing efficient, tumor-targeted delivery (Jain and Stylianopoulos, 2010). It has been previously shown that particle size is critical for successful delivery of drugs to cells both *in vitro* as well as *in vivo* (Chithrani et al., 2006b; Rejman et al., 2004a; Wen et al., 2008). Recently, the effect of shape has also been found to play a major role (Chithrani and Chan, 2007; Decuzzi et al., 2009; Geng et al., 2007; Gratton et al., 2007; Huang et al., 2011; Huang et al., 2010; Mitragotri, 2009). Most natural structures including red blood cells, viruses and bacteria that circulate and infect human body are non-spherical. This motivates a study of the effect of particle geometry in cellular uptake, biodistribution and retention of nanoparticles in the body. Theoretical studies have predicted that both size and shape could play an important role on particle margination dynamics in blood vessels (Decuzzi et al., 2009). Geng *et al.* showed that filomicelles (cylindrically shaped micelles) up to 20 μm long and 50 nm in diameter were able to persist in circulation for more than a week while nanoscale spherical particles were eliminated quickly (Geng et al., 2007). Champion *et al.* showed that internalization of microparticles by macrophages was dependent on local shape of the particles (Champion and Mitragotri, 2006). Elliptical particles attached to macrophages at the pointed end were shown to be internalized in

minutes while the particles attached at the flat surface took over 12 hours for complete internalization. Despite these advances in synthesizing nanoscale and biocompatible carriers, one major drawback of these existing methods is the scale-up capability of nanoparticle production. In order to systematically study the effect of nanoscale geometry on cellular uptake, *in vivo* biodistribution and drug delivery, it is critical to develop high-throughput fabrication methods that allow large-scale production of nanoparticles.

Although a number of works have shown successful fabrication of soft polymeric particles of different shapes, only a few methods have been reported that succeed in fabricating shape and size specific, sub-200 nm particles (Buyukserin et al., 2009; Caldorera-Moore et al., 2011; Canelas et al., 2009; Glangchai et al., 2008; Gratton et al., 2007; Roy et al., 2007). Such particles are required to effectively reach tumor sites through the EPR effect by passing through leaky endothelial fenestrations as well as for efficient uptake by non-phagocytic target cells (Schädlich et al., 2011). The fabrication processes generally involves stamping out (imprinting) polymeric particles using a mold to give the required shape and size. After the nanoparticles are formed, they need to be removed from the imprint substrate (harvesting) into a bio-compatible liquid. Gratton *et al.* reported physically scraping of the particles from the substrate by moving an acetone drop over the molded pattern with a glass slide (Gratton et al., 2007). Such a physical process may damage and alter the shape of the soft polymeric particles and could be difficult to scale up. Enlow *et al.* described a modified particle harvesting process by attaching the molded pattern with an excipient layer and reheating the assembly, thereby causing the polymeric particles to melt at the contact and transfer to the excipient layer which can then be dissolved to harvest particles (Enlow et al., 2011). Merkel *et al.* also reported an improved method to harvest particles from molded patterns by placing the mold over 0.1% Poly (Vinyl Alcohol) (PVA) solution in water and then cooling the

assembly in a -80°C cooler causing the particles to get trapped in the resulting ice layer. The mold is then peeled away leaving the particles embedded in ice (Merkel et al., 2011). In a different work, Buyukserin *et al.* have used Poly (Methyl Methacrylate) (PMMA) as a sacrificial layer that was later dissolved using acetone to harvest SU-8 (an epoxy based photoresist) particles (Buyukserin et al., 2009). However, exposure of biological drugs and polymeric drug carriers to acetone and other non-biocompatible chemicals are a cause of concern in drug delivery applications. To address these issues, Glangchai *et al.* reported a nanoimprint lithography process that used a water-soluble PVA release layer for fabricating sub-100 nm, shape-specific hydrogel particles (Glangchai et al., 2008; Roy et al., 2007). Although this process was completely water based, dispensing of the water-based imprint solution of Poly (Ethylene Glycol Di-acrylate) (PEGDA) can result in local dissolution of the water-soluble PVA sacrificial layer, resulting in low adhesion force between the sacrificial layer (PVA) and the cured resist (PEGDA). This causes peel off of the cured resist onto the template resulting in template contamination and hence preventing continuous, large-scale imprinting. In addition, higher molecular weight PEGDA (700 Da) used in these earlier studies was more viscous and required dispensing at higher volumes to ensure uniform spreading and resulting in thicker residual layers (thus needing a longer etching step) as well as limited shape retention when imprinting vertical, high-aspect ratio, sub-100 nm particles.

Previously, Linder *et al.* reported that Poly (Acrylic Acid) (PAA) can be used as a water soluble sacrificial layer in surface micromachining (Linder et al., 2005). The group also showed that solubility of thin layers of PAA can be chemically controlled by varying the ion concentration. Here, we report a large-scale imprinting (whole wafer scale imprinting yielding approximately 2.5×10^{11} particles of 100nm diameter and 80nm height per 8 inch silicon wafer) and particle-harvesting method based on a sacrificial PAA

release layer with switchable water solubility *i.e.* the water solubility of the sacrificial layer changes depending on the presence of divalent cations. Specifically, the PAA layer becomes insoluble in water in the presence of Ca^{2+} ions, while removal of calcium “switches” it to a soluble layer. This allows for continuous imprinting and efficient, one-step aqueous-based release of nanoparticles. The PAA release layer is compatible with both aqueous and organic solvent-based imprinting. The use of this switchable sacrificial layer also enables us to readily modify imprinted particles in both aqueous and organic solvents prior to particle harvesting. In addition, sub-10 nm residual layer thickness was achieved through the use of a low molecular weight, low viscosity PEGDA. This also resulted in improved shape replication of imprinted particles. This versatile, switchable layer-based imprinting provides a robust method for large-scale fabrication of shape-specific nanoparticles, both for fundamental studies on shape-effects for nanoscale particle transport as well as for applied studies on the effects of particle geometry on drug and contrast agent delivery.

3.2 MATERIALS AND METHODS

3.2.1 Materials and Reagents

Poly (Ethylene Glycol) diacrylate (PEGDA, Mw 200 and 400) was purchased from Sartomer, Exton, PA. The ultraviolet (UV) photoinitiator, 2-hydroxy-1-[4-(hydroxyethoxy) phenyl]-2-methyl-1 propanone (I2959) was purchased from Ciba, Basel, Switzerland. Fluorescein-o-acrylate monomer (97%), Poly (Vinyl Alcohol) (PVA, Mw 31 000) (Fluka), and dimethyl sulfoxide (DMSO) were purchased from Sigma Aldrich, St. Louis, MO. PAA Sodium salt, Mw 60 000 was purchased from Polysciences, Warrington, PA. Contact angle measurements were done using a Kruss - Drop Shape

analysis System DSA 10 Mk2. Scanning Electron Microscopy (SEM) was done on a Zeiss Supra 40VP SEM model and fluorescence microscopy was done on a Zeiss Axiovert 200M.

3.2.2 Imprinting Solution

Two types (i.e. water and DMSO based) of imprinting solution were prepared. 50% w/v Poly Ethylene Glycol Di-acrylate (Mw: 400 Da) was mixed with de-ionized water or Poly Ethylene Glycol Di-acrylate (Mw: 200 Da) was mixed with DMSO and a 0.07% w/v final concentration I2959 as photoinitiator. To allow fluorescence microscopy, 2% fluorescein -o-Acrylate was dissolved in the water based solution with help of 15% v/v DMSO or upto 16% fluorescein -o-Acrylate for DMSO based solution.

3.2.3 Release Layer

Many different chemicals at different concentrations were tried as potential release layer materials followed by imprinting tests over successful spin-coating over the wafers. Briefly, about 5mL of each solution was spincoated on an 8" Silicon wafer at 3000 rpm for 1 minute and the wafer was then baked on a hot plate at 160°C for 1 minute. Imprinting was done as described in section 3.2.5.

3.2.4 PAA Release Layer

A diluted 2% w/v PAA solution was prepared in water. About 5mL of this PAA solution was spincoated on an 8" Silicon wafer at 3000 rpm for 40 seconds and the wafer was then baked on a hot plate at 160°C for 1 minute. To make this layer suitable for water based imprinting, the wafer was submerged in a 0.5M CaCl₂ solution in water for 5 minutes, washed with 50mM CaCl₂ solution and finally washed with deionized water. The wafer was spun at 3000 rpm and baked again at 160°C for 1 minute to remove any remaining residual water.

3.2.5 Imprinting Parameters

Nanoimprinting was carried out using the J-FIL process on an Imprio 100, Molecular Imprints Inc., Austin, TX.(L. C. Glangchai et al., 2008) In the J-FIL process, a pre-patterned transparent quartz template was pressed onto resist droplets inkjetted on silicon wafers pre-coated with PAA release layer, causing it to spread, and fill the features in the quartz mold. The resist was then exposed to UV light (at 365nm wavelength at 5 mW/cm² intensity), for 25 seconds to photopolymerize the molded resist. The template was then removed revealing the desired nanostructures. The imprints were sputter coated with 3 nm of platinum layer to make them conductive and residual layer was measured using cross-sectional SEM. A low power (35 Watts) Argon plasma etch (Oxford Instruments Plasma Lab 80+) was performed at a pressure of 10 mTorr with Ar (20 sccm) and O₂ (4 sccm) yielding an etch rate of 0.6nm/sec.

3.2.6 Release and Imaging of Nanoparticles

Imprints were washed twice with DMSO after etching on the wafer to remove any unreacted polymer. Imprints were submerged in DMSO, incubated for 5 minutes and blow dried with Nitrogen. To release the particles, 50μl of de-ionized water was added per 5mmx5mm imprint area and incubated for 1 minute to dissolve the underlying PAA layer. The water containing nanoparticles was dialyzed for 2 days using 20K MWCO Slide-A-Lyzer Mini Dialysis devices (Pierce Inc.).

For SEM, 3μl of nanoparticle suspension was dispensed on a SEM stub, air dried and sputter coated with 3nm of Platinum layer to make the sample conductive. For fluorescence microscopy, 3μl of nanoparticle suspension was dispensed on a glass slide and covered with a glass cover slip. Fluorescence imaging was done at 100X magnification objective by exciting the sample using a 488nm wavelength laser.

3.2.7 In vitro Cytotoxicity

HeLa cells were used for *in vitro* cytotoxicity assay of the fabricated PEGDA nanocarriers using an MTS assay (CellTiter 96 AQueous One Solution Cell Proliferation Assay, Promega). 10,000 cells were plated overnight in a 96 well plate. Assays were performed by adding the MTS reagent solution to culture wells and recording the absorbance (at 490nm) at after particle incubation of 4, 24 and 48 hours. A ratio of 10^5 nanocarriers per cell was used. All the experiments were done in groups of 6.

3.2.8 Doxorubicin release kinetics

Imprinting resist was made with 55% PEGDA solution in DMSO containing 50 μ g/ml of Doxorubicin and imprinted on a PAA sacrificial layer to form cylindrical features with 325nm diameter and 100nm height. These cylindrical, doxorubicin containing nanoparticles were released in water and dialyzed over 72 hours using 20K MWCO Slide-A-Lyzer Mini Dialysis devices (Pierce Inc.). Fluorescence measurements of the particle solution were taken at different time intervals using a plate reader (Biotek, Synergy) and normalized against the initial reading to calculate percent drug released from the particles over time. Fluorescence microscopy images were also taken at different time intervals using a 100X magnification objective.

3.2.9 Encapsulation of fluorescent molecules

To encapsulate molecules in the nanoparticles, chemicals were added to imprinting solution prior to imprinting. Texas Red (1.66mg/ml final concentration), Texas Red conjugated to 10KDa Dextran (1.66mg/ml final concentration), Rhodamine Acrylate (20mg/ml final concentration) and Alexa Fluor 647 (0.16mg/ml final concentration) were added to separate 50% w/w PEGDA imprinting solutions and imprinting was carried out as described in section 3.2.5. Particles were then visualized

under fluorescence microscope as described in section 3.2.6. For all particles imaging was done at an excitation wavelength of 570nm.

3.3 RESULTS AND DISCUSSION

3.3.1 Imprint with a PVA Release Layer

We first examined the imprint results with the use of a PVA release layer. Imprint of water-based PEGDA solution on PVA was found to be initially uniform. However, the quality of imprints deteriorated during scale up with increasing number of imprints. Figure 3.1(a) shows a zoomed out scanning electron microscopy (SEM) image of the third PEGDA imprints on a PVA release layer with the use of water-based imprint solution. Both the SEM and the fluorescence images in Fig 3.1 (b) and (c) show non-uniform surface features. The high-resolution SEM images of Fig. 3.1 (d), (e) and (f) further reveal that some areas of the imprints were peeled off from the substrate, deformed or folded. When Di-Methyl Sulfo-Oxide (DMSO) based imprint solution was used, even the first imprint was not uniform due to fast dissolution of PVA in DMSO (data not shown).

It is known that wetting and adhesion of the imprint solution on the substrate and template surfaces influence imprint quality. Template filling by the imprint solution depends on the contact angles of the imprint solution on the substrate and the template surfaces (Kim et al., 2008; Sreenivasan, 2010). If the template surface is made highly non-wetting to improve release performance, it will cause partial filling of the features on the template and poor imprint pattern fidelity (Sreenivasan, 2010). Moreover, adhesion between the imprint solution and the underlying release layer needs to be greater than the adhesion between the imprint solution and the template surface. When PVA is used as the

underlying release layer, the PEGDA imprint solution adheres to the PVA surface due to weak H-bonds and physical entanglement of the polymeric PEGDA chains into the PVA surface. This bonding is not adequate for imprinting a densely packed nano-feature pattern that leads to large contact area between the imprint solution and the template surface. Moreover, the water or DMSO based solvent in the imprint solution may dissolve the underlying PVA layer, further weakening the adhesion between the sacrificial PVA layer and the cured resist, thereby causing peel-off of the UV-cured imprint pattern from the substrate and onto the template.

The results found with the PVA release layer suggested the need of an alternative release layer material that could be water soluble to allow particle harvesting using simple, one-step aqueous processes, and yet is insoluble in water-based imprinting solutions to avoid local dissolution and template contamination. Besides this apparently conflicting requirement, it is desirable that the release layer materials can be spun coated uniformly on the substrate so that nanoscale features can be reproducibly imprinted on the release layer. Moreover, the release layer needs to yield high adhesion strength and low contact angle with the imprint solution to avoid peel off during molding and complete filling of the template.

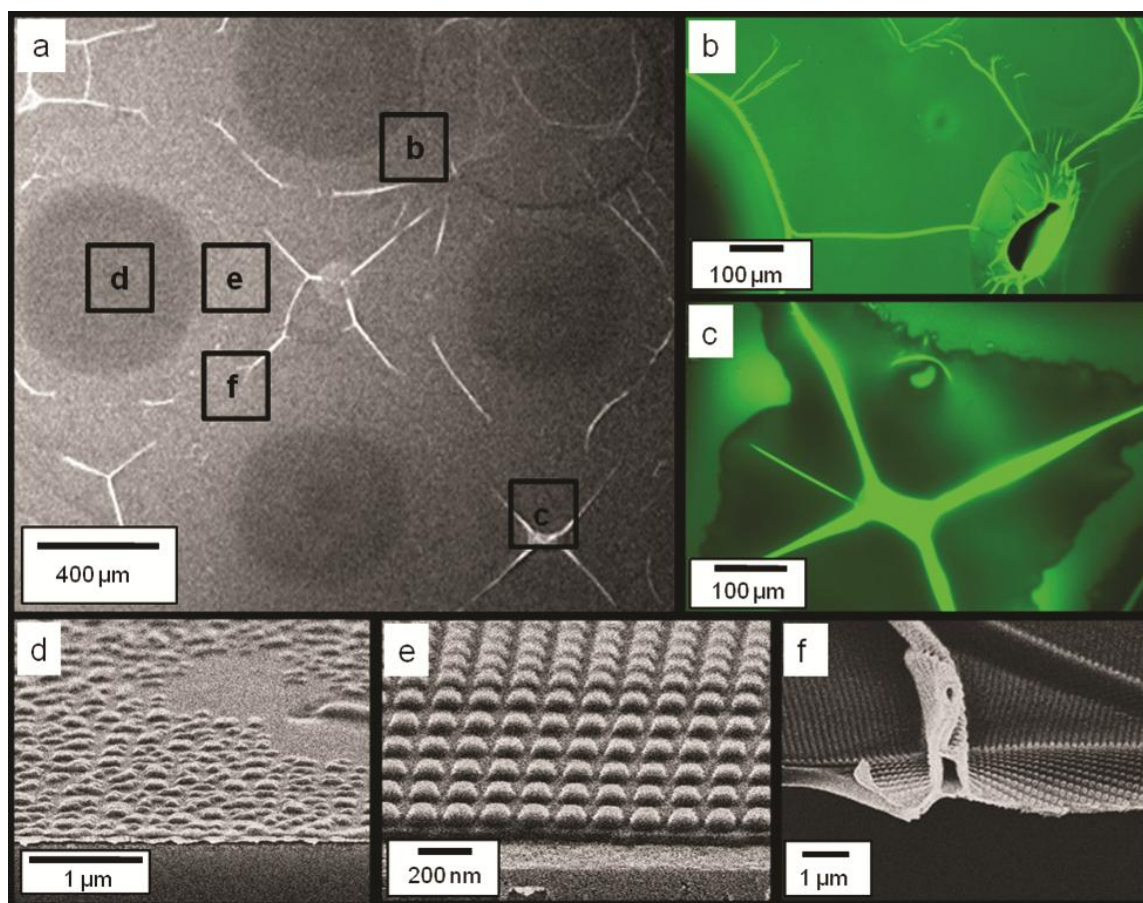


Figure 3.1: Representative SEM and Fluorescence Microscopy images of PEG imprints on a PVA release layer with the use of a water-based imprint solution. a) SEM image of imprint at low magnification, b) and, c) Fluorescence microscopy images of the imprint region at excitation wavelength of 488 nm and emission at 520 nm. d), e), f) - Zoomed in SEM images of the imprints highlighting different regions of defective and good imprints.

3.3.2 Release Layer Optimization

Many different chemicals at different concentrations were tried as potential release layer materials followed by imprinting tests over successful spin-coating over the wafers. Only PAA gave good results for imprinting. Results are summarized in Table 3.1

Table 3.1: Release Layer Optimization

Chemical	Molecular Weight (Da)	Concentration	Spin Coating	Imprinting Results
PVA	60,000	20mg/ml	Uniform	Non-Uniform
PAA	6,000	20mg/ml	Uniform	Non-Uniform
	60,000	20mg/ml	Uniform	Uniform
PEG	5,000	5mg/ml	Non-Uniform	NA
		10mg/ml	Non-Uniform	NA
		20mg/ml	Non-Uniform	NA
PEI (Poly Ethylene Imine)	60,000	10mg/ml	Non-Uniform	NA
		20mg/ml	Non-Uniform	NA

3.3.3 Imprint with a PAA Release Layer

Poly (Acrylic Acid) (PAA) is insoluble in many organic solvents such as DMSO. Moreover, the acryl functional groups in PAA promote covalent bonding between the PEGDA imprint and the surface of PAA, which is also non-toxic. Hence, we have explored PAA as an alternative release layer. When 2% w/v 60KDa PAA solution in water was spun at 3000 rpm on the silicon substrate, we were able to achieve a uniform PAA thickness of 20-30 nm on the substrate. Because PAA is not soluble in DMSO, we found that DMSO-based PEGDA solutions can be directly imprinted on a substrate coated with an untreated PAA release layer. The imprints were highly uniform and showed good template replication at sub 100 nm scale, as shown in Fig 3.2(a). SEM images show complete filling of template even to the edges. Fluorescence microscopy images of imprinted resist over PAA showed uniform fluorescence intensity, as shown in

Fig 3.2(c). Furthermore, we have also successfully encapsulated a hydrophobic, anti-cancer drug doxorubicin in these nanoimprinted particles, as shown by fluorescence microscopy images of released nanoparticles (Fig 3.2(d)).

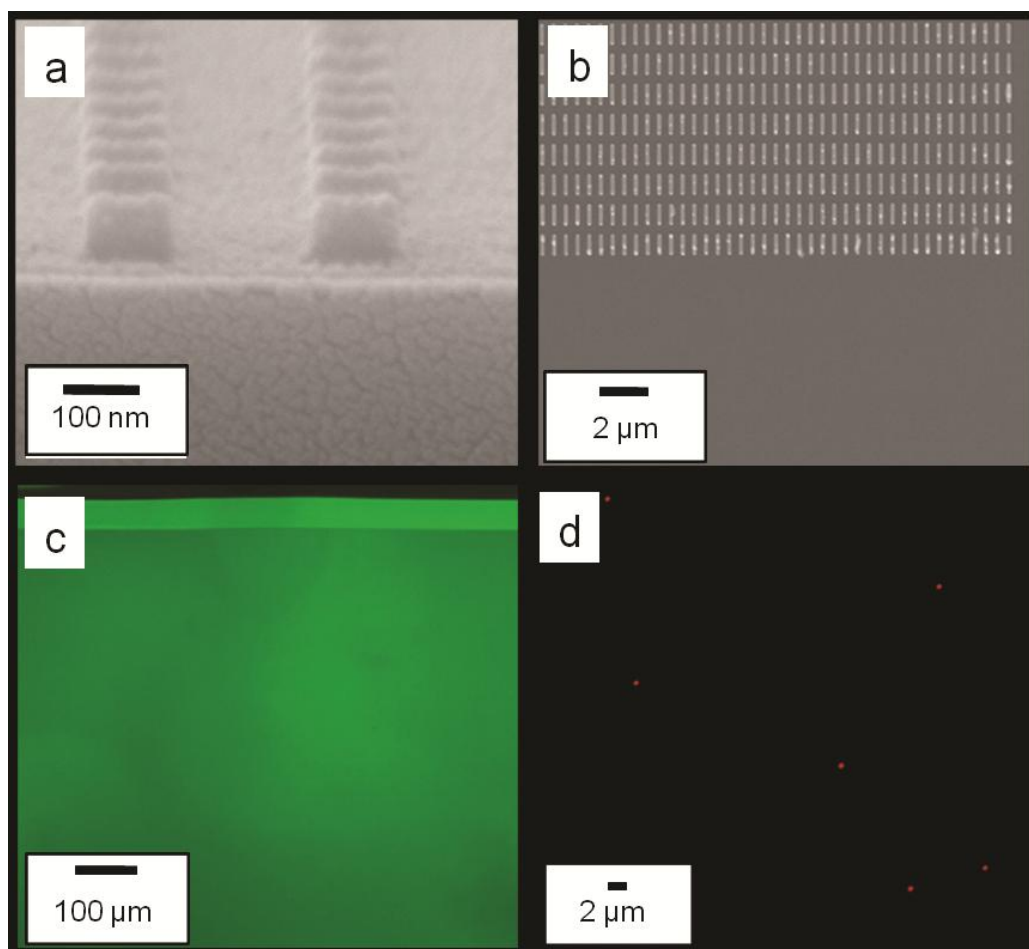


Figure 3.2: Imprints over PAA using a DMSO based imprint solution (a) Cross-sectional SEM images of 100 nm diameter x 80 nm height cylindrical particles (b) Top SEM images of 800 nm x 100 nm x 100 nm cuboidal particles (c) Fluorescence images of FITC containing 100 nm diameter x 80 nm height cylindrical particles (d) Fluorescence images of Doxorubicin containing 325 nm diameter x 100 nm height cylindrical particles taken 2 hours after being released in water.

We found that the PAA layer allows successful automated 350 imprints of DMSO-based PEGDA with FITC encapsulation that covers an entire 8 inch wafer, as shown in Figure 3.3. This is a significant improvement over the previous process and does not represent the limit of the scalability of the process. In this study, we stopped imprinting at 325 imprints as it provided adequate evidence of the scalability of the process. The cross section SEM in Fig. 3.3(b) shows that the residual layer thickness (RLT) is as small as 9 nm. In comparison, the RLT achieved in the previous imprint process was 30-40 nm (L. C. Glangchai et al., 2008). Because the residual layer needs to be etched with oxygen plasma prior to particle harvesting, the reduced RLT helps to reduce wastage of expensive biomaterials during oxygen plasma etching. The RLT depends on the viscosity of the imprinting solution, crosslinking density of polymer chains, and aspect ratio of particles being formed. The reduced RLT was achieved here with the use of PEG-di-acrylate (PEGDA) with a lower molecular weight (MW: 200 and 400 Da) and lower viscosity, which in turn allowed a smaller drop dispensing volume (reduction by 50% compared to drops formed when using higher molecular weight (700Da). The lower molecular weight formulation also allows for better template replication and shape retention which, in conjunction with the PAA sacrificial layer, resulted in an improved and scalable nanoimprinting process.

In this study, the imprint throughput was limited by the relatively small 5 mm x 5 mm imprint field on the template to 20 hours per wafer. This throughput can be potentially improved to less than 1 minute per wafer with the use of a large-area template and high-speed, high-resolution material jetting, as demonstrated for similar imprint processes for applications in light-emitting diodes (LEDs), magnetic storage and electronic devices (Sreenivasan, 2010).

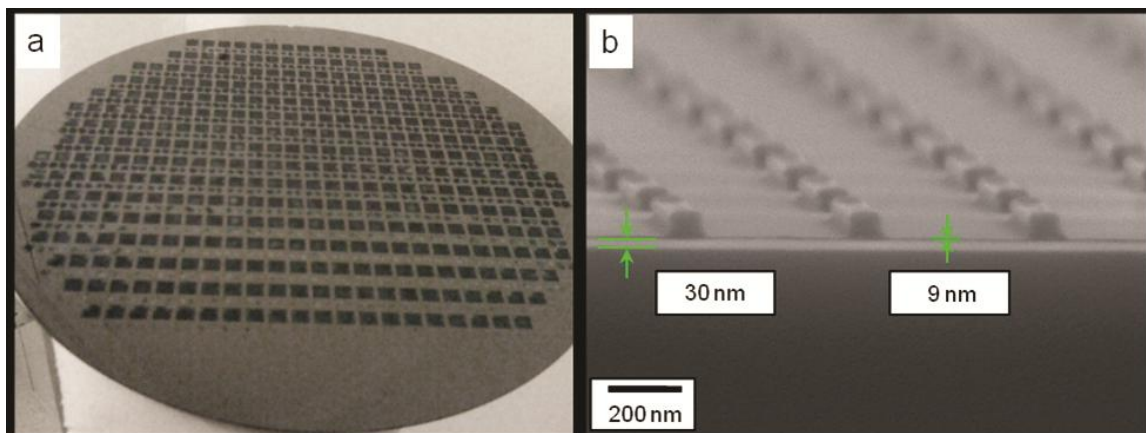


Figure 3.3: (a) Optical photograph of a wafer showing more than 325 successful automated repeatable imprints of a dense 5 mm x 5 mm template with 100-nm-diameter and 80-nm-height imprint features. (b) Cross-sectional SEM of 800 nm x 100 nm x 100 nm cuboids with sub 10 nm residual layer thickness

Because most therapeutic biomolecules are only active and stable under aqueous conditions, it is desirable to use water as the solvent for the imprint solution and the release layer. As mentioned above, the release layer used should not dissolve in the aqueous imprint solution but must dissolve in water-based harvesting solution after imprinting. Commercially available sodium salt of PAA rapidly solubilizes in water so it cannot be used directly as the release layer for water-based imprint solution. However, PAA is known to reversibly change its solubility in water depending on the concentration of monovalent and divalent ions.(Schweins and Huber, 2001) As shown in Fig. 3.4, in presence of Ca^{2+} ions, PAA ionically crosslinks to become water insoluble, and can be made water soluble after the Ca^{2+} ions are exchanged with Na^+ ions. We performed an ion exchange process by treating the wafer coated with the PAA release layer with 0.5M CaCl_2 solution. The wafer was then washed with de-ionized water leaving the PAA layer ionically crosslinked with Ca^{2+} ions. This procedure makes the PAA layer insoluble in

water. We found that Ca^{2+} treated PAA allows successful automated imprinting of at least 30 successive imprints.

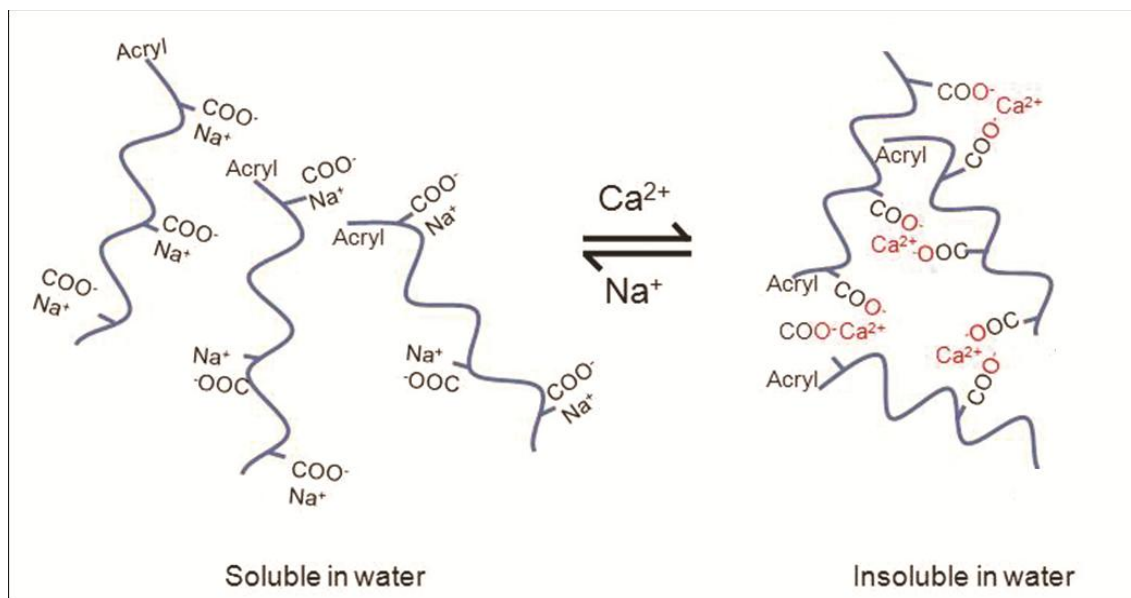


Figure 3.4: Reversible tuning of the solubility of PAA in water by exchanging between Ca^{2+} and Na^+ ions.

As shown in Table 3.2, we have conducted contact angle measurements of various imprinting solutions on different sacrificial layers including PAA, Ca^{2+} treated PAA, and PVA, as well as on a fused silica template treated with a fluorinated self assembled layer (FSAM) (Bailey et al., 2000; Beck et al., 2002; Jung et al., 2005; Sreenivasan, 2010). The contact angle was found to increase somewhat when the Ca^{2+} treated PAA release layer is used with the water- or DMSO- based imprint solutions, suggesting decreased wetting behavior. This however did not affect the template filling and there was adequate adhesion between the cured resist and the Ca^{2+} treated PAA surface as shown by successful imprinting and release of particles in Fig. 3.5.

Table 3.2: Contact angle (in degrees) measurement results

Substrate	Solution			
	DI Water	50% w/v PEGDA400 mw in Water	DMSO	50% w/v PEGDA400 mw in DMSO
PVA	20.0 ± 0.9	8.5 ± 0.3	10.8 ± 0.5	8.5 ± 0.4
PAA	7.0 ± 0.6	10.4 ± 1.2	10.9 ± 1.1	8.4 ± 1.0
PAA Treated with Ca ²⁺	8.3 ± 0.7	17.0 ± 0.7	35.7 ± 0.5	27.9 ± 0.5
Fused Silica coated SAM	7.4 ± 0.9	16.6 ± 0.6	7.6 ± 0.6	11.5 ± 0.3

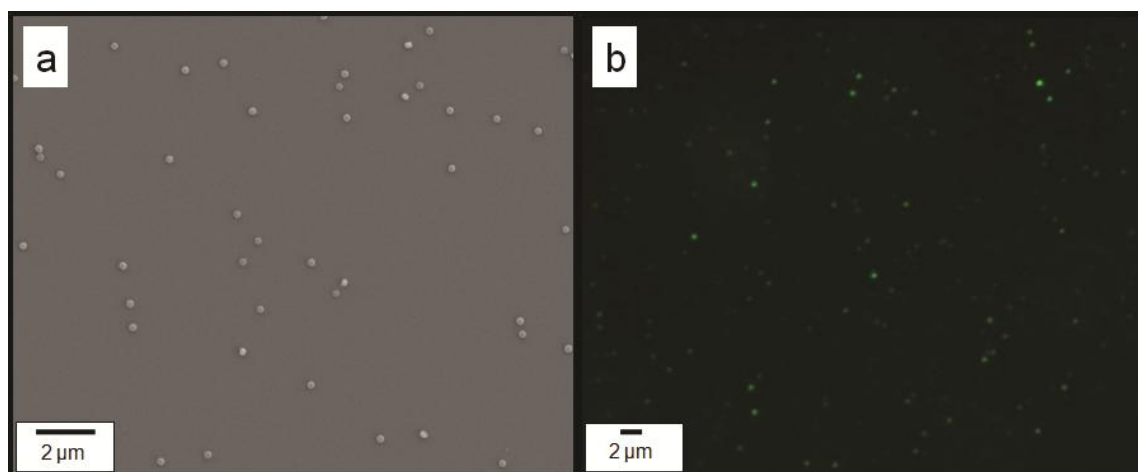


Figure 3.5: (a) SEM and (b) fluorescence microscopy images of 220 nm diameter and 125 nm height cylindrical, FITC-loaded particles imprinted over Ca²⁺ treated PAA layer using a water-based PEGDA resist. Imprints were released from the imprint substrate into water and subsequently drop casted on a different clean silicon wafer substrate for SEM imaging.

Furthermore, because the Ca^{2+} treated PAA layer is water insoluble, chemical functionalization of the imprinted nanoparticles can be carried out in a water-based environment before releasing the particles from the imprint substrate. As an example, Figure 3.6(a-b) shows that the as-imprinted particles can be washed in water multiple times without being released. This process is advantageous compared to functionalization of released particles as it avoids loss and distortion of particles caused by filtration and high speed centrifugation. After the PAA layer solubility is switched to be water soluble with the addition of monovalent ions (Na^+), the fabricated nanoparticles can be harvested readily into water, as shown in Fig. 3.6(d).

3.3.4 In vitro Cytotoxicity

Two types of particles (100nm diameter x 80nm height and 400nm x 100nm x 100nm cuboids) fabricated using this process was tested for cytotoxicity in HeLa cells using an MTS assay (after 4, 24 and 48 hours of incubation). Particles were found to be essentially non-toxic. For 100nm diameter x 80nm height particles administered at a dose of 10^5 particles per cell, cell viability was found to be $100.2 \pm 6.4\%$, 99.3 ± 2.1 and $101.7 \pm 5.2\%$ after 4, 24 and 48 hours respectively. For 400nm x 100nm x 100nm cuboidal particles administered at a dose of 10^5 particles per cell, cell viability was found to be $98.9 \pm 1.3\%$, $101.4 \pm 6.2\%$ and $103.6 \pm 0.86\%$ after 4, 24 and 48 hours respectively.

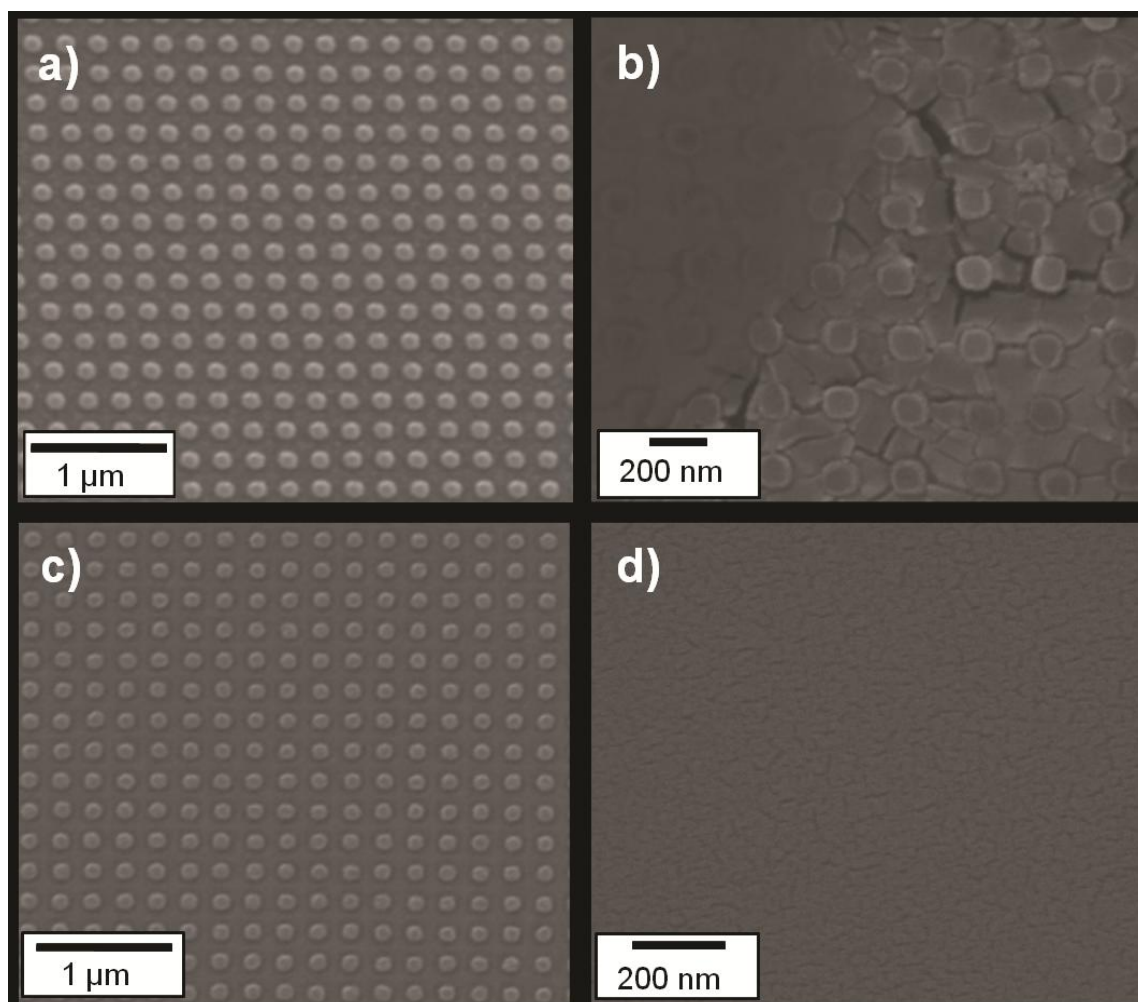


Figure 3.6: SEMs of (a) 100 nm diameter x 80 nm height cylindrical imprinted PEGDA particles in DMSO after imprinting and etching, (b) after incubation in 0.1M CaCl₂ water solution for 5 minutes, (c) after washing twice with deionized water for 5 minutes each time, (d) after washing with 0.1M NaOH water solution

3.3.5 Doxorubicin Release Kinetics

Theoretical maximum loading of Doxorubicin in imprinted particles was 41.66 μg of Dox per gram of particles). We have shown that doxorubicin is present within these imprinted nanoparticles (55% PEGDA imprints in DMSO) even 72 hours after particle

harvesting and release in water (Fig 3.7). Dox release kinetics over a 72 hour period was also studied and showed a sustained release pattern (Fig 3.8).

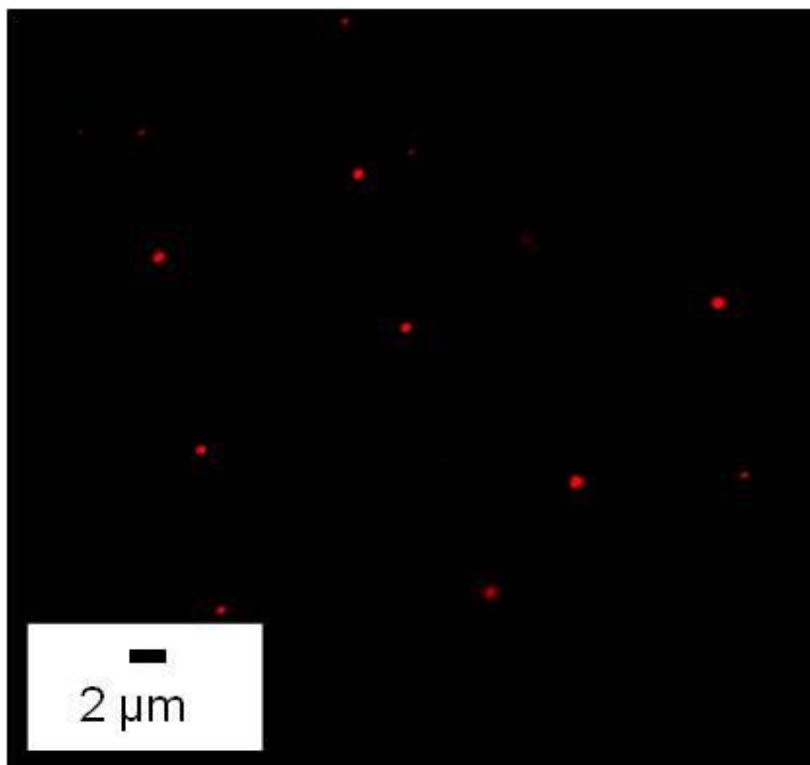


Figure 3.7: Fluorescence images of Doxorubicin containing 325 nm diameter x 100 nm height cylindrical particles taken after 72 hours of dialysis in water.

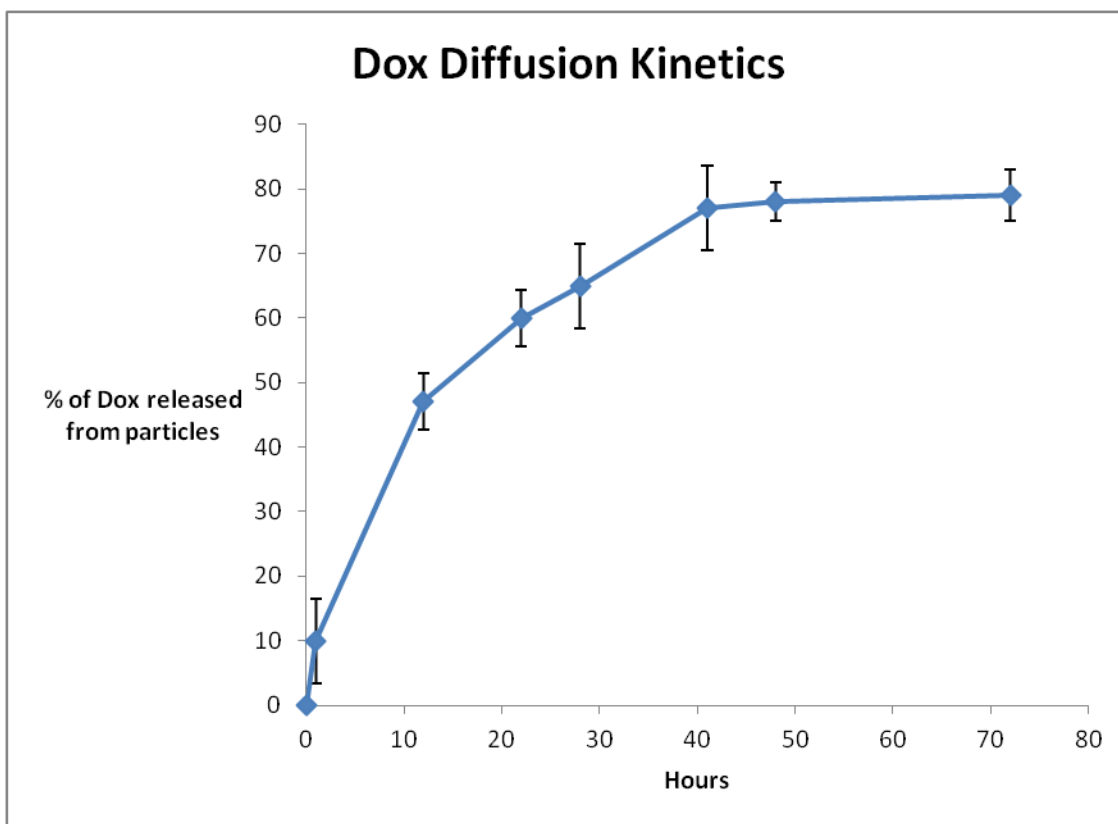


Figure 3.8: Kinetics of release of Doxorubicin from imprinted nanoparticles (325nm diameter x 100nm height) fabricated with 55% PEGDA resist in DMSO

3.3.6 Encapsulation of fluorescent molecules

Various fluorescent molecules were successfully encapsulated in the nanoparticles by mixing with imprinting solution prior to imprinting. Figure 3.9 shows Texas Red (1.66mg/ml final concentration), Texas Red conjugated to 10KDa Dextran (1.66mg/ml final concentration), Rhodamine Acrylate (20mg/ml final concentration) and Alexa Fluor 647 (0.16mg/ml final concentration) encapsulated in 220nm x 100nm disc shaped particles. Interestingly, Alexa Fluor 647 was also imaged at 570nm excitation wavelength and was not visible when excited at 630nm where there is an absorption maximum for this dye for reason unknown.

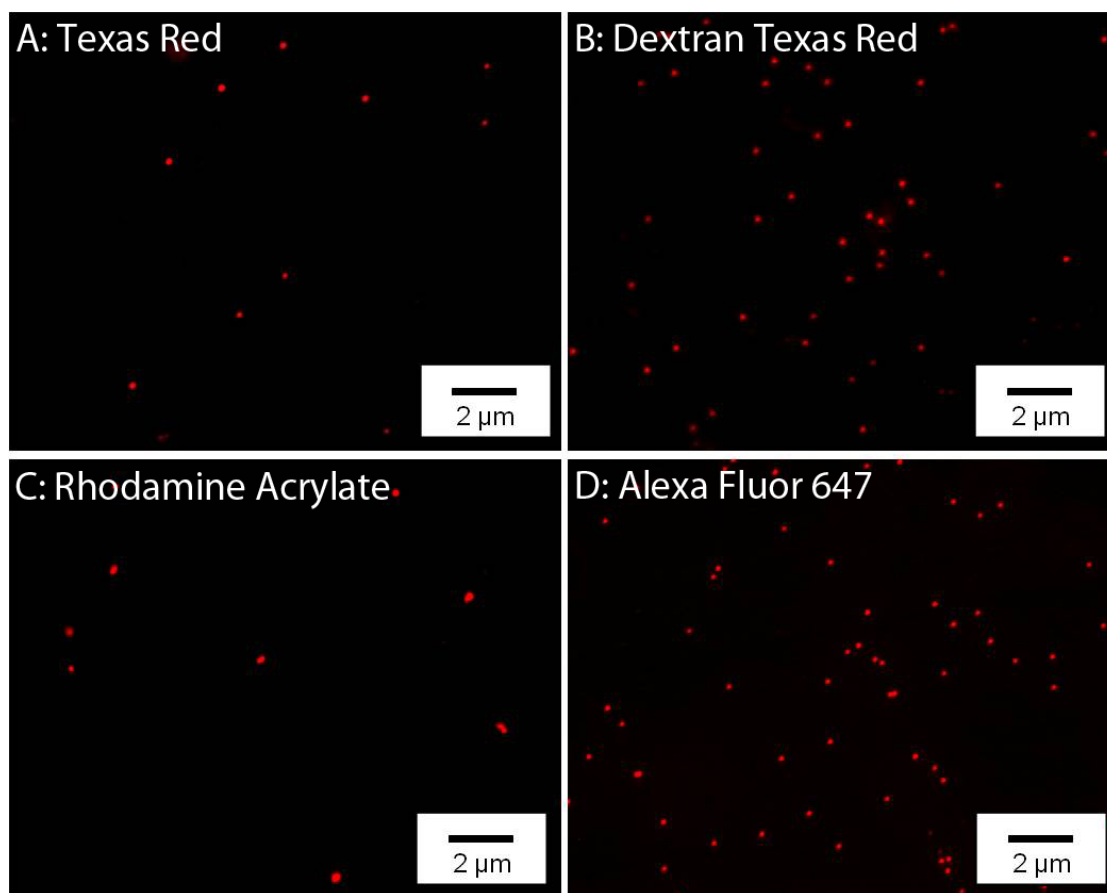


Figure 3.9: Fluorescence images of 220 nm diameter x 100 nm height cylindrical particles encapsulating **A.** Texas Red, **B.** Texas Red conjugated to 10KDa Dextran, **C.** Rhodamine Acrylate and **D.** Alexa Fluor 647.

3.4 CONCLUSIONS

These experiments show that PAA can be used as a highly versatile release layer for UV based nanoimprint lithography of biocompatible polymers. The water solubility of PAA is switchable by exchanging monovalent and divalent cations. This feature allows for large scale, repeatable, high-fidelity imprinting of nanoparticles and nanostructures in both water- and organic solvent-based imprint solutions. In addition, this method allows aqueous environment-based surface-functionalization of imprinted

particles directly on the imprint substrate as well as a simple method for particle release in water-based solutions. It offers advantage over other organic solvent-based sacrificial layers that may not be biocompatible because of the exposure of the particles to acetone, toluene, or other toxic solvents during the fabrication process. Moreover, with the use of a small-molecular weight PEGDA, the residual layer thickness was reduced to below 10 nm so as to minimize wastage of expensive biomaterials *via* oxygen plasma etching of the residual layer. In addition, successful encapsulation and release kinetics of model small molecule model drug is demonstrated. These results represent important advancements toward high-throughput, biocompatible fabrication of drug nanocarriers and nanostructures using top-down nanoimprint lithography.

3.5 REFERENCES

- Bailey, T., Choi, B., Colburn, M., Meissl, M., Shaya, S., Ekerdt, J. G., Sreenivasan, S. V., and Willson, C. G. (2000). Step and flash imprint lithography: Template surface treatment and defect analysis. *Journal of Vacuum Science & Technology B* 18, 3272-3277.
- Beck, M., Graczyk, M., Maximov, I., Sarwe, E. L., Ling, T. G. I., Keil, M., and Montelius, L. (2002). Improving stamps for 10 nm level wafer scale nanoimprint lithography. *Microelectronic Engineering* 61-62, 441-448.
- Buyukserin, F., Aryal, M., Gao, J., and Hu, W. (2009). Fabrication of polymeric nanorods using bilayer nanoimprint lithography. *Small* 5, 1632-1636.
- Caldorera-Moore, M., Kang, M. K., Moore, Z., Singh, V., Sreenivasan, S. V., Shi, L., Huang, R., and Roy, K. (2011). Swelling behavior of nanoscale, shape- and size-specific, hydrogel particles fabricated using imprint lithography. *Soft Matter* 7, 2879-2887.
- Canelas, D. A., Herlihy, K. P., and DeSimone, J. M. (2009). Top-down particle fabrication: control of size and shape for diagnostic imaging and drug delivery. *Wiley Interdiscip Rev Nanomed Nanobiotechnol* 1, 391-404.

- Champion, J. A., and Mitragotri, S. (2006). Role of target geometry in phagocytosis. *Proc Natl Acad Sci U S A* *103*, 4930-4934.
- Chithrani, B. D., and Chan, W. C. (2007). Elucidating the mechanism of cellular uptake and removal of protein-coated gold nanoparticles of different sizes and shapes. *Nano Lett* *7*, 1542-1550.
- Chithrani, B. D., Ghazani, A. A., and Chan, W. C. W. (2006). Determining the Size and Shape Dependence of Gold Nanoparticle Uptake into Mammalian Cells. *Nano Letters* *6*, 662-668.
- Davis, M. E., Chen, Z., and Shin, D. M. (2008). Nanoparticle therapeutics: an emerging treatment modality for cancer. *Nat Rev Drug Discov* *7*, 771-782.
- Decuzzi, P., Pasqualini, R., Arap, W., and Ferrari, M. (2009). Intravascular delivery of particulate systems: does geometry really matter? *Pharm Res* *26*, 235-243.
- Enlow, E. M., Luft, J. C., Napier, M. E., and DeSimone, J. M. (2011). Potent Engineered PLGA Nanoparticles by Virtue of Exceptionally High Chemotherapeutic Loadings. *Nano Letters* *11*, 808-813.
- Ferrari, M. (2005). Cancer nanotechnology: opportunities and challenges. *Nat Rev Cancer* *5*, 161-171.
- Geng, Y., Dalhaimer, P., Cai, S., Tsai, R., Tewari, M., Minko, T., and Discher, D. E. (2007). Shape effects of filaments versus spherical particles in flow and drug delivery. *Nat Nanotechnol* *2*, 249-255.
- Glangchai, L. C., Caldorera-Moore, M., Shi, L., and Roy, K. (2008). Nanoimprint lithography based fabrication of shape-specific, enzymatically-triggered smart nanoparticles. *J Control Release* *125*, 263-272.
- Gratton, S. E., Pohlhaus, P. D., Lee, J., Guo, J., Cho, M. J., and Desimone, J. M. (2007). Nanofabricated particles for engineered drug therapies: a preliminary biodistribution study of PRINT nanoparticles. *J Control Release* *121*, 10-18.
- Hamidi, M., Azadi, A., and Rafiei, P. (2008). Hydrogel nanoparticles in drug delivery. *Advanced Drug Delivery Reviews* *60*, 1638-1649.
- Huang, X., Li, L., Liu, T., Hao, N., Liu, H., Chen, D., and Tang, F. (2011). The shape effect of mesoporous silica nanoparticles on biodistribution, clearance, and biocompatibility in vivo. *ACS Nano* *5*, 5390-5399.
- Huang, X., Teng, X., Chen, D., Tang, F., and He, J. (2010). The effect of the shape of mesoporous silica nanoparticles on cellular uptake and cell function. *Biomaterials* *31*, 438-448.
- Jain, R. K., and Stylianopoulos, T. (2010). Delivering nanomedicine to solid tumors. *Nat Rev Clin Oncol* *7*, 653-664.

- Jung, G.-Y., Li, Z., Wu, W., Chen, Y., Olynick, D. L., Wang, S.-Y., Tong, W. M., and Williams, R. S. (2005). Vapor-Phase Self-Assembled Monolayer for Improved Mold Release in Nanoimprint Lithography. *Langmuir* *21*, 1158-1161.
- Kim, K.-D., Kwon, H.-J., Choi, D.-g., Jeong, J.-H., and Lee, E.-s. (2008). Resist Flow Behavior in Ultraviolet Nanoimprint Lithography as a Function of Contact Angle with Stamp and Substrate. *Japanese Journal of Applied Physics* *47*, 8648-8651.
- L. C. Glangchai, M. Caldorera-Moore, L. Shi, and Roy, K. (2008). Nanoimprint lithography based fabrication of shape-specific, enzymatically-triggered smart nanoparticles. *J Control Release* *125*, 263-272.
- Linder, V., Gates, B. D., Ryan, D., Parviz, B. A., and Whitesides, G. M. (2005). Water-soluble sacrificial layers for surface micromachining. *Small* *1*, 730-736.
- Merkel, T. J., Jones, S. W., Herlihy, K. P., Kersey, F. R., Shields, A. R., Napier, M., Luft, J. C., Wu, H., Zamboni, W. C., Wang, A. Z., *et al.* (2011). Using mechanobiological mimicry of red blood cells to extend circulation times of hydrogel microparticles. *Proc Natl Acad Sci U S A* *108*, 586-591.
- Mitragotri, S. (2009). In drug delivery, shape does matter. *Pharm Res* *26*, 232-234.
- Panyam, J., and Labhasetwar, V. (2003). Biodegradable nanoparticles for drug and gene delivery to cells and tissue. *Advanced Drug Delivery Reviews* *55*, 329-347.
- Peppas, N. A. (2004). Intelligent therapeutics: biomimetic systems and nanotechnology in drug delivery. *Advanced Drug Delivery Reviews* *56*, 1529-1531.
- Rejman, J., Oberle, V., Zuhorn, I. S., and Hoekstra, D. (2004). Size-dependent internalization of particles via the pathways of clathrin- and caveolae-mediated endocytosis. *Biochem J* *377*, 159-169.
- Roy, K., Shi, L., and Glangchai, L. C. (2007). Methods for fabricating nano and microparticles for drug delivery. In, (US).
- Schädlich, A., Caysa, H., Mueller, T., Tenambergen, F., Rose, C., Göpferich, A., Kuntsche, J., and Mäder, K. (2011). Tumor Accumulation of NIR Fluorescent PEG-PLA Nanoparticles: Impact of Particle Size and Human Xenograft Tumor Model. *ACS Nano* *5*, 8710-8720.
- Schweins, R., and Huber, K. (2001). Collapse of sodium polyacrylate chains in calcium salt solutions. *The European Physical Journal E: Soft Matter and Biological Physics* *5*, 117-126.
- Sreenivasan, S. V., Choi, J., Schumaker, P., and Xu, F. (2010). Status of UV Lithography for Nanoscale Manufacturing. *Handbook of Nanofabriation Edited by Wiederrecht, GP Chapter 5*, 149-182.
- Wen, J., Kim, B. Y. S., Rutka, J. T., and Chan, W. C. W. (2008). Nanoparticle-mediated cellular response is size-dependent. *Nature Nanotechnology* *3*, 145-150.

Chapter 4: Effect of Shape of Nanoparticles on Uptake by Cells

4.1 INTRODUCTION

Polymeric nanoparticles have gained significant interest in biomedical applications and are widely studied for delivering therapeutic and imaging payloads to cells (Ferrari, 2005; Jain and Stylianopoulos, 2010). Understanding how particle properties affect cellular internalization is not only critical for designing improved therapeutic and diagnostic agents (Peer et al., 2007) but also essential for efficient *in vitro* cell manipulation (Dobson, 2006; Jang et al., 2012; Tseng et al., 2012) and evaluating the toxicity of nanomaterials (Nel et al., 2006; Teeguarden et al., 2007). Nanoparticle uptake by cells has been shown to depend on particle size, surface charge and material composition (He et al., 2010). Recently, shape-specific micro and nanoparticles, inspired by the diverse, evolutionarily conserved shapes of pathogens and cells, are being studied to elucidate whether particle shape plays an important role in cellular internalization, *in vivo* transport and organ distribution (Chauhan et al., 2011; Chithrani and Chan, 2007; Decuzzi et al., 2005; Decuzzi et al., 2009; Geng et al., 2007; Gratton et al., 2007; Gratton et al., 2008; Huang et al., 2011; Huang et al., 2010; Jiang et al., 2012; Mitragotri, 2009). Chithrani *et al.* reported that *in vitro* cell uptake of gold nanospheres is more efficient than nanorods (Chithrani et al., 2006a). In contrast, Huang *et al.* showed that for mesoporous silicon, long aspect ratio nanoparticles outperform nanospheres (Huang et al., 2010). In each of these studies, differences in both particle size and surface chemistry between rods and spheres could have played a significant role in cell uptake. Chauhan *et al.* compared silica-quantum dot nanospheres with nanorods and showed that rods accumulated faster and in higher numbers inside tumor tissues and were also able to penetrate deeper than nanospheres (Chauhan et al., 2011). Gratton *et al.* used PRINT-

fabricated (Rolland et al., 2005) polymer nanoparticles and showed that cellular uptake and biodistribution of the particles were influenced by particle shape (Gratton et al., 2008). At the microscale, Champion *et al.* (Champion and Mitragotri, 2006) showed that macrophage uptake of micro-ellipsoids was dependent on local interactions of particle shape with cell membranes (Champion and Mitragotri, 2006). Long thin filamentous particles have also been shown to circulate in blood for up to a week while spherical nanoparticles were cleared within 48 hours (Geng et al., 2007). Recently, Van de ven *et al.* compared disc and rod-shaped mesoporous silicon microparticles and showed that disc-shaped particles accumulate more near tumor vasculatures (van de Ven et al., 2012). Theoretical models have also predicted that non-spherical particles could marginate more in blood vessels and are therefore more prone to flow into budding capillaries and through gaps in leaky blood vessels to deliver cargo to diseased tissues (Decuzzi et al., 2005; Shah et al., 2011).

Despite these developments, there remains a significant knowledge gap in our fundamental understanding of the interplay between nanoscale shape and size on cellular internalization, especially for polymeric nanoparticles. It is unclear how internalization of various non-spherical particles varies with size across different cell-types and how their kinetics and uptake mechanisms differ. Here we present a comprehensive study showing the complex effects of nanoparticle geometry on uptake in epithelial, endothelial, and immune cells. Specifically, we compare discoidal and rod-shaped polymeric nanohydrogels of equivalent volume and dimensions and show that compared to spherical particles, nanodiscs and nanorods have unique, geometry-dependent, cell-type specific internalization kinetics and uptake mechanisms.

Understanding the effect of nanoscale particle geometry on cell-uptake requires highly monodispersed nanoparticles of equivalent volumes, identical surface properties,

and material compositions that differ only in shape and size. These particles should also have minimal interference from serum protein adsorption and electrostatic adsorption with cell membranes. Further different cell lines need to be tested to understand the effect of shape of carriers based on the type of cells used before making generalizations.

4.2 MATERIALS AND METHODS

4.2.1 Materials and Reagents

4.2.1 Nanoimprinting

50% Poly (ethylene Glycol) Di-acrylate (Mw: 200 Da), 0.1% w/v final concentration of 2-hydroxyl-1-[4-(hydroxyl) phenyl]-2-methyl-1propanone (I2959, Ciba) as the photoinitiator and 5% Fluorescein Acrylate were dissolved in DMSO. A diluted 2% w/v Poly(acrylic acid) (PAA) solution was prepared in water. About 5mL of this PAA solution was spincoated on an 8" Silicon wafer at 4500 rpm for 40 seconds. The wafer was then baked on a hot plate at 160°C for 1 minute. Nanoimprinting was carried out on an Imprio® 100 using the Jet and Flash Imprint Lithography (J-FIL™) process at Molecular Imprints Inc. in Austin, TX. In the J-FIL™ process, resist droplets are first ink-jetted onto a silicon wafer pre-coated with a PAA release layer. Then, a pre-patterened transparent quartz template was pressed onto the resist droplets, causing them to spread and fill the features of the quartz mold. The resist was then exposed to UV light (365nm wavelength at 5 mW/cm² intensity), for 25 seconds to photopolymerize the molded resist. The template was then demolded, revealing the desired nanostructures. The imprints were sputter coated with a 3nm layer of Platinum and the residual layer was measured using cross-sectional SEM. A low power (35 Watts) Argon plasma etch

(Oxford Instruments Plasma Lab 80+) was performed at a pressure of 10 mTorr with Ar (20 sccm) and O₂ (4 sccm), yielding an etch rate of 0.6nm/sec.

4.2.2 Release and Characterization of Nanoparticles

After etching on the wafer, imprints were washed twice with DMSO to remove any unreacted polymer. The imprints were then submerged in DMSO, incubated for 5 minutes and blow dried with Nitrogen. Nanoparticles were harvested from the imprints by pipetting 50 μ l of filtered de-ionized (DI) water over a 5mmx5mm imprint area. The DI water dissolved the underlying PAA layer and the DI water containing the released nanoparticles was collected after 1 minute. The water containing nanoparticles was dialyzed for 3 days using 300KDa Float-A-Lyzers (SpectrumLabs Inc.). For SEM, 3 μ l of nanoparticle suspension was dispensed on a SEM stub, air-dried and sputter coated with a 3nm layer of Platinum to make the sample conductive. For fluorescence microscopy, 3 μ l of nanoparticle suspension was dispensed on a glass slide and covered with a glass cover slip. Imaging was performed at 100X magnification by exciting the sample using a 488nm wavelength laser. Zeta potential and dynamic light scattering analysis were performed using a Zetasizer Nano ZS tool (Malvern Inc.). Zeta potential analysis was performed by Dr. Claudia Mujat of Malvern Inc. For serum stability tests, dialyzed nanoparticles were mixed with 10% serum containing PBS and imaged using fluorescence microscopy directly in serum containing PBS. For long term serum stability, dialyzed nanoparticles were mixed with 10% serum containing PBS or just PBS as a control and incubated at 37°C for 48 hours. The solution was then dialyzed for 2 days against deionized water using a 1000KDa float-a-lyzer (Spectrum Labs).

4.2.3 Cell Culture

HeLa (ATCC) and HEK 293 (ATCC) cells were cultured in Dulbecco's Modified Eagle Medium (DMEM) (Hyclone) supplemented with 10% fetal bovine serum (Characterized FBS, Hyclone) and 1% antibiotics (penicillin and streptomycin, Invitrogen). HUVEC (ATCC) cells were cultured in MCDB 131 medium (Life Technologies) supplemented with 10% fetal bovine serum (Characterized FBS, Hyclone) and 1% antibiotics (penicillin and streptomycin, Invitrogen) and further supplemented with EGM2 Supplement and Growth Factor Kit (Lonza Inc.). The mCherry labeled clathrin cell lines of RPE cells (gift from Dr. Marcel Mettlen at UT Southwestern Medical Center, Dallas) were cultured in DMEM/Ham's F12 1:1 mixture supplemented with 10% fetal bovine serum (Characterized FBS, Hyclone) and 1% antibiotics (penicillin and streptomycin, Invitrogen). Similar green fluorescent protein (GFP) labeled clathrin cell lines have been previously reported (Loerke et al., 2011). For all cell lines, media was changed every other day and cells were passaged at 80-90% confluency. Bone Marrow Dendritic Cells (BMDCs) were derived from bone marrow isolated progenitor cells of female Balb/c mice (H-2d, 5-10 weeks old, Jackson Laboratories). RPMI-1640 Glutamax® (Invitrogen, Carlsbad, CA) medium, supplemented with 20 ng/ml mouse GM-CSF and 10 ng/ml IL4 (eBioscience, San Diego, CA) was used to differentiate progenitor cells into the myeloid lineage. Loosely adherent APCs (a mixture of cells with mostly DCs) were harvested on days 6-7 and found to be 70-75% CD11c+. All of the experimental and surgical procedures involving animals were approved by the University of Texas at Austin Institutional Animal Care and Use Committee. BMDCs were used immediately and isolated fresh from mice for each experiment.

4.2.4 Cytotoxicity Assay

HeLa, HEK293 and HUVEC cells were used for *in vitro* cytotoxicity analysis of the fabricated PEGDA nanocarriers using an MTS assay (CellTiter 96 AQueous One Solution Cell Proliferation Assay, Promega). To perform the MTS assay, 10,000 cells were plated in a 96 well plate and incubated overnight. Assays were performed by adding the MTS reagent solution to the culture wells and recording the absorbance (at 490nm) after particle incubation for 4, 24 and 48 hours. A ratio of 10^5 nanoparticles of dimension 400nm x 100nm x 100nm per cell was used. All of the experiments were conducted in groups of 6.

4.2.5 Thermo-Gravimetric Analysis

The weights of known amounts of fluorescence unit containing nanoparticles for different shapes were measured using thermo-gravimetric analysis (TGA) (Mettler Toledo). Fluorescence intensities of 50 and 100 units were measured on a Biotech plate reader for 3 different shapes of nanoparticles solutions using 480/20nm excitation filters and 520/20nm emission filters. The solution was then subjected to heating till 150°C for 20 mins to evaporate all solvent and the dry weight was then measured.

4.2.6 Confocal Microscopy

For Confocal Microscopy, HeLa and RPE cells were seeded (20,000 cells per well) on poly-l-lysine coated coverslips (BD Biocoat™) in a 24 well tissue culture plate and allowed to adhere overnight. Cells were then incubated with nanoparticles for 24 hours. Cells were then fixed, permeabilized and their nuclei stained using DAPI (Molecular Probes). The cytoskeleton of HeLa cells was also stained using Texas red conjugated phalloidin (Molecular Probes). RPE cells have inherent red fluorescently

labeled (mCherry) clathrin pits. Slides were imaged using a Leica SP2 AOBS confocal microscope.

4.2.7 Flow Cytometry

For flow cytometry, HeLa, HEK293 and HUVEC cells were seeded (20,000 cells per well) in a 24 well tissue culture plate and then allowed to adhere overnight in 10% serum containing medium. Cells were then incubated with an equal mass of shape-specific particles or polystyrene beads for 12, 24 and 48 hours. The cells were then trypsinized, washed with phosphate buffer saline (PBS) and resuspended into 2% FACS buffer (2% FBS in PBS). Flow cytometry was done using an Accuri C6 cytometer (BD Accuri™). All conditions were tested in triplicates. For BMDCs, 100,000 cells per well were seeded in a 48 well tissue culture plate and same process repeated. Change in median fluorescence was calculated and plotted against time. To compare the number of particles internalized among various shapes, 80nm x 70nm disc particles were used to normalize all particles. It was assumed that the change in median fluorescence for an 80nm diameter disc corresponded to 100 particles per cell, and the number of particles for other shapes was computed relative to this using the following formula:

$$\text{Number of particles of a specific shape} = \frac{\text{Change in Median Fluorescence for that shape} \times \text{Volume of (80nm x 70nm) disc} \times 100}{\text{Volume of that Specific Shape}}$$

4.2.8 Inverted Culture Studies

For inverted culture studies, HEK 293 and HUVEC cells were seeded (20,000 cells per well) on poly-L-lysine coated cover slips in a 24 well tissue culture plate and then allowed to adhere overnight. Cover slips were then gently placed inverted onto 2

glass pegs of equal size (1mm cube) and media filled up to 1.3 mm in each well. Equal fluorescence of polystyrene beads and shape specific particles were then incubated with cells for 24 hours after which cover slips were transferred into a fresh 24 well plate. Cells were then trypsinized, washed with phosphate buffer saline (PBS) and resuspended into 2% FACS buffer (2% FBS in PBS) for flow cytometry.

4.2.9 Pharmacological Inhibition Studies

For Pharmacological inhibitors Studies, HEK293 and HUVEC cells were seeded (20,000 cells per well) in a 24 well tissue culture plate and then allowed to adhere overnight. Various pharmacological inhibitors were used and added to cells at the concentration described in Fig 4a. Specifically, chlorampramazine, a cationic drug which results in loss of clathrin and AP2 adaptor complexes from the cell surface and specifically blocks the clathrin mediated pathway, was used (Ivanov, 2008). Filipin causes aggregation of cholesterol in biological membranes and disruption of caveolar pits while still allowing other cellular mechanisms (Ivanov, 2008) to continue. Amiloride blocks the exchange of Na^+/H^+ in the cell membrane while cytochalasin D blocks actin polymerization, thereby blocking membrane ruffling and macropinocytosis. However, actin filaments are involved in various other endocytic pathways and inhibition by cytochalasin D is hence not very specific (Ivanov, 2008). Nocodazole hinders microtubule polymerization and, hence, vesicular transport (dos Santos et al., 2011). Cells were incubated for 1 hour after which particles were added to cells containing inhibitors for 5 more hours. Cells were then trypsinized, washed with phosphate buffer saline (PBS) and resuspended into 2% FACS buffer (2% FBS in PBS) for flow cytometry.

4.3 RESULTS AND DISCUSSION

4.3.1 Particle Characterization

Poly(ethylene glycol)-diacrylate (PEGDA)-based discoidal (220nm diameter, $d \times 100\text{nm}$ height, h , 325nm $d \times 100\text{nm}$ h and 80nm $d \times 70\text{nm}$ h) and cuboidal (rod-shaped) nanoparticles (100nm \times 100nm \times 400nm and 100nm \times 100nm \times 800nm) were fabricated using Jet and Flash Imprint Lithography (J-FILTM) (Agarwal et al., 2012; Caldorera-Moore et al., 2011; Glangchai et al., 2008) (Fig. 4.1 A-G). The 220x100nm discs and 100x100x400nm rods as well as 325x100nm discs and 100x100x800nm rods represent particles of similar volumes. All particles had an average zeta potential of -55mV (Fig. 4.1 H) which, along with the material composition (PEGDA), ensured minimal aggregation and protein absorption in serum (Fig. 4.2, Table 4.1) as well as minimized electrostatic adsorption to cell-membranes.

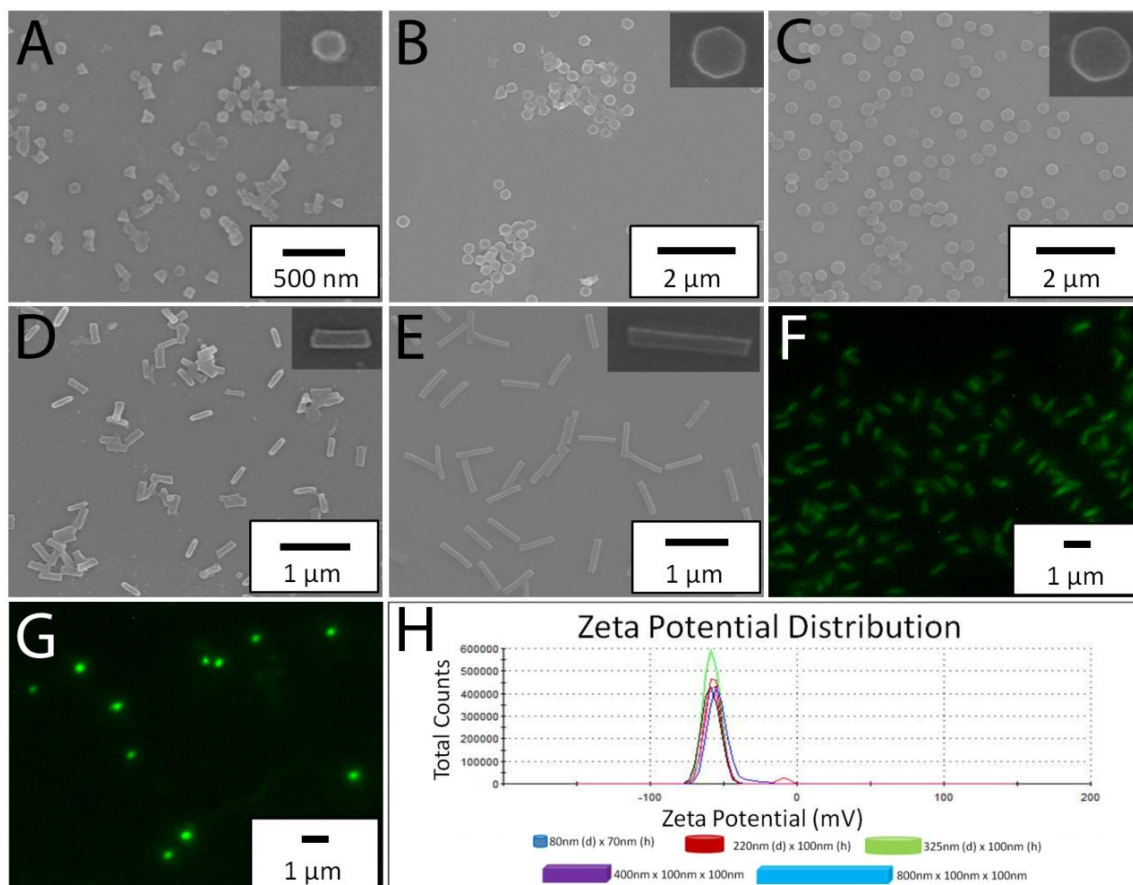


Figure. 4.1: Nanoparticle Characterization – Specific Shapes, Uniform Fluorescence and Equivalent Surface Charge: SEM micrograph of A) 80nm diameter x 70nm height discs, B) 220nm diameter x 100nm height discs, C) 325nm diameter x 100nm height discs, D) 400nm x 100nm x 100nm rods, E) 800nm x 100nm x 100nm rods. Fluorescence images of F) 800nm x 100nm x 100nm rods, G) 325nm diameter x 100nm height discs. H) Zeta potential plot for all particles.

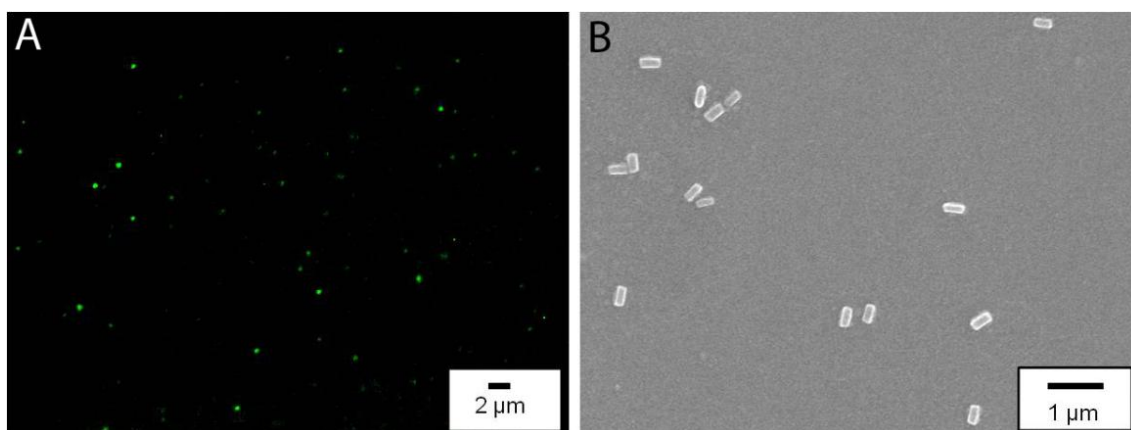


Figure 4.2: Particle characterization in presence of serum shows no aggregation of particles: A) Fluorescence Microscopy images of 220nm diameter x 100nm height particles at excitation wavelength of 488nm and emission at 520nm, B) SEM image of 400nm x 100nm x 100nm particles after incubation in 10% serum.

Table 4.1: DLS and Zeta potential characterization of particles after incubation in 10% serum:

400x100x100nm particles	Particle in PBS	Particle in FBS
DLS	452.2 ± 20nm	458.9 ± 16nm
Zeta	-55 ± 4 mV	-48 ± 3 mV

4.3.2 Cytotoxicity Assay

Particles were tested with various cell lines for cytotoxicity and were found to be non-toxic (Fig. 4.3).

Nanoparticle Cytotoxicity

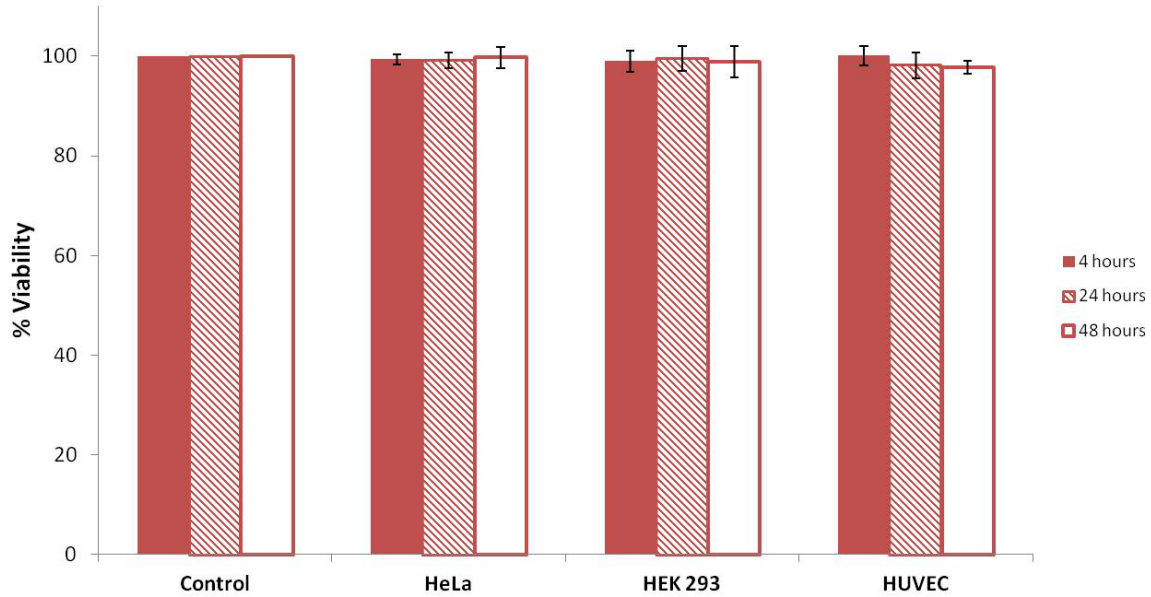


Figure. 4.3: In vitro cytotoxicity assay show particles are non-toxic. Cytotoxicity assay for HeLa, HEK 293 and HUVEC cells done with 400 nm x 100 nm x 100nm particles.

4.3.2 Thermo-Gravimetric Analyzer

All nanoparticles were synthesized with fluorescein-acrylate distributed throughout the matrix and administered at equal total fluorescence intensity (to mimic equal drug dosage) which also corresponded to an equal particle mass (verified using Thermo Gravimetric Analyzer (TGA), Fig. 4.4). Figure 4.4 shows that for all particles tested, fluorescence can be used as a measure of mass of particles and that fluorescence is uniformly distributed throughout the matrix of each particle.

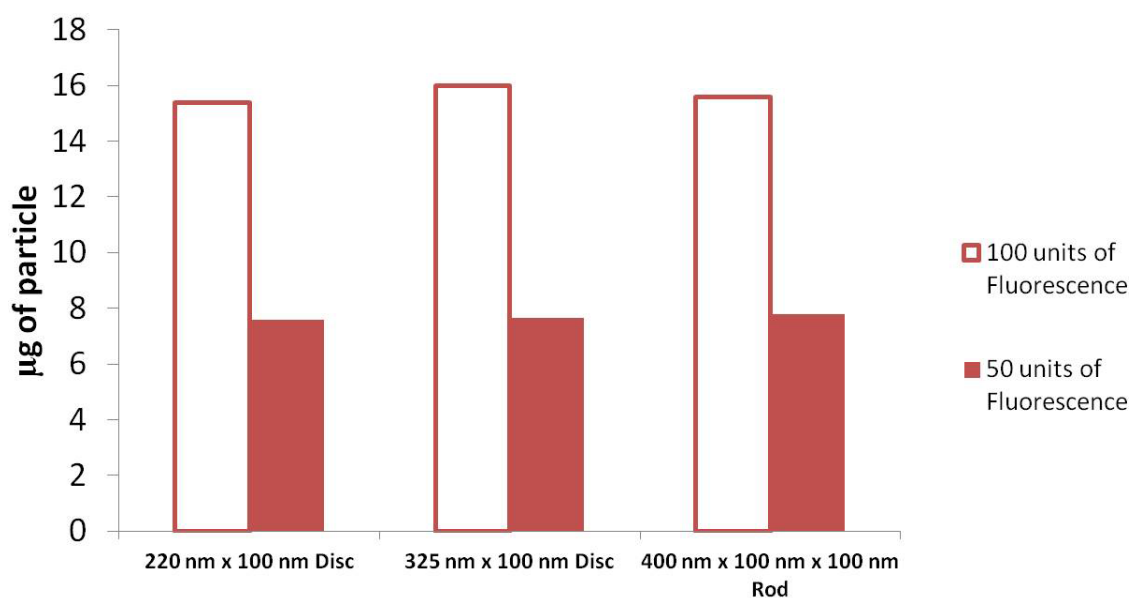


Figure. 4.4: Correlation of fluorescence signal with mass of nanoparticle. Plot showing correlation between fluorescence units and mass of particles.

4.3.3 Confocal Microscopy

Uptake studies were performed on HeLa cells and assessed using confocal microscopy. All shapes of particles were found to be internalized (Figure 4.5) and there was no signal from the surface of the cells after washing.

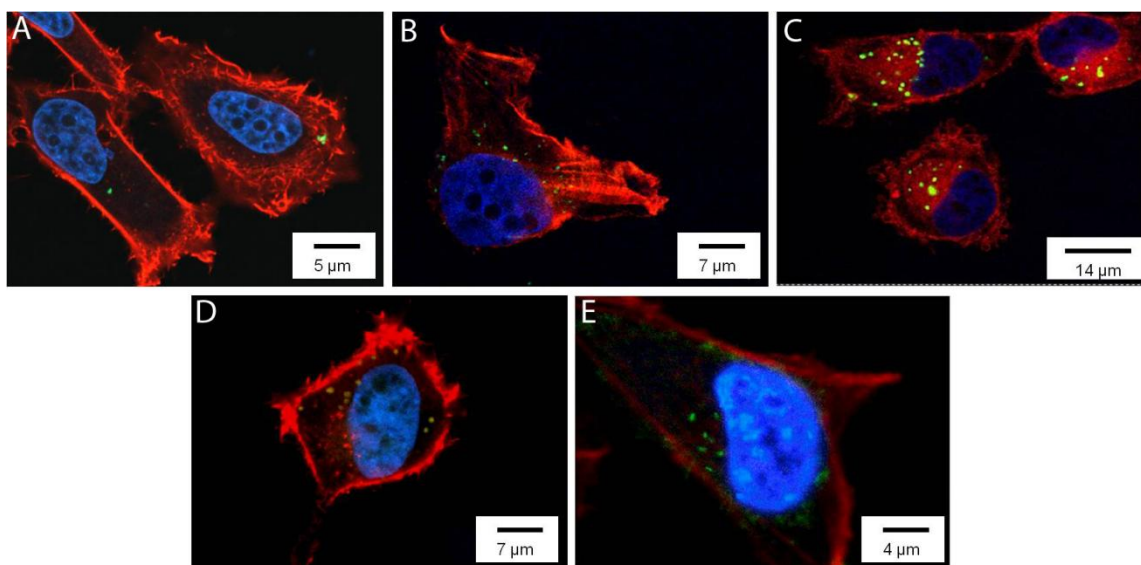


Figure. 4.5: Confocal Microscopy of particle uptake by HeLa cells. Confocal cross-section images of HeLa cells showing internalization of shape-specific particles A) 80nm diameter x 70nm height discs, B) 220nm diameter x 100nm height discs, C) 325nm diameter x 100nm height discs, D) 400nm x 100nm x 100nm rods, E) 800nm x 100nm x 100nm rods.

4.3.4 Flow Cytometry

For quantitative analysis, flow cytometry was performed and data showing median fluorescence increase in cells were captured over time (Fig. 4.6A). Between discoidal and rod-shaped nanoparticles of similar volume, nanodiscs were more efficiently internalized at all time-points. Interestingly, Barua *et al.* reported that for non-specific hydrophobic polystyrene particles, nanorods and nanodiscs have similar uptake in epithelial breast cancer cells (Barua *et al.*, 2013). These differences highlight the effect of hydrophobic versus hydrophilic surfaces and emphasize the importance of material composition. Furthermore in our studies, for both discs and rods, nanoparticles with larger volumes were taken up more effectively compared to their smaller counterparts. This is counter intuitive when compared to spherical polymer particles where smaller particles show higher uptake in HeLa cells (Chithrani *et al.*, 2006a; He *et al.*, 2010) (Fig.

4.7A). Although, Huang *et al.* have shown similar effect with rod-shaped mesoporous silica particles in human melanoma A375 cells (Huang et al., 2010), this has not been previously reported for polymeric nanodiscs or nanorods. To ensure that this is not cell line specific, these experiments were repeated on another epithelial cell line, HEK 293, and similar trends were observed (Fig. 4.6B, Fig. 4.7B).

To determine the effect of particle shape on other types of cells that nanoparticles encounter *in vivo*, human umbilical vein endothelial cells (HUVECs) and primary mouse Bone Marrow Dendritic Cells (BMDCs) were used. BMDCs showed similar disc versus rod uptake preference to that of epithelial cells (Fig. 4.6C), i.e. nanodiscs were internalized more efficiently than nanorods and larger particles were internalized more efficiently than smaller particles. HUVEC cells, however, showed unique trends wherein intermediate sized discs (220nm diameter) were internalized more efficiently than either smaller or larger volume discs as well as nanorods (Fig. 4.6D). Surprisingly, although in these studies the nanoparticle-to-cell ratio was ten times less than that used in epithelial cells, the median fluorescence values were similar indicating significantly higher uptake efficacy in endothelial cells. Decrease in median fluorescence observed at 48 hours in HUVECs could be a result of faster particle dilution per cell because of cell division and low particle-dose, or due to endothelial cell-specific exocytosis (Bartczak et al., 2012).

All uptake experiments were repeated several times using nanohydrogels manufactured in different batches and cells of different passage numbers (passage 3 to 18; representative reproducible results are shown in Fig. 4.8).

Further, assuming that fluorescein-acrylate is uniformly distributed throughout the particle matrix, we estimated the relative number of particles present per cell (normalized to 80nm diameter discs) at the maximum internalization time points. The 220nm and 325nm diameter discs have similar volumes to 400nm and 800nm rods respectively. Thus

for these particles, equal fluorescence administration also means administration at equal numbers. We found that between 220nm discs and 400nm rods, nanodiscs were internalized more efficiently than nanorods in all cell-types (Fig. 4.6E). Similarly, as shown in Fig. 4.6F, for the larger, equivalent volume disc-rod pair (325nm discs, 800nm rods), 40-60% more disc-shaped particles were internalized in epithelial and immune cells. Interestingly, this trend is reversed in endothelial cells, although less significantly, further confirming that the effect of particle geometry is cell-type specific.

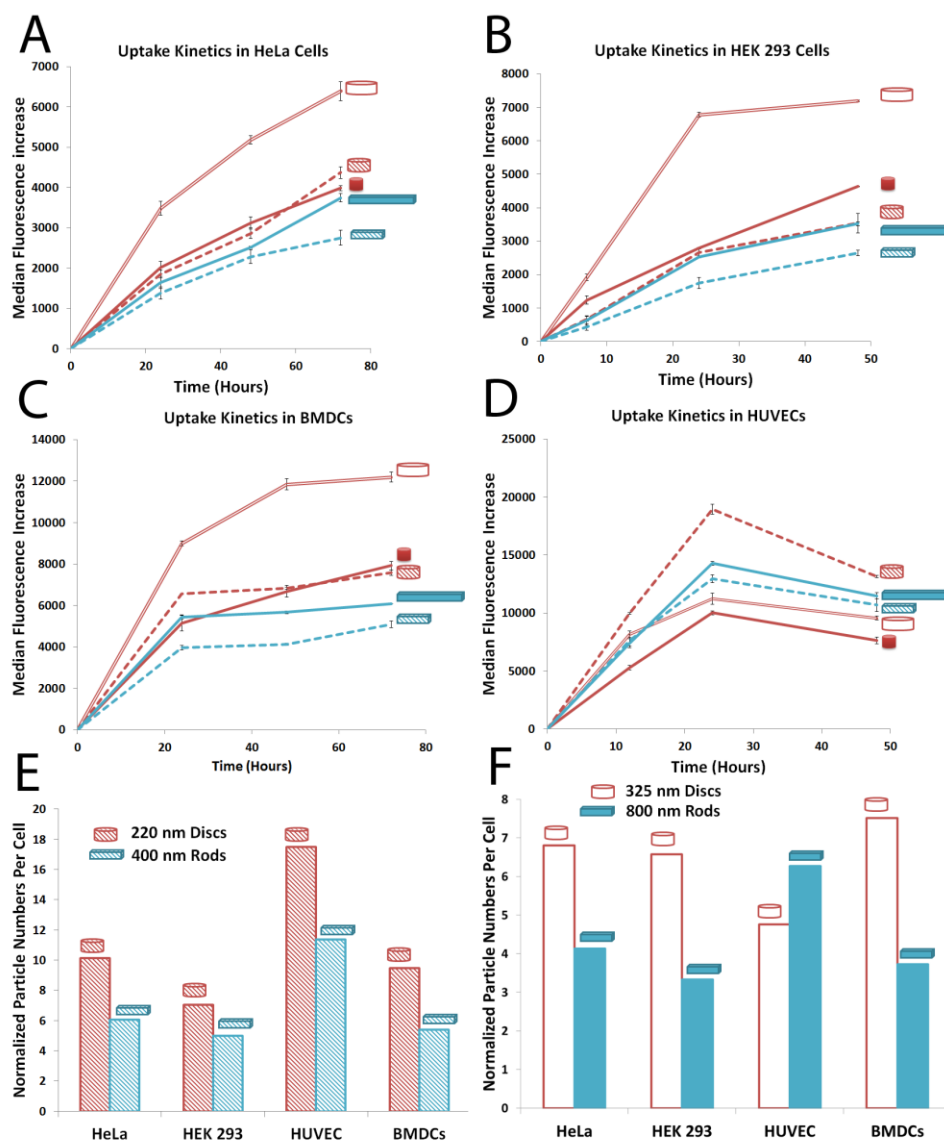


Figure. 4.6: Cellular uptake kinetics of different shape-specific nanoparticles in various cell lines. A) HeLa cells, B) HEK 293 cells, C) HUVEC cells, D) BMDCs. In figure A-D, red lines are for discs (hollow for 325x100nm disc, dashed for 220x100nm disc and solid for 80x70nm disc) and blue lines for rods (dashed for 400x100x100nm rods and solid for 800x100x100nm rods). Error bars are standard deviation with n=3 for each data point. E-F) Normalized median particle uptake per cell (indicates relative number of particles internalized by cells when normalized to 80x70nm disc) at the maximum internalization time point (72 hours for HeLa and BMDC, 48 hours for HEKs and 24 hours for endothelial cells)

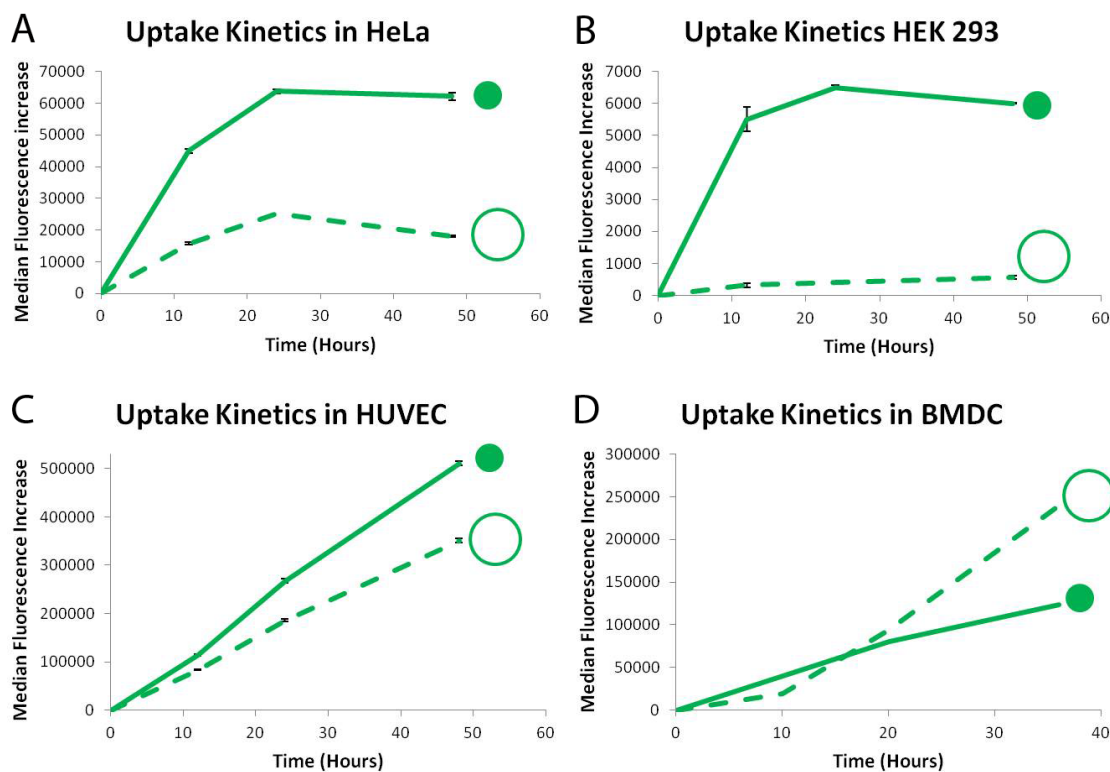


Figure. 4.7: Flow cytometry kinetic plots for uptake of polystyrene beads in 4 cell lines. Effect of size of nanoparticles on uptake kinetics in A) HeLa cells, B) HEK 293 cells, C) HUVEC cells, D) BMDCs. In figure a-d, dashed green line for 200nm polystyrene spherical particles and solid green line for 100nm polystyrene spherical particles. Error bars are standard deviation with n=3 for each data point.

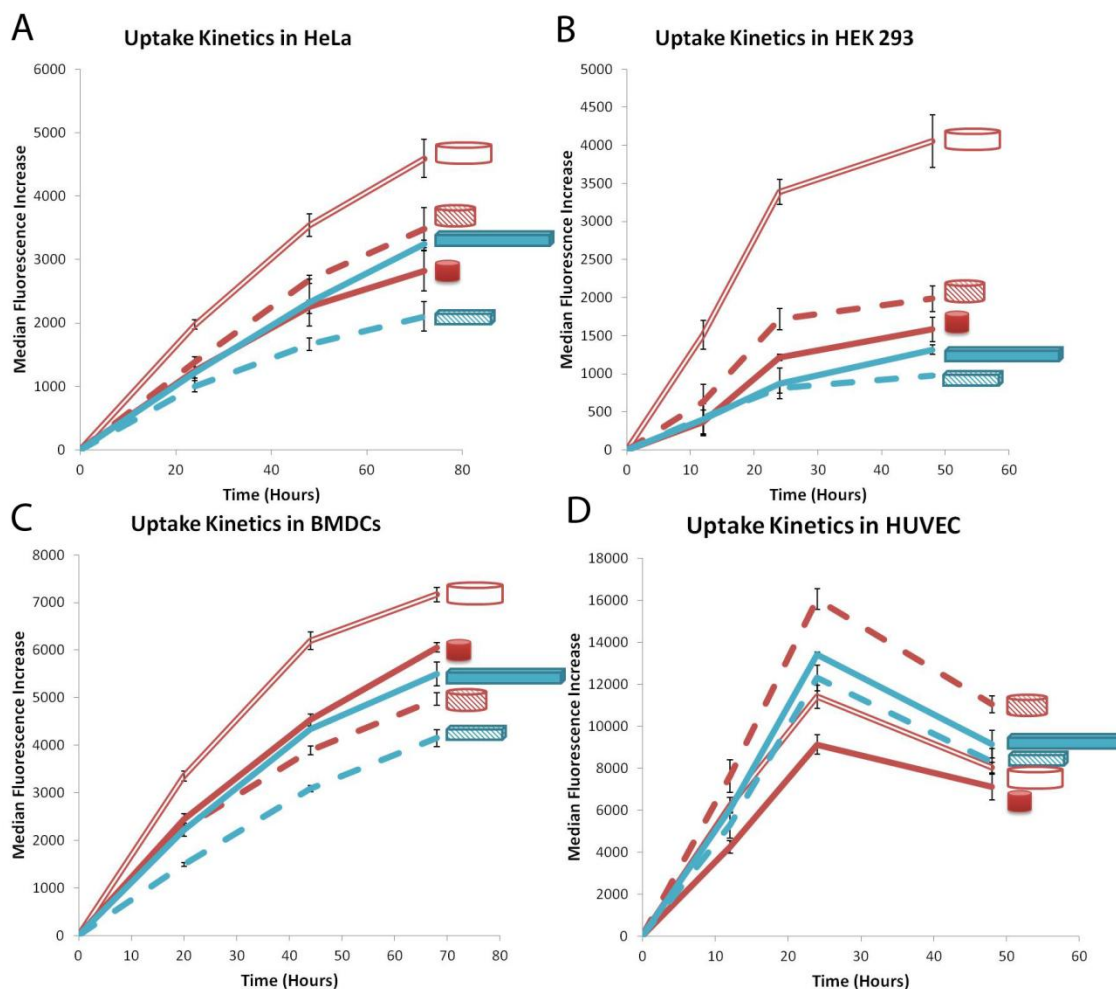


Figure. 4.8: Cellular uptake kinetics of different shape-specific nanoparticles in various cell lines. A) HeLa cells, B) HEK 293 cells, C) HUVEC cells, D) BMDCs. In figure A-D, red lines are for discs (hollow for 325x100nm disc, dashed for 220x100nm disc and solid for 80x70nm disc) and blue lines for rods (dashed for 400x100x100nm rods and solid for 800x100x100nm rods). Error bars are standard deviation with n=3 for each data point.

4.3.5 Inverted Culture Studies

It has been previously reported that sedimentation plays an important role when performing *in vitro* cell-uptake studies (Cho et al., 2011; Teeguarden et al., 2007).

Nanoparticles can form concentration gradients *in vitro* under the influence of gravity, resulting in higher concentrations of particles near the bottom surface of well plates (Cho et al., 2011). This could be a significant factor as to why larger discs and rods, with more weight per particle, are uptaken more efficiently compared to smaller discs and rods. To study this gravitational effect, uptake studies were also performed in an inverted culture model (Fig 4.9). The results indicate that nanodiscs still outperform nanorods and, although the uptake of 325nm discs was significantly reduced, in epithelial cells the 220nm discs outperformed the 80nm ones (Fig 4.9C). Though this difference was not statistically significant in endothelial cells, the mean uptake was still higher for 220nm discs (Fig 4.9D). In contrast, when inverted uptake studies were performed with spherical Polystyrene (PS) beads, smaller diameter beads (100nm compared to 200nm diameter) still showed higher uptake compared to larger diameter beads (Fig 4.9B) (Cho et al., 2011). It is also important to note that in inverted cell cultures, larger particles are at a lower concentration near the cell surface as compared to smaller particles. Yet the fact that an intermediate size disc outperforms both smaller and larger size discs indicates that sedimentation alone cannot explain the observed internalization kinetics of hydrogel nanodiscs and nanorods and that shape plays an important role. A possible explanation is that for disc and rod-shaped nanoparticles, larger size provides larger surface-contact areas for multivalent interactions with the cell membrane. This effect may increase the probability of initiating cellular uptake. For spherical nanoparticles, such interactions are minimal as there is a smaller contact area (theoretically only a point-contact) irrespective of the size of the particle and therefore, smaller nanoparticles, which require less membrane activation, are uptaken more efficiently.

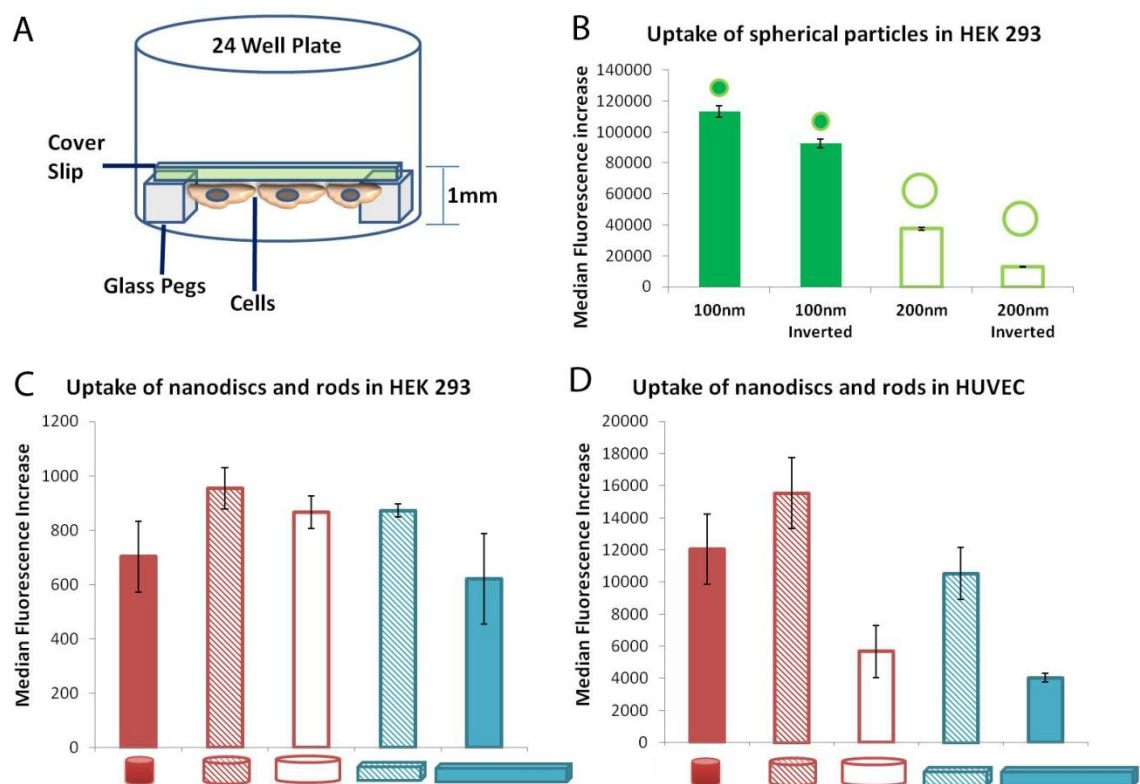


Figure. 4.9: Inverted Culture Uptake studies: Shape still matters. A) Experimental setup for uptake studies in inverted conditions B) Inverted cellular uptake of spherical polystyrene beads after 24 hours in HEK 293. Inverted cellular uptake of shape specific nanoparticles after 24 hours in C) HEK 293 cells, D) HUVEC cells. In figure b, hollow green bars are for 200nm diameter spherical polystyrene bead and solid green bars are for 100nm diameter spherical polystyrene bead. In figure c-d, red bars are for discs (hollow red bars for 325nm x 100nm disc, dashed red bars for 220nm x 100nm disc and solid red bars for 80nm x 70nm disc) and blue bars for rods (dashed blue bars for 400nm x 100nm x 100nm and solid blue bars for 800nm x 100nm x 100nm). Error bars are standard deviation with n=3 for each data point.

This hypothesis also suggests that for non-spherical particles, soluble proteins in media can potentially compete for interaction sites and thereby decrease uptake. To test the effects of soluble proteins on uptake, we performed uptake experiments in medium containing different amounts of serum (0, 10 and 50%) and found our hypothesis to be

true, with the highest uptake seen in serum free media and the lowest in 50% serum medium (Supplementary Fig. 4.10).

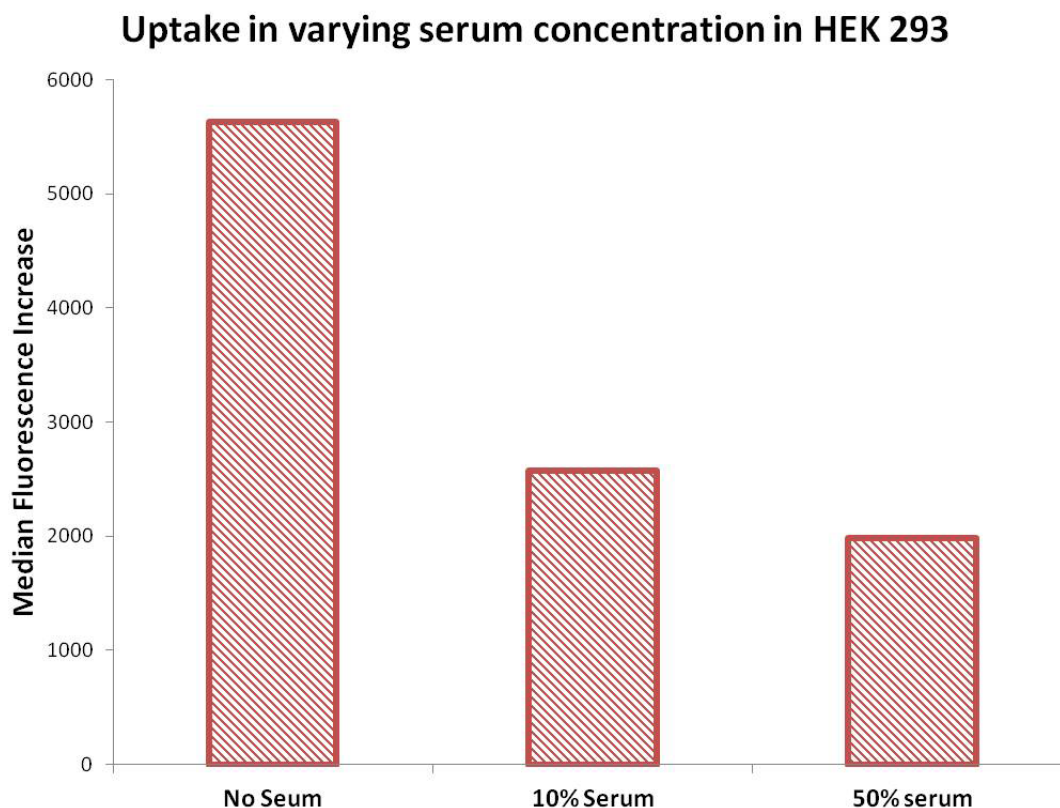


Figure 4.10: Effect of serum concentration on uptake of 220 nm x 100 nm disc shaped nanoparticles by HEK 293 cells after 24 hours. Plot showing effect of serum concentration on uptake of nanoparticle by HEK 293 after 24 hour of incubation.

4.3.6 Pharmacological Inhibition Studies

To further understand the specific mechanisms involved in cellular internalization of nanohydrogels, pharmacological inhibitors were used to interfere with various uptake pathways. It should be noted that inhibitory effects of these agents are cell-type

dependent (Vercauteren et al., 2010). Five types of inhibitors were chosen based on their selectivity and applications (Fig. 4.11). Inhibitor concentrations were optimized to achieve a minimum of 90% cell viability over 8 hours for both epithelial and endothelial cells. In both cell-types (Fig. 4.11B-C), macropinocytosis was found to be the common internalization pathway. Interestingly, in HEK cells, nanodiscs (but not nanorods) were also internalized using caveolae-mediated endocytosis. This could partially explain why discs outperformed rods. Since the caveolae pathway is involved in transcytosis, this has significant implications in delivering therapeutic and diagnostic agents across epithelial barriers (Kim and Malik, 2003).

In contrast to epithelial cells, HUVECs used macropinocytosis and clathrin-mediated pathways for both nanorods as well as nanodiscs and were affected by pathway inhibition to a larger extent than epithelial cells. This can either indicate that these two pathways play a more efficient role in nanoparticle uptake or that there is a more complete inhibition in HUVECs. For spherical PS beads of different sizes (100nm, 200nm and 500nm; Fig. 4.12), the inhibition studies indicated that cells utilize multiple uptake pathways for nanospheres depending on their size, including clathrin-mediated (200nm and 500nm), macropinocytosis (all sizes), and caveolae-mediated (200nm). It should be noted that the PS beads used have different surface and bulk material composition compared to the non-spherical nanoparticles.

A	Inhibitor	Cellular Mechanism Inhibited	Concentration used		Time used
			HEK 293	HUVEC	
	Chlorpromazine	Clathrin	30 μ M	28 μ M	6 hour
	Amiloride	Macropinocytosis	850 μ M	800 μ M	6 hour
	Cystochalsin D	Macropinocytosis	150nM	500nM	6 hour
	Nocodazole	Microtubules	20 μ M	13 μ M	6 hour
	Filipin	Caveolae	50 μ g/ml	40 μ g/ml	6 hour

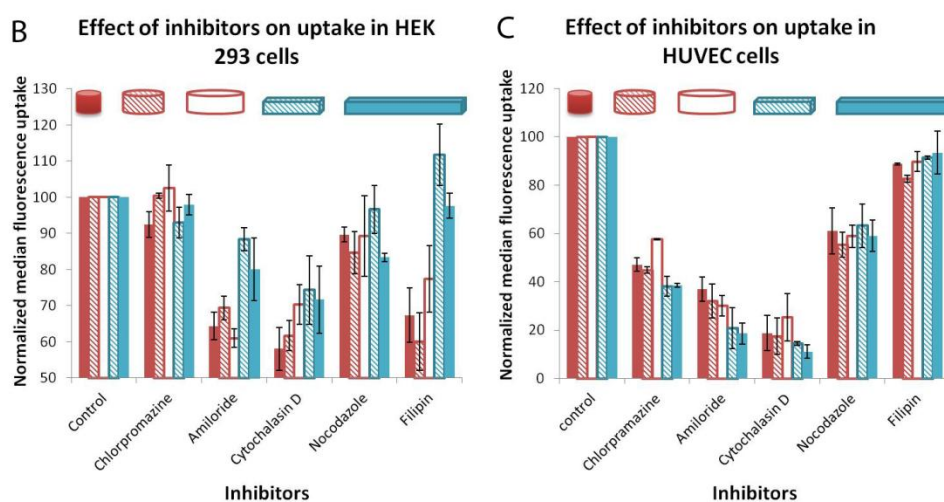


Figure. 4.11: Effect of pharmacological inhibitors on uptake of various shape-specific nanoparticles A) Inhibitors used (with function and concentration) for the uptake experiments. B-C) Change in normalized median fluorescence uptake due to presence of inhibitors in HEK 293 and HUVEC cells. Error bars are standard deviation with n=5 for each data point. Red bars are for discs (solid for 80nm diameter discs, dashed for 220nm diameter and hollow for 325nm diameter) and blue lines for rods (dashed for 400x100x100nm rods and solid for 800x100x100nm rods).

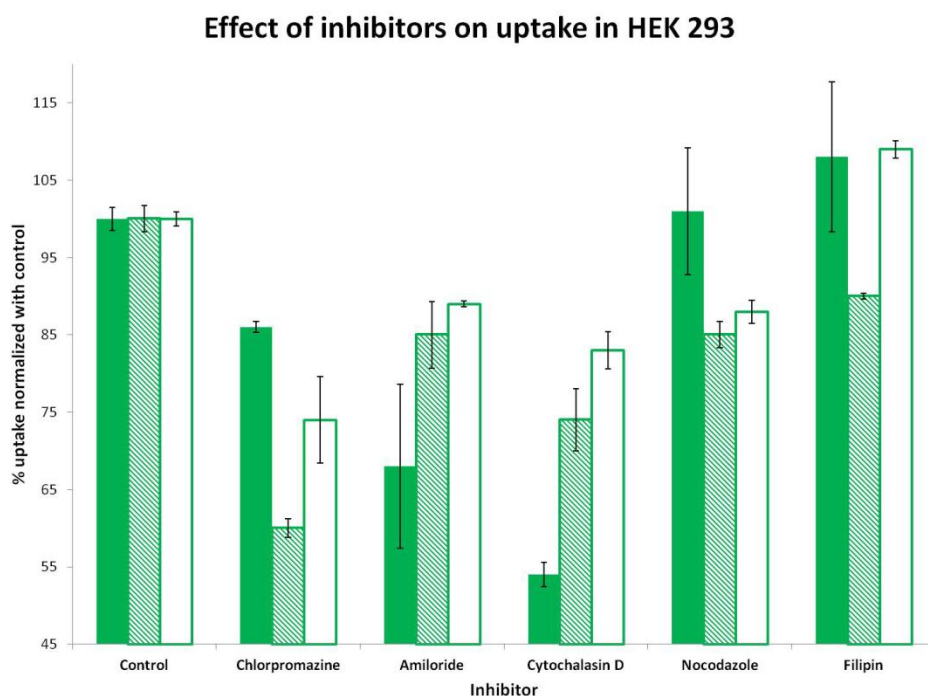


Figure. 4.12: Effect of Pharmacological Inhibitors on uptake of spherical polystyrene nanoparticles. Change in normalized median fluorescence uptake due to presence of inhibitors in HEK 293 Cells. Solid green bars are for 100nm diameter polystyrene beads, dashed green bars are for 200nm diameter polystyrene beads and hollow green bars are for 500nm diameter polystyrene beads. Error bars are standard deviation with n=5 for each data point.

4.3.7 Confocal Microscopy with RPE cells

To further confirm that the clathrin pathway was indeed not involved in epithelial cells, confocal microscopy images were gathered with an epithelial cell line (Retinal Pigment Epithelium (RPE) cells) where the clathrin was labeled with a red fluorescent tag (mCherry). These stably transfected cells were a gift from Dr. Marcel Mettlen at University of Texas Southwestern Medical Center, Dallas. Confocal imaging showed little to no co-localization of nanoparticles with clathrin pits (Fig. 4.13).

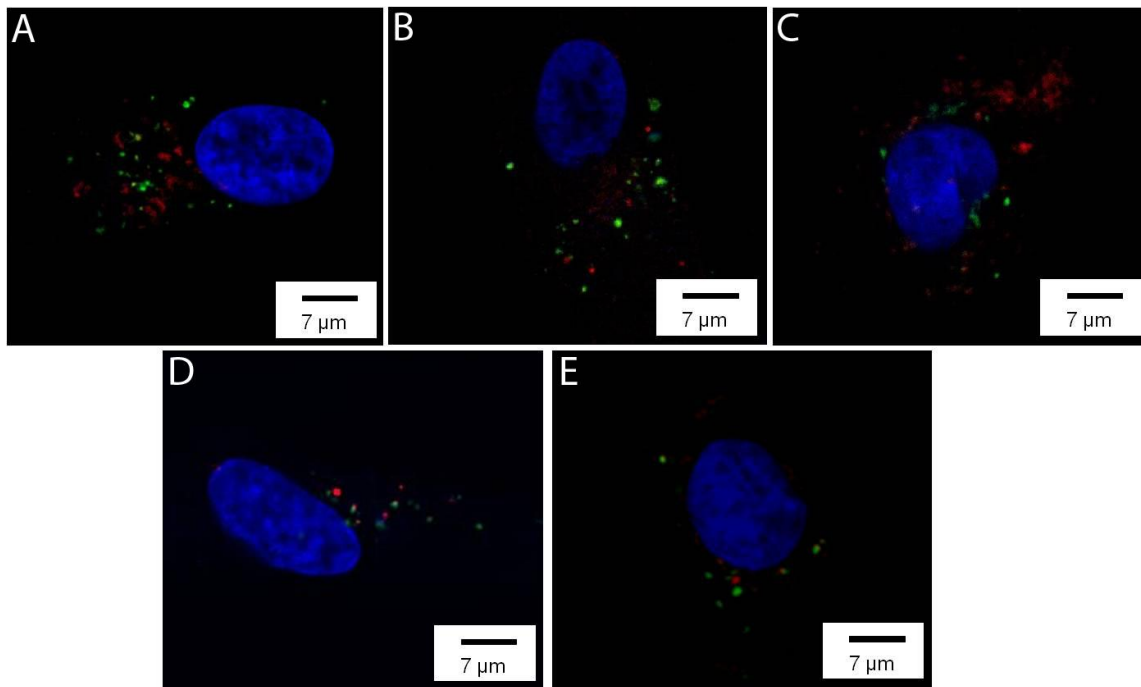


Figure. 4.13: Confocal Microscopy of particle uptake and localization by clathrin labeled RPE cells. Confocal Images of RPE cell lines incubated with shape-specific particles to test the co-localization of particles with clathrin pits. A) 80nm diameter x 70nm height discs, B) 220nm diameter x 100nm height discs, C) 325nm diameter x 100nm height discs, D) 400nm x 100nm x 100nm rods, E) 800nm x 100nm x 100nm rods.

4.4 CONCLUSIONS

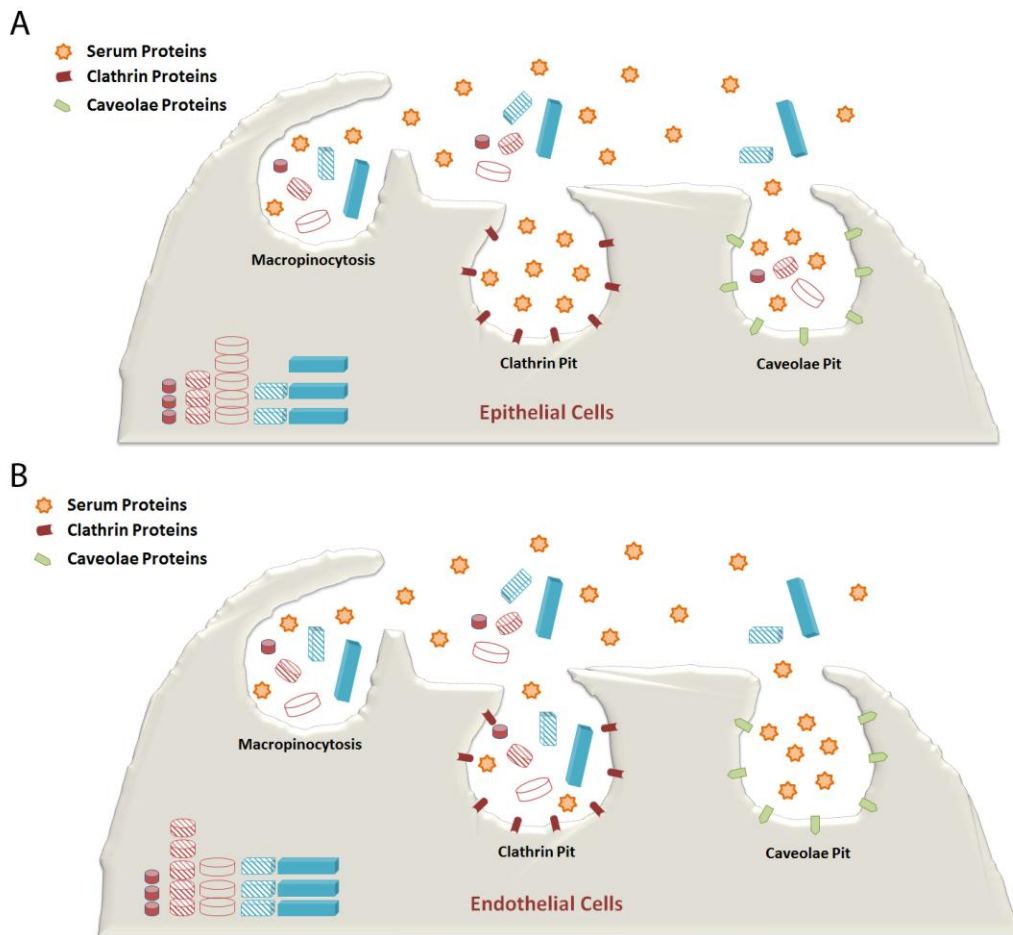


Figure. 4.14: Summary of cell-uptake mechanisms: Illustrative image showing differences in mechanisms and relative efficiencies for cell uptake of shape-specific nanoparticles in A) Epithelial and B) Endothelial cells.

Based on our overall results, Fig. 4 summarizes the uptake mechanisms and relative internalization efficacy of polymeric nanodiscs and nanorods in epithelial and endothelial cells. In conclusion, we demonstrate that there is significant interplay between nanoscale shape and size in cell-uptake of polymeric hydrophilic nanoparticles. In all cell types, nanodiscs of larger or intermediate sizes were internalized more

efficiently compared to nanorods or the smallest size discs. Furthermore, we show that cellular mechanisms for nanohydrogel uptake vary significantly with particle geometry and are cell-type specific. We propose that when nanoparticle surface properties and composition are kept constant, each cell-type can “sense” the nanoscale geometry (both shape and size), trigger unique uptake pathways and thus have different shape-dependent internalization efficiencies. These results provide fundamental insights into the effect of nanoscale shape on cellular uptake and offer unique opportunities for the use of particle geometry as a design criterion to control cellular internalization as well as affect cell targeting, therapeutics and diagnostics delivery, and nanotoxicity.

4.5 REFERENCES

- Agarwal, R., Singh, V., Journey, P., Shi, L., Sreenivasan, S. V., and Roy, K. (2012). Scalable Imprinting of Shape-Specific Polymeric Nanocarriers Using a Release Layer of Switchable Water Solubility. *ACS Nano* 6, 2524-2531.
- Bartczak, D., Nitti, S., Millar, T. M., and Kanaras, A. G. (2012). Exocytosis of peptide functionalized gold nanoparticles in endothelial cells. *Nanoscale* 4, 4470-4472.
- Barua, S., Yoo, J. W., Kolhar, P., Wakankar, A., Gokarn, Y. R., and Mitragotri, S. (2013). Particle shape enhances specificity of antibody-displaying nanoparticles. *Proc Natl Acad Sci U S A*.
- Caldorera-Moore, M., Kang, M. K., Moore, Z., Singh, V., Sreenivasan, S. V., Shi, L., Huang, R., and Roy, K. (2011). Swelling behavior of nanoscale, shape- and size-specific, hydrogel particles fabricated using imprint lithography. *Soft Matter* 7, 2879-2887.
- Champion, J. A., and Mitragotri, S. (2006). Role of target geometry in phagocytosis. *Proc Natl Acad Sci U S A* 103, 4930-4934.
- Chauhan, V. P., Popovic, Z., Chen, O., Cui, J., Fukumura, D., Bawendi, M. G., and Jain, R. K. (2011). Fluorescent nanorods and nanospheres for real-time in vivo probing of nanoparticle shape-dependent tumor penetration. *Angew Chem Int Ed Engl* 50, 11417-11420.

- Chithrani, B. D., and Chan, W. C. (2007). Elucidating the mechanism of cellular uptake and removal of protein-coated gold nanoparticles of different sizes and shapes. *Nano Lett* 7, 1542-1550.
- Chithrani, B. D., Ghazani, A. A., and Chan, W. C. (2006). Determining the size and shape dependence of gold nanoparticle uptake into mammalian cells. *Nano Lett* 6, 662-668.
- Cho, E. C., Zhang, Q., and Xia, Y. (2011). The effect of sedimentation and diffusion on cellular uptake of gold nanoparticles. *Nat Nanotechnol* 6, 385-391.
- Decuzzi, P., Lee, S., Bhushan, B., and Ferrari, M. (2005). A theoretical model for the margination of particles within blood vessels. *Ann Biomed Eng* 33, 179-190.
- Decuzzi, P., Pasqualini, R., Arap, W., and Ferrari, M. (2009). Intravascular delivery of particulate systems: does geometry really matter? *Pharm Res* 26, 235-243.
- Dobson, J. (2006). Gene therapy progress and prospects: magnetic nanoparticle-based gene delivery. *Gene Ther* 13, 283-287.
- dos Santos, T., Varela, J., Lynch, I., Salvati, A., and Dawson, K. A. (2011). Effects of transport inhibitors on the cellular uptake of carboxylated polystyrene nanoparticles in different cell lines. *PLoS One* 6, e24438.
- Ferrari, M. (2005). Cancer nanotechnology: opportunities and challenges. *Nat Rev Cancer* 5, 161-171.
- Geng, Y., Dalhaimer, P., Cai, S., Tsai, R., Tewari, M., Minko, T., and Discher, D. E. (2007). Shape effects of filaments versus spherical particles in flow and drug delivery. *Nat Nanotechnol* 2, 249-255.
- Glangchai, L. C., Caldorera-Moore, M., Shi, L., and Roy, K. (2008). Nanoimprint lithography based fabrication of shape-specific, enzymatically-triggered smart nanoparticles. *J Control Release* 125, 263-272.
- Gratton, S. E., Pohlhaus, P. D., Lee, J., Guo, J., Cho, M. J., and Desimone, J. M. (2007). Nanofabricated particles for engineered drug therapies: a preliminary biodistribution study of PRINT nanoparticles. *J Control Release* 121, 10-18.
- Gratton, S. E., Ropp, P. A., Pohlhaus, P. D., Luft, J. C., Madden, V. J., Napier, M. E., and DeSimone, J. M. (2008). The effect of particle design on cellular internalization pathways. *Proc Natl Acad Sci U S A* 105, 11613-11618.
- He, C., Hu, Y., Yin, L., Tang, C., and Yin, C. (2010). Effects of particle size and surface charge on cellular uptake and biodistribution of polymeric nanoparticles. *Biomaterials* 31, 3657-3666.
- Huang, X., Li, L., Liu, T., Hao, N., Liu, H., Chen, D., and Tang, F. (2011). The shape effect of mesoporous silica nanoparticles on biodistribution, clearance, and biocompatibility in vivo. *ACS Nano* 5, 5390-5399.

- Huang, X., Teng, X., Chen, D., Tang, F., and He, J. (2010). The effect of the shape of mesoporous silica nanoparticles on cellular uptake and cell function. *Biomaterials* 31, 438-448.
- Ivanov, A. I. (2008). Pharmacological inhibition of endocytic pathways: is it specific enough to be useful? *Methods Mol Biol* 440, 15-33.
- Jain, R. K., and Stylianopoulos, T. (2010). Delivering nanomedicine to solid tumors. *Nat Rev Clin Oncol* 7, 653-664.
- Jang, E. S., Shin, J. H., Ren, G., Park, M. J., Cheng, K., Chen, X., Wu, J. C., Sunwoo, J. B., and Cheng, Z. (2012). The manipulation of natural killer cells to target tumor sites using magnetic nanoparticles. *Biomaterials* 33, 5584-5592.
- Jiang, X., Qu, W., Pan, D., Ren, Y., Williford, J. M., Cui, H., Luijten, E., and Mao, H. Q. (2012). Plasmid-Templated Shape Control of Condensed DNA-Block Copolymer Nanoparticles. *Adv Mater*.
- Kim, K. J., and Malik, A. B. (2003). Protein transport across the lung epithelial barrier. *Am J Physiol Lung Cell Mol Physiol* 284, L247-259.
- Loerke, D., Mettlen, M., Schmid, S. L., and Danuser, G. (2011). Measuring the hierarchy of molecular events during clathrin-mediated endocytosis. *Traffic* 12, 815-825.
- Mitragotri, S. (2009). In drug delivery, shape does matter. *Pharm Res* 26, 232-234.
- Nel, A., Xia, T., Madler, L., and Li, N. (2006). Toxic potential of materials at the nanolevel. *Science* 311, 622-627.
- Peer, D., Karp, J. M., Hong, S., Farokhzad, O. C., Margalit, R., and Langer, R. (2007). Nanocarriers as an emerging platform for cancer therapy. *Nat Nano* 2, 751-760.
- Rolland, J. P., Maynor, B. W., Euliss, L. E., Exner, A. E., Denison, G. M., and DeSimone, J. M. (2005). Direct fabrication and harvesting of monodisperse, shape-specific nanobiomaterials. *J Am Chem Soc* 127, 10096-10100.
- Shah, S., Liu, Y., Hu, W., and Gao, J. (2011). Modeling particle shape-dependent dynamics in nanomedicine. *J Nanosci Nanotechnol* 11, 919-928.
- Teeguarden, J. G., Hinderliter, P. M., Orr, G., Thrall, B. D., and Pounds, J. G. (2007). Particokinetics in vitro: dosimetry considerations for in vitro nanoparticle toxicity assessments. *Toxicol Sci* 95, 300-312.
- Tseng, P., Judy, J. W., and Di Carlo, D. (2012). Magnetic nanoparticle-mediated massively parallel mechanical modulation of single-cell behavior. *Nat Methods* 9, 1113-1119.
- van de Ven, A. L., Kim, P., Haley, O., Fakhoury, J. R., Adriani, G., Schmulen, J., Moloney, P., Hussain, F., Ferrari, M., Liu, X., *et al.* (2012). Rapid tumorotropic accumulation of systemically injected plateloid particles and their biodistribution. *J Control Release* 158, 148-155.

Vercauteren, D., Vandenbroucke, R. E., Jones, A. T., Rejman, J., Demeester, J., De Smedt, S. C., Sanders, N. N., and Braeckmans, K. (2010). The use of inhibitors to study endocytic pathways of gene carriers: optimization and pitfalls. *Mol Ther* 18, 561-569.

Chapter 5: Effect of Shape of Nanoparticles on Uptake and Penetration in Spheroids

5.1 INTRODUCTION

In newly formed tumors, vasculatures are immature and leaky. Due to their small size, nanoparticles are capable of passively accumulating around such leaky vasculatures (known as Enhanced Permeability and Retention Effect (EPR)) (Jain and Stylianopoulos, 2010). Such “leaks” allow small particles to extravasate from the vessels into the vicinity of the tumor cells. Additionally, great numbers of nanoparticles accumulate and are retained within the tumor matrix due to poor lymphatic drainage within the site (Peer et al., 2007). This accumulation makes nanoparticles ideal candidates for tumor drug delivery. However, multiple factors make the uniform delivery of particles to all regions of a tumor difficult. Tumors have a very low density vascular network and, hence, large inter-vessel space which makes the uniform delivery of particles to all regions of the tumor difficult. Further, nanoparticles accumulate near the peripheral regions of solid tumors and are unable to penetrate deep inside tumor tissue due to the dense collagen matrix and high interstitial pressure that lies within. The permeability of the vessels may also vary throughout a tumor, potentially leading to an uneven distribution of the particles within the tumor tissue. In order to effectively treat tumors, nanoparticles must be designed such that they are not only able to extravasate through the tumor vasculature, but also penetrate deep inside the dense tumor matrix, composed of collagen, glycosaminoglycans, and proteoglycans.

As diffusion is the primary means of distribution of the particles inside a tumor, various strategies have been investigated to increase the diffusion of particles in order to

overcome interstitial tissue barriers. Kim *et al.* used cylindroids as *in vitro* tumor models to see the effect of surface charge on 6 nm particle penetration inside the tissue matrix (Kim *et al.*, 2010). The group showed that cationic nanoparticles are taken up by proliferating cells and do not penetrate deep into the matrix, while in contrast, anionic particles diffuse quickly into the deep tissue matrix. In another study, Wong *et al.* used a strategy in which the size of nanoparticles shrunk from 100nm to 10nm upon their entrance into the tumor matrix in order to increase the diffusion and penetration of particles in the interstitial tissue (Wong *et al.*, 2011). The 10 nm quantum dots were encapsulated in gelatin coating such that the final size of each nanoparticle was 100 nm. The gelatin was degraded in the presence of proteases which are upregulated in tumor microenvironments, releasing 10 nm quantum dots which diffused rapidly throughout the interstitial spaces of the tumor. Park *et al.* showed that cylindrical gold nanoparticles diffuse more in solid tumors compared to spherical gold nanoparticles after intra-tumor injections (J. Park *et al.*, 2010). When tissue sections were made and stained for blood vessels, spherical particles were found within 400 μm of vessel edges, and rod shaped particles were found up to 1.5 mm away from the blood vessels. Uster *et al.* showed that PEGylated commercially available CAELYX[®] distributed more uniformly in tumors as compared to free doxorubicin drug after 24 hours of administration. The results of the Uster *et al.* experiments indicated that particles with hydrophilic and inert coatings can penetrate deep inside the tumor tissues even at larger size dimension due to low surface interactions with surrounding cells (Uster *et al.*, 1998).

While drugs have shown success *in vitro*, difficulties arise when studying drug penetration *in vivo* in mice tissues due to the high complexity and number of variables present. Recently, spheroids have been proposed as *in vitro* tumor models and are known to closely resemble the architecture, biological properties, and physiological

characteristics of human tumor tissue (Friedrich et al., 2009; Herrmann et al., 2008; Ivascu and Kubbies, 2006; Mueller-Klieser, 1987; Yuhas et al., 1977). Not only do spheroids provide a good model to closely resemble the state of cells in tumor tissues, but also, due to their three dimensional architecture, they provide an opportunity to study tissue penetration and distribution. Here we propose to study the effects of geometry of NPs on diffusion in spheroids acting as *in vitro* tumor models.

5.2 MATERIALS AND METHODS

5.2.1 Spheroid Synthesis (Poly-HEMA)

The spheroids were synthesized as previously described by Ivascu *et al.* (Ivascu and Kubbies, 2006). Briefly, a round-bottom, 96 well plate was coated with 50 μ l 0.5% poly-HEMA in 95% ethanol and air dried at 37° C for 3 days prior to use. 5000 HeLa or HEK-293 cells were then seeded in each well and the plate was centrifuged at 1000rcf for 10 minutes to initiate spheroid formation. Following this, the spheroids were incubated under standard cell culture conditions, at 37° C, 5% CO₂ in humidified incubators, for four days. The media was intermittently changed after every two days.

5.2.2 Spheroid Synthesis (Agarose Gel)

1.6g agarose was weighed and suspended in 100ml of phosphate buffer saline (PBS). The solution was microwaved until all agarose dissolved in the PBS, then 80 μ l was added to each of 40 wells in a tissue culture, flat-bottomed 96 well plate. The solution was air dried at 25° C for 20 minutes to form a gel. Each well was washed twice with 200 μ l of PBS, waiting 10 minutes before and after each wash. Then, 1000-4000

HEK-293 cells were seeded in each well to initiate spheroid formation. Following this, the spheroids were incubated under standard cell culture conditions, at 37° C, 5% CO₂ in humidified incubators, for four days. Another set of spheroids were incubated over an orbital shaker (BT4000 IncuShaker) rotating at 240 rpm under standard cell culture conditions, at 37° C, 5% CO₂ in humidified incubators, for four days. The media was intermittently changed after every two days.

5.2.3 SEM of Spheroids

The spheroids were washed with PBS and then fixed in 4% para-formaldehyde for an hour at room temperature. The spheroids were then twice washed with PBS and dehydrated using a series of graded ethyl alcohols (70%, 90% and 100% for 15 minutes each). This was followed by chemical drying using Hexamethyldisilazane (HMDS). The spheroids were incubated with a 2:1 ratio of 100% ethyl alcohol and HMDS, followed by a 1:2 ratio, and finally 100% HMDS for 15 minutes each. All HMDS reagents were handled in glass containers in the hood. The samples were lastly air dried in a hood for 24 hours and then mounted and imaged using Scanning Electron Microscopy.

5.2.4 2-Photon Microscopy

Three types of polystyrene beads (100 nm, 200 nm, and 500 nm diameter) or previously synthesized shape specific nanoparticles were incubated with spheroids for 48 hours with or without shaking at 240 rpm. After 48 hours, the spheroids were twice washed with PBS to remove any loosely attached particles and then incubated with 4% para-formaldehyde for 30 minutes at room temperature to fix the cells. Spheroids were then again washed with PBS and put inside 0.5mm depth coverwell imaging chambers (Grace Bio-Labs) over a glass slide. 2-photon microscopy was then performed at an

excitation wavelength of 965 nm. Images were taken up to a depth of 200 μm using a 10X objective and voxel size of 4 μm .

5.2.5 Image Analysis

Image stacks were analyzed using ImageJ (NIH). Total particle association with spheroids was computed by counting the pixel intensity in all images and subtracting the background intensity obtained from untreated spheroids. For radial distribution of particles, a customized script in ImageJ was used to generate radial intensity plots. Average radial intensities were obtained by adding the pixel intensities at a given radius and dividing by the number of pixels. Distances were normalized by the spheroid radius at which greatest pixel intensity was found, and fluorescence intensities were normalized by the maximum fluorescence intensity.

5.2.6 Flow Cytometry Analysis

Three types of polystyrene beads (100 nm, 200 nm, and 500 nm diameter) or previously synthesized shape specific nanoparticles were incubated with spheroids for 48 hours with or without shaking at 240 rpm. After 48 hours, 3 spheroids were pooled together and twice washed with PBS to remove any loosely attached particles and then incubated with 100 μl of 6 mg/ml Collagenase D solution in trypsin for 10 minutes. Trypsin was neutralized by adding 100 μl of media, and dissociated into single cells by gentle pipetting with a micropipette. Cells were then washed with phosphate buffer saline (PBS) and resuspended in 2% FACS buffer (2% FBS in PBS). Flow cytometry was performed using an Accuri C6 Cytometer (BD AccuriTM). All conditions were tested in triplicates. Change in median fluorescence was calculated and plotted against time.

5.3 RESULTS

5.3.1 Spheroid Formation

Spheroids were successfully formed in both static and rotator conditions, as shown in figure 5.1 below.

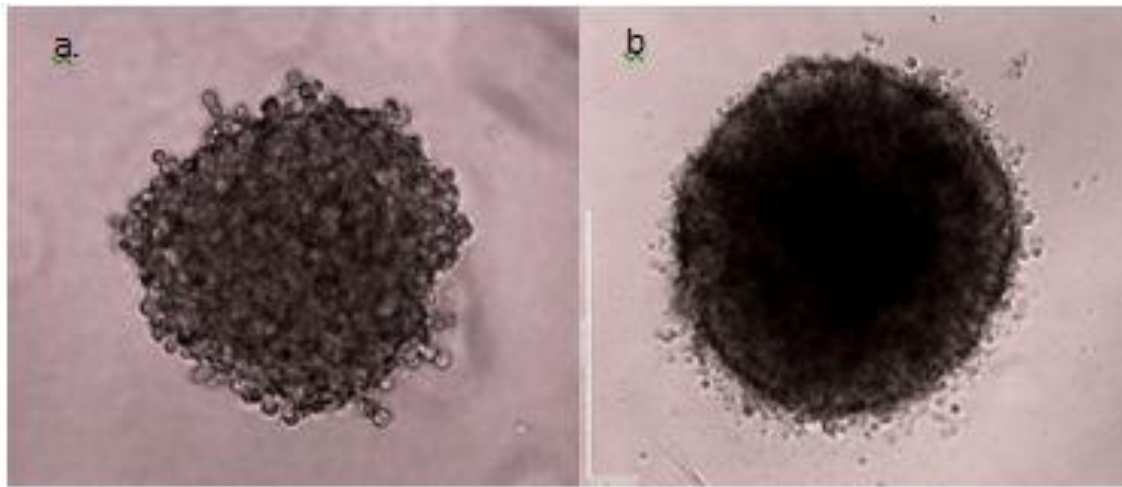


Figure 5.1: Light microscopy images of Spheroids cultured over PolyHEMA under static conditions a) HeLa spheroid on day one b) HeLa spheroid on day four

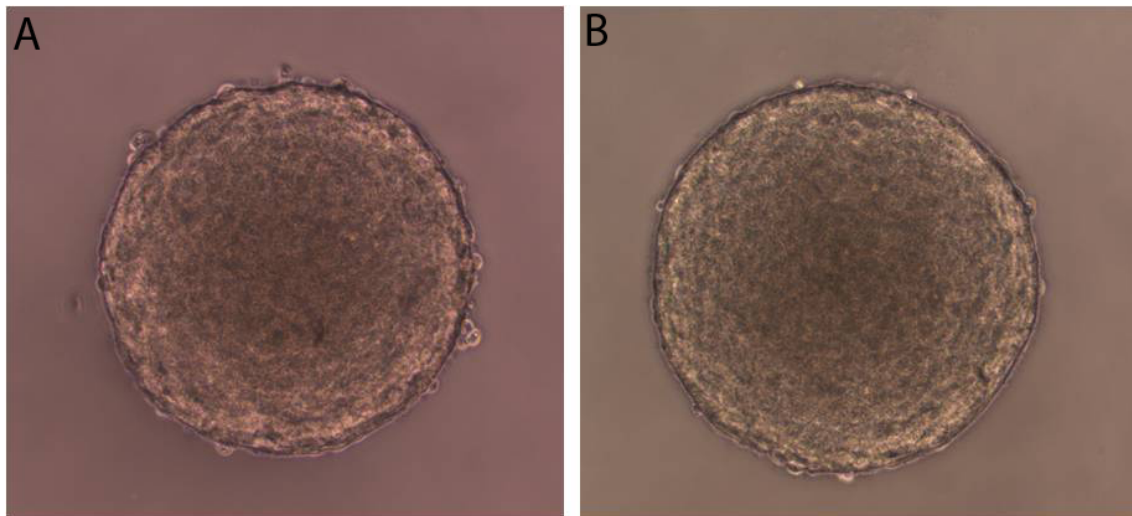
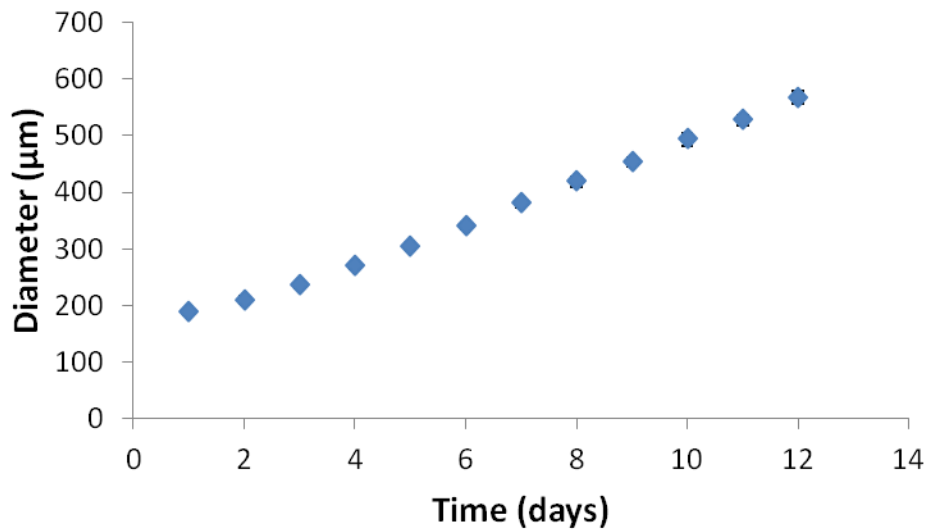


Figure 5.2: Light microscopy images of HEK spheroids cultured over 2% agarose gel under A) static conditions for 72 hours and B) rotatory shaker for 72 hours at 240rpm.

Average Diameter in Static Condition



Average Diameter in Shaker Condition

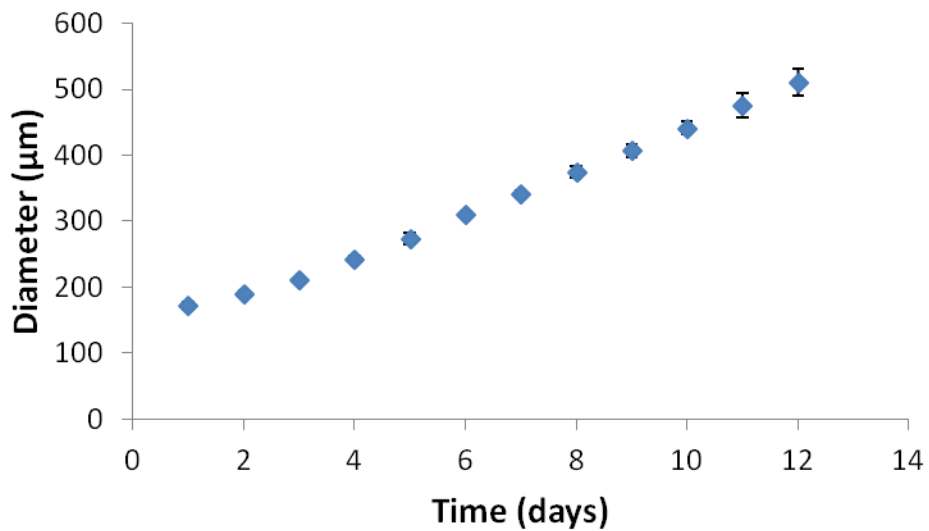


Figure 5.3: Growth Kinetics of spheroids showing change in diameter of spheroids grown in A) static conditions and B) rotatory shaker at 240rpm.

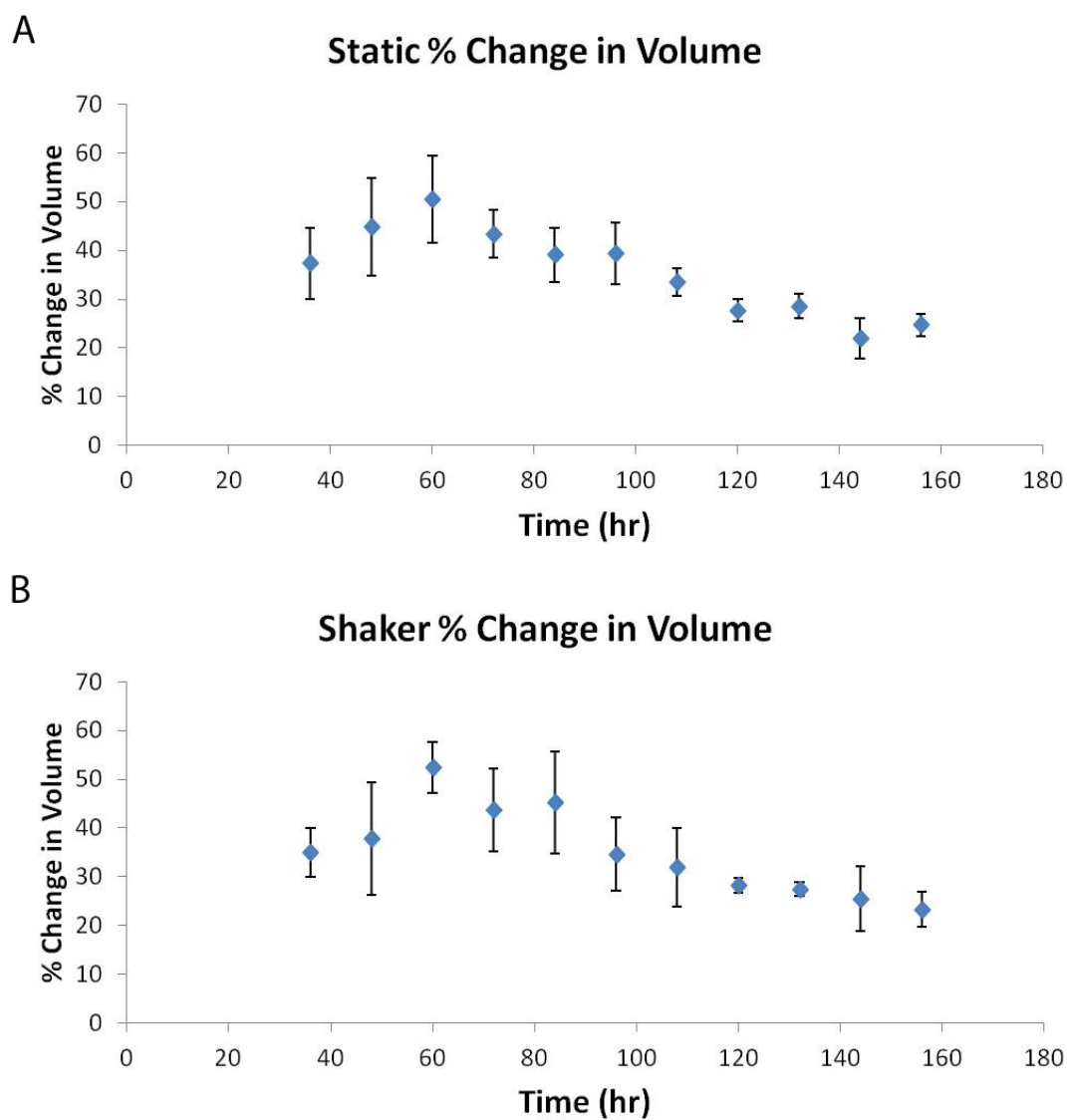


Figure 5.4: Growth Kinetics of spheroids showing percent change in volume of spheroids grown in A) static conditions and B) on rotatory shaker at 240rpm.

SEM images of spheroids were successfully obtained and showed the presence of dense networks of cells within the extracellular matrix.

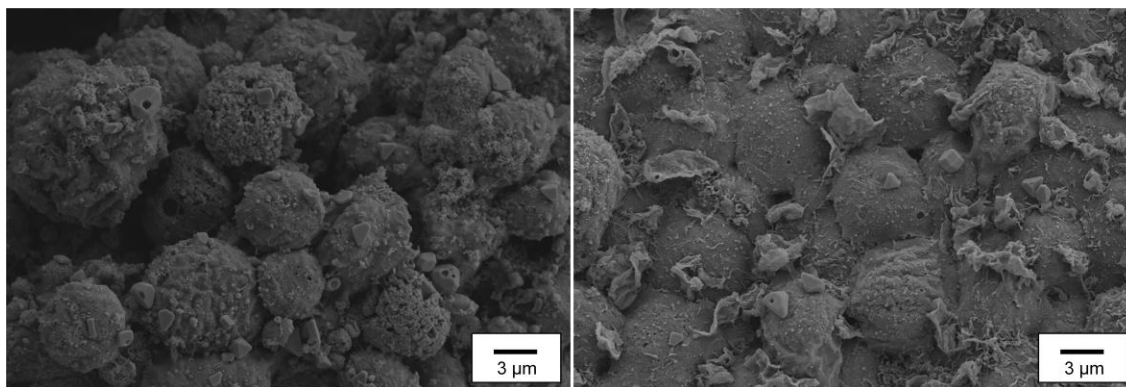


Figure 5.5: Scanning Electron Microscopy images of HEK spheroid cultured over 2% agarose gel on rotatory shaker for 72 hours at 240rpm.

5.3.2 2-Photon Microscopy

Particles were successfully shown to be associated with spheroids. Polystyrene particles were first examined using 100, 200 and 500 nm diameter beads. All three sizes of beads displayed association with spheroids. However, beads only localized near the surface of each spheroid and did not show deep penetration. Figure 5.6 shows characteristic images of spheroids near the center. Total pixel intensity associated with each spheroid was counted and normalized per slice (4 μm depth) to compare between different particle sizes, as shown in figure 5.7. To study the radial distribution of particles, circles were drawn around the spheroids (Fig 5.8) and custom imageJ script was used to find average characteristic pixel intensity as a function of distance from the center. Both the distance from the center and pixel intensity were normalized to compare across different conditions. No significant difference in particle penetration depth for different sizes of polystyrene beads was found. This can be attributed to the fact that these beads are hydrophobic and get stuck to the cell membrane, thereby limiting their penetration (Fig 5.9).

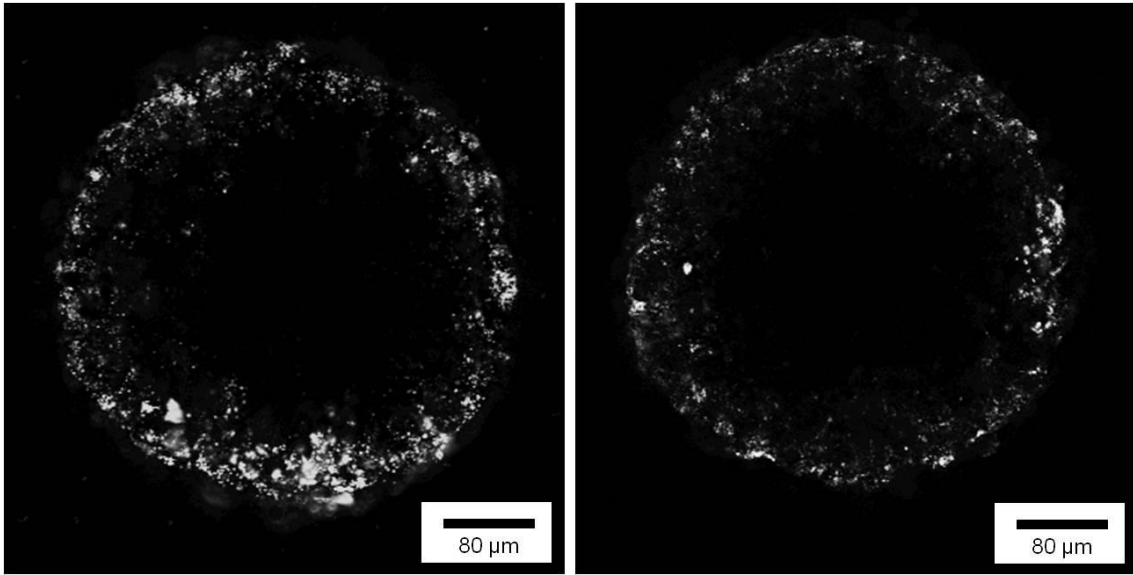


Figure 5.6: 2-Photon microscopy images of spheroids at 200 μm deep from the top edge of the spheroids incubated with A) 200 nm polystyrene beads and B) 500 nm polystyrene beads.

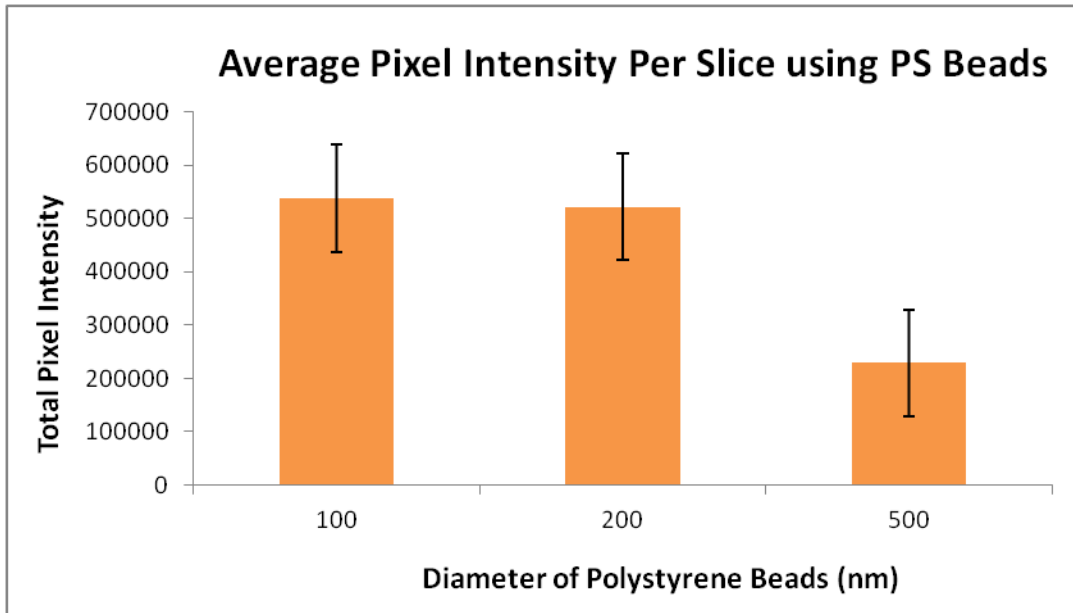


Figure 5.7: Graph showing comparison of normalized pixel intensity associated with spheroid per slice with different diameter polystyrene beads

Radial Intensity of Polystyrene Beads

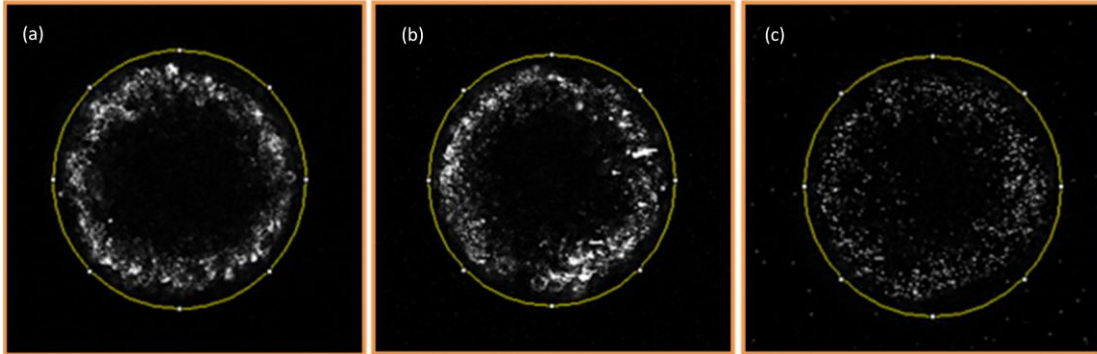


Figure 5.8: Picture showing spheroid optical sections at 120 μm depth and an area selection circle used to compute the radial intensity distribution for polystyrene beads of diameters A) 100 nm, B) 200 nm and C) 500 nm.

Radial Intensity Distribution

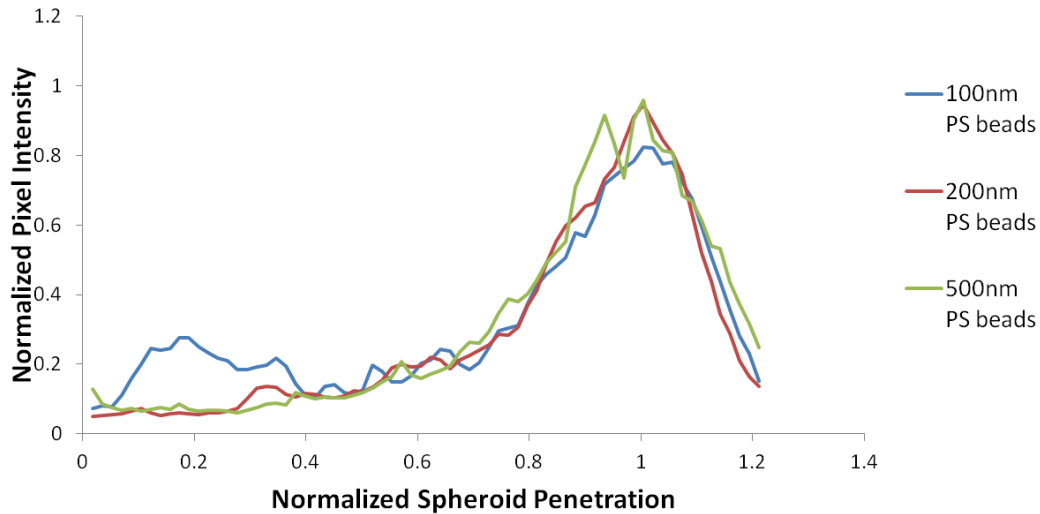


Figure 5.9: Normalized radial intensity distribution of polystyrene nanoparticles as a function of distance from the center of the spheroid.

Similar experiments were performed on PEG based shape specific particles and preliminary results show differences in penetration depth of disc shaped particles, as

shown in Figure 5.10. Since PEG is an inert material, it is expected to interact less with the cell membrane and hence penetrate deeper into dense tissue matrixes.

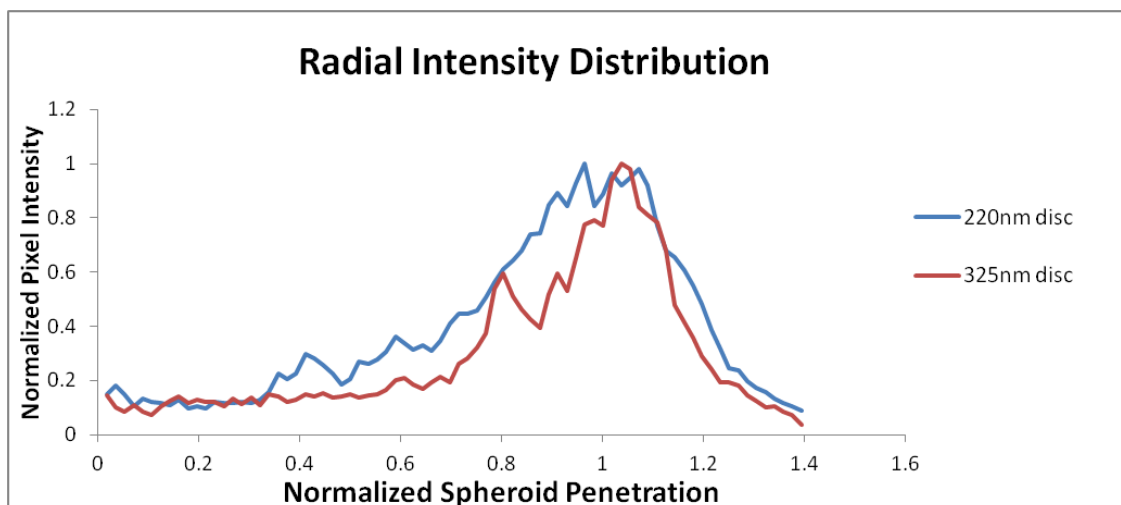


Figure 5.10: Normalized radial intensity distribution of Disc-shaped nanoparticles as a function of distance from the center of the spheroid.

5.3.3: Flow Cytometry

Particle association with spheroids was quantified using flow cytometry. Polystyrene particles were examined using 100, 200 and 500 nm diameter beads. All beads showed association with spheroids. Surprisingly, 200 nm polystyrene beads showed nearly equal uptake as 100 nm beads (figure 5.11), which was not seen in 2D cultures (as seen in chapter 4). However, we also saw a similar trend when spheroids were analyzed using 2-photon microscopy, and hence this trend seems to be consistent with 3D models.

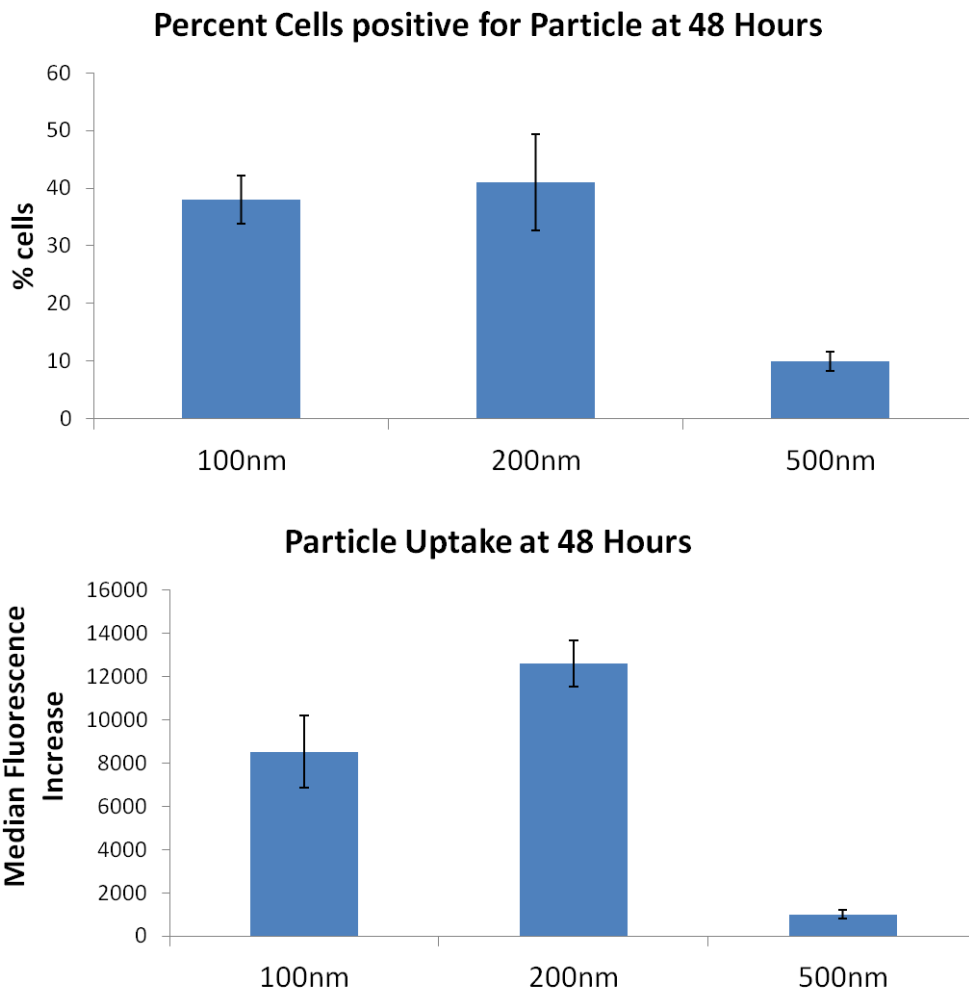


Figure 5.11: Graph showing comparison of particle association with spheroid after 48 hours of incubation with different size polystyrene beads analyzed using flow cytometry.

5.4 CONCLUSIONS

In conclusion we demonstrate that 3-D tumor models, spheroids, can be successfully formed and used to carry out various uptake tests with nanoparticles. Polystyrene beads of 100, 200 and 500 nm were first used to see the effect of size on uptake by HEK 293 spheroids. In contrast to 2D tissue plate cultures, 3D models showed that 200 nm beads were equally uptaken by cells as compared to 100 nm beads. This was

verified using both imaging and flow cytometry. Surprisingly, when penetration into the spheroids was studied using 2-photon microscopy, none of the sizes showed any discernable differences in amount of penetration into the spheroids. This could be attributed to the hydrophobic nature of the beads, which could result in strong association with cell membranes and hence inhibition in penetration. When similar experiments were performed using hydrophilic PEG based particles of disc shape, 220 nm diameter discs showed enhanced penetration compared to 325 nm discs. These results show that hydrophilic particles can more deeply penetrate into the spheroids.

5.5 REFERENCES

- Friedrich, J., Seidel, C., Ebner, R., and Kunz-Schughart, L. A. (2009). Spheroid-based drug screen: considerations and practical approach. *Nat Protoc* 4, 309-324.
- Herrmann, R., Fayad, W., Schwarz, S., Berndtsson, M., and Linder, S. (2008). Screening for Compounds That Induce Apoptosis of Cancer Cells Grown as Multicellular Spheroids. *Journal of Biomolecular Screening* 13, 1-8.
- Ivascu, A., and Kubbies, M. (2006). Rapid generation of single-tumor spheroids for high-throughput cell function and toxicity analysis. *J Biomol Screen* 11, 922-932.
- J. Park, A. Estrada, J. A. Schwartz, P. Diagaradjane, S. Krishnan, A. K. Dunn, and Tunnell, J. W. (2010). Intra-Organ Biodistribution of Gold Nanoparticles Using Intrinsic Two-Photon-Induced Photoluminescence. *Lasers in Surgery and Medicine* 42, 630-639.
- Jain, R. K., and Stylianopoulos, T. (2010). Delivering nanomedicine to solid tumors. *Nat Rev Clin Oncol* 7, 653-664.
- Kim, B., Han, G., Toley, B. J., Kim, C. K., Rotello, V. M., and Forbes, N. S. (2010). Tuning payload delivery in tumour cylindroids using gold nanoparticles. *Nat Nanotechnol* 5, 465-472.
- Mueller-Klieser, W. (1987). Multicellular spheroids. A review on cellular aggregates in cancer research. *J Cancer Res Clin Oncol* 113, 101-122.
- Peer, D., Karp, J. M., Hong, S., Farokhzad, O. C., Margalit, R., and Langer, R. (2007). Nanocarriers as an emerging platform for cancer therapy. *Nat Nano* 2, 751-760.

- Uster, P. S., Working, P. K., and Vaage, J. (1998). Pegylated liposomal doxorubicin (DOXIL®, CAELYX®) distribution in tumour models observed with confocal laser scanning microscopy. *International Journal of Pharmaceutics* *162*, 77-86.
- Wong, C., Stylianopoulos, T., Cui, J., Martin, J., Chauhan, V. P., Jiang, W., Popovic, Z., Jain, R. K., Bawendi, M. G., and Fukumura, D. (2011). Multistage nanoparticle delivery system for deep penetration into tumor tissue. *Proc Natl Acad Sci U S A* *108*, 2426-2431.
- Yuhas, J. M., Li, A. P., Martinez, A. O., and Ladman, A. J. (1977). A simplified method for production and growth of multicellular tumor spheroids. *Cancer Res* *37*, 3639-3643.

Chapter 6: Conclusions and Future Work

6.1 RESEARCH SUMMARY

The aim of this dissertation was to fabricate and evaluate the effect of shape and size of nanoparticles for biomedical applications. Jet and Flash Imprint lithography (J-FIL) was shown as a biocompatible and high throughput methods to fabricate nanoparticles with precise geometry. Various biomolecules were shown to be encapsulated and effect of shape on internalization by mammalian cells was studied. Finally 3D tumor models were used to study particle uptake by cells in a 3D micro-environment and their penetration into tissue models was evaluated.

6.2 CONCLUSIONS AND FUTURE DIRECTIONS

6.2.1: Fabrication of Particles

In chapter 3, the J-FIL process was optimized to fabricate nanoparticles at high throughput. Poly (Acrylic Acid) (PAA) was shown to be a highly versatile release layer for UV based nanoimprint lithography of biocompatible polymers. The water solubility of PAA is can be switched by exchanging monovalent and divalent cations. This feature allows for large scale, repeatable, high-fidelity imprinting of nanoparticles and nanostructures in both water and organic solvent-based imprint solutions. In addition, the J-FIL method allows aqueous environment-based surface-functionalization of imprinted particles directly on the imprint substrate as well as a simple method for particle release in water-based solutions. It offers advantages over other organic solvent-based sacrificial layers that may not be biocompatible because of the exposure of the particles to acetone, toluene, or other toxic solvents during the fabrication process. Moreover, with the use of

a small-molecular weight PEGDA, the residual layer thickness was reduced to below 10 nm so as to minimize wastage of expensive biomaterials *via* plasma etching of the residual layer. In addition, successful encapsulation and release kinetics of model small molecule drugs was demonstrated. These results represent important advancements toward high-throughput, biocompatible fabrication of drug nanocarriers and nanostructures using top-down nanoimprint lithography.

In future, various shapes such as triangles and different aspect ratio rods and discs need to be synthesized to provide a comprehensive data set so as to better predict and model the effects of particle shape on cellular uptake. The Imprinting process also needs to be optimized to result in wafer scale production. Although some scale up was shown in chapter 3, but the amount of particles needed for animal studies is still significantly more than what can be achieved from one wafer worth of particles. Imprio 1100, an improved version of Imprio 100, is already being used utilizing a similar process and needs to be adapted for this purpose, as it can result in a 100 times enhancement of particle dose fabricated for a given time. The Imprio 1100 process would make it possible to obtain enough particles to perform nanoparticle bio-distribution and tumor therapeutic studies in mice. Elasticity and charge of nanoparticles can also be varied to produce particles of different elastic moduli and charges to see the effects of these parameters on the internalization and uptake mechanisms of shape specific particles. Further surface chemistries need to be developed that allow for surface modification of nanoparticles with specific ligands such as peptides, proteins and antibodies.

6.2.2: Cellular Uptake Studies

In chapter 4, it was demonstrated that there is significant interplay between nanoscale shape and size in cell-uptake of polymeric hydrophilic nanoparticles. Particles were tested in epithelial, endothelial and immune cells and in all cell types, nanodiscs of larger or intermediate sizes were internalized more efficiently compared to nanorods or the smallest size discs. Furthermore, it was shown that cellular mechanisms for nanohydrogel uptake vary significantly with particle geometry and are cell-type specific. While epithelial cells showed higher uptake for all discs shaped nanoparticles compared to equal size rods, the same trend was not true for endothelial cells. 325nm diameter disc shaped particles were found to outperform smaller diameter discs in epithelial cells, whereas an intermediate diameter disc of 220nm was shown to be most efficiently uptaken in endothelial cells. Further, the differences in uptake between different geometries were partially explained by the uptake mechanisms that cells utilize in epithelial cells. This indicates that when nanoparticle surface properties and composition are kept constant, each cell-type can “sense” the nanoscale geometry (both shape and size), trigger unique uptake pathways, and thus have different shape-dependent internalization efficiencies. These results provide fundamental insights into the effects of nanoscale shape on cellular uptake and offer unique opportunities for the use of particle geometry as a design criterion to control cellular internalization and affect cell targeting, therapeutics and diagnostics delivery, and nanotoxicity.

Uptake studies needs to be done with newer shapes to understand the science and physics behind the uptake mechanisms of shape specific particles. As previously described, all internalization and uptake mechanism studies should be performed with particles of different elasticity, charge and surface ligands. It will be interesting to see if

whether, due to the presence of specific ligands on the particle surface, the effects seen with shape are enhanced or diminished.

In chapter 5, effects of shape and surface properties of nanoparticles were evaluated in 3-D tumor models, spheroids. Spherical polystyrene beads of 100, 200 and 500 nm were first used to see the effect of size on uptake by HEK 293 spheroids. In contrast to 2D tissue plate cultures, 3D models showed that 200 nm beads were equally uptaken by cells when compared to 100 nm beads. This was verified using both imaging and flow cytometry. When penetration into the spheroids was studied using 2-photon microscopy, surprisingly there were no discernable differences between any of the sizes in the amount of penetration into the spheroids. This can be attributed to the hydrophobic nature of the beads, which could result in strong association with cell membranes and hence inhibition of penetration. When similar experiments were done using hydrophilic PEG based particles of disc shape, 220 nm diameter discs showed enhanced penetration compared to 325 nm discs. This shows that hydrophilic particles can result in deeper penetration into spheroids.

Penetration and uptake studies in spheroids should be performed with all shape-specific particles. These studies will give us a better idea of the behavior of nanoparticles in 3D models. These studies should also be conducted with particles of different elasticity, charge and surface ligands. Additionally, bio-distribution studies after tail vein administration of nanoparticles should be performed in both healthy and tumor bearing mice. An intra-tumoral distribution study should also be performed to demonstrate the influence of shape on particle distribution. Finally, drug loaded particles should be used to evaluate their therapeutic potentials for cancer treatment.

Glossary

ABBREVIATIONS

Da	Dalton
DH ₂ O	Deionized Water
DMEM	Dulbecco's Modified Eagle Medium
DMSO	Dimethyl Sulfoxide
DNA	Deoxyribonucleic Acid
EPR	Enhanced Permeability and Retention Effect
FBS	Fetal Bovine Serum
FSAM	Fluoriated Self Assembled Monolayer
GFLGK-DA	Glycine-Phenylalanine-Leucine-Glycine-Lysine- Diacrylate
HEK	Human Embryonic Kidney
I100	Imprio 100
I2959	2-hydroxy-1-[4-(hydroxyethoxy) phenyl]-2-methyl-1 propanone
J-FIL	Jet and Flash Imprint Lithography
MW	Molecular Weight
NIL	Nano-Imprint Lithography
PAA	Poly(acrylic acid)
PEG	Poly(ethylene glycol)
PEGDA	Poly(ethylene glycol) diacrylate
PEI	Polyethylenimine
PRINT	Particle Replication on Non-Wetting Templates
PVA	Poly(vinyl alcohol)
RIE	Reactive Ion Etching
RPM	Revolution per Minute

SEM	Scanning Electron Microscopy
Si	Silicon
siRNA	Small Interfering RNA
TEM	Transmission Electron Microscopy
UV	Ultraviolet

References

- Acharya, G., Shin, C. S., McDermott, M., Mishra, H., Park, H., Kwon, I. C., and Park, K. (2010). The hydrogel template method for fabrication of homogeneous nano/microparticles. *J Control Release* *141*, 314-319.
- Agarwal, R., Singh, V., Journey, P., Shi, L., Sreenivasan, S. V., and Roy, K. (2012). Scalable Imprinting of Shape-Specific Polymeric Nanocarriers Using a Release Layer of Switchable Water Solubility. *ACS Nano* *6*, 2524-2531.
- Albanese, A., Tang, P. S., and Chan, W. C. (2012). The effect of nanoparticle size, shape, and surface chemistry on biological systems. *Annu Rev Biomed Eng* *14*, 1-16.
- Arvizo, R. R., Miranda, O. R., Thompson, M. A., Pabelick, C. M., Bhattacharya, R., Robertson, J. D., Rotello, V. M., Prakash, Y. S., and Mukherjee, P. (2010). Effect of nanoparticle surface charge at the plasma membrane and beyond. *Nano Lett* *10*, 2543-2548.
- Bailey, T., Choi, B., Colburn, M., Meissl, M., Shaya, S., Ekerdt, J. G., Sreenivasan, S. V., and Willson, C. G. (2000). Step and flash imprint lithography: Template surface treatment and defect analysis. *Journal of Vacuum Science & Technology B* *18*, 3272-3277.
- Ballou, B., Lagerholm, B. C., Ernst, L. A., Bruchez, M. P., and Waggoner, A. S. (2004). Noninvasive imaging of quantum dots in mice. *Bioconjug Chem* *15*, 79-86.
- Banquy, X., Suarez, F., Argaw, A., Rabanel, J.-M., Grutter, P., Bouchard, J.-F., Hildgen, P., and Giasson, S. (2009). Effect of mechanical properties of hydrogel nanoparticles on macrophage cell uptake. *Soft Matter* *5*, 3984-3991.
- Bartczak, D., Nitti, S., Millar, T. M., and Kanaras, A. G. (2012). Exocytosis of peptide functionalized gold nanoparticles in endothelial cells. *Nanoscale* *4*, 4470-4472.
- Barua, S., Yoo, J. W., Kolhar, P., Wakankar, A., Gokarn, Y. R., and Mitragotri, S. (2013). Particle shape enhances specificity of antibody-displaying nanoparticles. *Proc Natl Acad Sci U S A*.
- Beck, M., Graczyk, M., Maximov, I., Sarwe, E. L., Ling, T. G. I., Keil, M., and Montelius, L. (2002). Improving stamps for 10 nm level wafer scale nanoimprint lithography. *Microelectronic Engineering* *61-62*, 441-448.
- Belting, M. (2003). Heparan sulfate proteoglycan as a plasma membrane carrier. *Trends Biochem Sci* *28*, 145-151.

- Bhattacharya, S., Roxbury, D., Gong, X., Mukhopadhyay, D., and Jagota, A. (2012). DNA conjugated SWCNTs enter endothelial cells via Rac1 mediated macropinocytosis. *Nano Lett* 12, 1826-1830.
- Bhowmick, T., Berk, E., Cui, X., Muzykantov, V. R., and Muro, S. (2012). Effect of flow on endothelial endocytosis of nanocarriers targeted to ICAM-1. *J Control Release* 157, 485-492.
- Brandenberger, C., Muhlfeld, C., Ali, Z., Lenz, A. G., Schmid, O., Parak, W. J., Gehr, P., and Rothen-Rutishauser, B. (2010). Quantitative evaluation of cellular uptake and trafficking of plain and polyethylene glycol-coated gold nanoparticles. *Small* 6, 1669-1678.
- Brannon-Peppas, L., and Blanchette, J. O. (2004). Nanoparticle and targeted systems for cancer therapy. *Adv Drug Deliv Rev* 56, 1649-1659.
- Buyukserin, F., Aryal, M., Gao, J., and Hu, W. (2009). Fabrication of polymeric nanorods using bilayer nanoimprint lithography. *Small* 5, 1632-1636.
- Caldorera-Moore, M., Guimard, N., Shi, L., and Roy, K. (2010). Designer nanoparticles: incorporating size, shape and triggered release into nanoscale drug carriers. *Expert Opin Drug Deliv* 7, 479-495.
- Caldorera-Moore, M., Kang, M. K., Moore, Z., Singh, V., Sreenivasan, S. V., Shi, L., Huang, R., and Roy, K. (2011). Swelling behavior of nanoscale, shape- and size-specific, hydrogel particles fabricated using imprint lithography. *Soft Matter* 7, 2879-2887.
- Callahan, J., and Kopecek, J. (2006). Semitelechelic HPMA copolymers functionalized with triphenylphosphonium as drug carriers for membrane transduction and mitochondrial localization. *Biomacromolecules* 7, 2347-2356.
- Campbell, R. B., Fukumura, D., Brown, E. B., Mazzola, L. M., Izumi, Y., Jain, R. K., Torchilin, V. P., and Munn, L. L. (2002). Cationic charge determines the distribution of liposomes between the vascular and extravascular compartments of tumors. *Cancer Res* 62, 6831-6836.
- Canelas, D. A., Herlihy, K. P., and DeSimone, J. M. (2009). Top-down particle fabrication: control of size and shape for diagnostic imaging and drug delivery. *Wiley Interdiscip Rev Nanomed Nanobiotechnol* 1, 391-404.
- Cedervall, T., Lynch, I., Foy, M., Berggård, T., Donnelly, S. C., Cagney, G., Linse, S., and Dawson, K. A. (2007a). Detailed Identification of Plasma Proteins Adsorbed on Copolymer Nanoparticles. *Angewandte Chemie International Edition* 46, 5754-5756.
- Cedervall, T., Lynch, I., Lindman, S., Berggård, T., Thulin, E., Nilsson, H., Dawson, K. A., and Linse, S. (2007b). Understanding the nanoparticle-protein corona using

- methods to quantify exchange rates and affinities of proteins for nanoparticles. *Proc Natl Acad Sci U S A* *104*, 2050-2055.
- Champion, J. A., Katare, Y. K., and Mitragotri, S. (2007). Particle shape: a new design parameter for micro- and nanoscale drug delivery carriers. *J Control Release* *121*, 3-9.
- Champion, J. A., and Mitragotri, S. (2006). Role of target geometry in phagocytosis. *Proc Natl Acad Sci U S A* *103*, 4930-4934.
- Chauhan, V. P., Popovic, Z., Chen, O., Cui, J., Fukumura, D., Bawendi, M. G., and Jain, R. K. (2011). Fluorescent nanorods and nanospheres for real-time in vivo probing of nanoparticle shape-dependent tumor penetration. *Angew Chem Int Ed Engl* *50*, 11417-11420.
- Chen, Y., Wang, S., Lu, X., Zhang, H., Fu, Y., and Luo, Y. (2011). Cholesterol sequestration by nystatin enhances the uptake and activity of endostatin in endothelium via regulating distinct endocytic pathways. *Blood* *117*, 6392-6403.
- Chithrani, B. D., and Chan, W. C. (2007). Elucidating the mechanism of cellular uptake and removal of protein-coated gold nanoparticles of different sizes and shapes. *Nano Lett* *7*, 1542-1550.
- Chithrani, B. D., Ghazani, A. A., and Chan, W. C. (2006a). Determining the size and shape dependence of gold nanoparticle uptake into mammalian cells. *Nano Lett* *6*, 662-668.
- Chithrani, B. D., Ghazani, A. A., and Chan, W. C. W. (2006b). Determining the Size and Shape Dependence of Gold Nanoparticle Uptake into Mammalian Cells. *Nano Letters* *6*, 662-668.
- Cho, E. C., Zhang, Q., and Xia, Y. (2011). The effect of sedimentation and diffusion on cellular uptake of gold nanoparticles. *Nat Nanotechnol* *6*, 385-391.
- Choi, H. S., Liu, W., Misra, P., Tanaka, E., Zimmer, J. P., Itty Ipe, B., Bawendi, M. G., and Frangioni, J. V. (2007). Renal clearance of quantum dots. *Nat Biotechnol* *25*, 1165-1170.
- Clark, S. J., Higman, V. A., Mulloy, B., Perkins, S. J., Lea, S. M., Sim, R. B., and Day, A. J. (2006). His-384 allotypic variant of factor H associated with age-related macular degeneration has different heparin binding properties from the non-disease-associated form. *J Biol Chem* *281*, 24713-24720.
- Conner, S. D., and Schmid, S. L. (2003). Regulated portals of entry into the cell. *Nature* *422*, 37-44.
- Davis, M. E., Chen, Z., and Shin, D. M. (2008). Nanoparticle therapeutics: an emerging treatment modality for cancer. *Nat Rev Drug Discov* *7*, 771-782.

- Decuzzi, P., Lee, S., Bhushan, B., and Ferrari, M. (2005). A theoretical model for the margination of particles within blood vessels. *Ann Biomed Eng* 33, 179-190.
- Decuzzi, P., Pasqualini, R., Arap, W., and Ferrari, M. (2009). Intravascular delivery of particulate systems: does geometry really matter? *Pharm Res* 26, 235-243.
- Desai, N., Trieu, V., Yao, Z., Louie, L., Ci, S., Yang, A., Tao, C., De, T., Beals, B., Dykes, D., *et al.* (2006). Increased antitumor activity, intratumor paclitaxel concentrations, and endothelial cell transport of cremophor-free, albumin-bound paclitaxel, ABI-007, compared with cremophor-based paclitaxel. *Clin Cancer Res* 12, 1317-1324.
- Discher, D. E., Janmey, P., and Wang, Y. L. (2005). Tissue cells feel and respond to the stiffness of their substrate. *Science* 310, 1139-1143.
- Dobson, J. (2006). Gene therapy progress and prospects: magnetic nanoparticle-based gene delivery. *Gene Ther* 13, 283-287.
- Doherty, G. J., and McMahon, H. T. (2009). Mechanisms of endocytosis. *Annu Rev Biochem* 78, 857-902.
- Domański, D. M., Klajnert, B., and Bryszewska, M. (2004). Influence of PAMAM dendrimers on human red blood cells. *Bioelectrochemistry* 63, 189-191.
- dos Santos, T., Varela, J., Lynch, I., Salvati, A., and Dawson, K. A. (2011). Effects of transport inhibitors on the cellular uptake of carboxylated polystyrene nanoparticles in different cell lines. *PLoS One* 6, e24438.
- Doshi, N., Zahr, A. S., Bhaskar, S., Lahann, J., and Mitragotri, S. (2009). Red blood cell-mimicking synthetic biomaterial particles. *Proc Natl Acad Sci U S A* 106, 21495-21499.
- Dykman, L., and Khlebtsov, N. (2012). Gold nanoparticles in biomedical applications: recent advances and perspectives. *Chem Soc Rev* 41, 2256-2282.
- Edidin, M. (2001). Shrinking patches and slippery rafts: scales of domains in the plasma membrane. *Trends Cell Biol* 11, 492-496.
- Enlow, E. M., Luft, J. C., Napier, M. E., and DeSimone, J. M. (2011). Potent Engineered PLGA Nanoparticles by Virtue of Exceptionally High Chemotherapeutic Loadings. *Nano Letters* 11, 808-813.
- Evans, C. W., Fitzgerald, M., Clemons, T. D., House, M. J., Padman, B. S., Shaw, J. A., Saunders, M., Harvey, A. R., Zdyrko, B., Luzinov, I., *et al.* (2011). Multimodal analysis of PEI-mediated endocytosis of nanoparticles in neural cells. *ACS Nano* 5, 8640-8648.
- Ferrari, M. (2005). Cancer nanotechnology: opportunities and challenges. *Nat Rev Cancer* 5, 161-171.

- Friedrich, J., Seidel, C., Ebner, R., and Kunz-Schughart, L. A. (2009). Spheroid-based drug screen: considerations and practical approach. *Nat Protoc* 4, 309-324.
- Gaur, U., Sahoo, S. K., De, T. K., Ghosh, P. C., Maitra, A., and Ghosh, P. K. (2000). Biodistribution of fluoresceinated dextran using novel nanoparticles evading reticuloendothelial system. *Int J Pharm* 202, 1-10.
- Geng, Y., Dalhaimer, P., Cai, S., Tsai, R., Tewari, M., Minko, T., and Discher, D. E. (2007). Shape effects of filaments versus spherical particles in flow and drug delivery. *Nat Nanotechnol* 2, 249-255.
- Georgieva, J. V., Kalicharan, D., Couraud, P. O., Romero, I. A., Weksler, B., Hoekstra, D., and Zuhorn, I. S. (2011). Surface characteristics of nanoparticles determine their intracellular fate in and processing by human blood-brain barrier endothelial cells in vitro. *Mol Ther* 19, 318-325.
- Glangchai, L. C., Caldorera-Moore, M., Shi, L., and Roy, K. (2008). Nanoimprint lithography based fabrication of shape-specific, enzymatically-triggered smart nanoparticles. *J Control Release* 125, 263-272.
- Gratton, S. E., Pohlhaus, P. D., Lee, J., Guo, J., Cho, M. J., and Desimone, J. M. (2007). Nanofabricated particles for engineered drug therapies: a preliminary biodistribution study of PRINT nanoparticles. *J Control Release* 121, 10-18.
- Gratton, S. E., Ropp, P. A., Pohlhaus, P. D., Luft, J. C., Madden, V. J., Napier, M. E., and DeSimone, J. M. (2008). The effect of particle design on cellular internalization pathways. *Proc Natl Acad Sci U S A* 105, 11613-11618.
- Hamad, I., Al-Hanbali, O., Hunter, A. C., Rutt, K. J., Andresen, T. L., and Moghimi, S. M. (2010). Distinct polymer architecture mediates switching of complement activation pathways at the nanosphere-serum interface: implications for stealth nanoparticle engineering. *ACS Nano* 4, 6629-6638.
- Hamidi, M., Azadi, A., and Rafiei, P. (2008). Hydrogel nanoparticles in drug delivery. *Advanced Drug Delivery Reviews* 60, 1638-1649.
- Han, J., Zern, B. J., Shuvaev, V. V., Davies, P. F., Muro, S., and Muzykantov, V. (2012). Acute and chronic shear stress differently regulate endothelial internalization of nanocarriers targeted to platelet-endothelial cell adhesion molecule-1. *ACS Nano* 6, 8824-8836.
- Harush-Frenkel, O., Debotton, N., Benita, S., and Altschuler, Y. (2007). Targeting of nanoparticles to the clathrin-mediated endocytic pathway. *Biochem Biophys Res Commun* 353, 26-32.
- Harush-Frenkel, O., Rozentur, E., Benita, S., and Altschuler, Y. (2008). Surface charge of nanoparticles determines their endocytic and transcytotic pathway in polarized MDCK cells. *Biomacromolecules* 9, 435-443.

- Hatakeyama, H., Akita, H., Kogure, K., Oishi, M., Nagasaki, Y., Kihira, Y., Ueno, M., Kobayashi, H., Kikuchi, H., and Harashima, H. (2007). Development of a novel systemic gene delivery system for cancer therapy with a tumor-specific cleavable PEG-lipid. *Gene Ther* *14*, 68-77.
- Hawkins, M. J., Soon-Shiong, P., and Desai, N. (2008). Protein nanoparticles as drug carriers in clinical medicine. *Adv Drug Deliv Rev* *60*, 876-885.
- He, C., Hu, Y., Yin, L., Tang, C., and Yin, C. (2010). Effects of particle size and surface charge on cellular uptake and biodistribution of polymeric nanoparticles. *Biomaterials* *31*, 3657-3666.
- Henson, P. M., Bratton, D. L., and Fadok, V. A. (2001). Apoptotic cell removal. *Curr Biol* *11*, R795-805.
- Herrmann, R., Fayad, W., Schwarz, S., Berndtsson, M., and Linder, S. (2008). Screening for Compounds That Induce Apoptosis of Cancer Cells Grown as Multicellular Spheroids. *Journal of Biomolecular Screening* *13*, 1-8.
- Hobbs, S. K., Monsky, W. L., Yuan, F., Roberts, W. G., Griffith, L., Torchilin, V. P., and Jain, R. K. (1998). Regulation of transport pathways in tumor vessels: role of tumor type and microenvironment. *Proc Natl Acad Sci U S A* *95*, 4607-4612.
- Hoffmann, P. R., deCathelineau, A. M., Ogden, C. A., Leverrier, Y., Bratton, D. L., Daleke, D. L., Ridley, A. J., Fadok, V. A., and Henson, P. M. (2001). Phosphatidylserine (PS) induces PS receptor-mediated macropinocytosis and promotes clearance of apoptotic cells. *J Cell Biol* *155*, 649-659.
- Huang, X., Li, L., Liu, T., Hao, N., Liu, H., Chen, D., and Tang, F. (2011). The shape effect of mesoporous silica nanoparticles on biodistribution, clearance, and biocompatibility in vivo. *ACS Nano* *5*, 5390-5399.
- Huang, X., Teng, X., Chen, D., Tang, F., and He, J. (2010). The effect of the shape of mesoporous silica nanoparticles on cellular uptake and cell function. *Biomaterials* *31*, 438-448.
- Huth, U. S., Schubert, R., and Peschka-Suss, R. (2006). Investigating the uptake and intracellular fate of pH-sensitive liposomes by flow cytometry and spectral bio-imaging. *J Control Release* *110*, 490-504.
- Ilium, L., Davis, S. S., Wilson, C. G., Thomas, N. W., Frier, M., and Hardy, J. G. (1982). Blood clearance and organ deposition of intravenously administered colloidal particles. The effects of particle size, nature and shape. *International Journal of Pharmaceutics* *12*, 135-146.
- Ishida, T., and Kiwada, H. (2008). Accelerated blood clearance (ABC) phenomenon upon repeated injection of PEGylated liposomes. *Int J Pharm* *354*, 56-62.

- Ishida, T., Wang, X., Shimizu, T., Nawata, K., and Kiwada, H. (2007). PEGylated liposomes elicit an anti-PEG IgM response in a T cell-independent manner. *J Control Release* *122*, 349-355.
- Ivanov, A. I. (2008). Pharmacological inhibition of endocytic pathways: is it specific enough to be useful? *Methods Mol Biol* *440*, 15-33.
- Ivascu, A., and Kubbies, M. (2006). Rapid generation of single-tumor spheroids for high-throughput cell function and toxicity analysis. *J Biomol Screen* *11*, 922-932.
- J. Park, A. Estrada, J. A. Schwartz, P. Diagaradjane, S. Krishnan, A. K. Dunn, and Tunnell, J. W. (2010). Intra-Organ Biodistribution of Gold Nanoparticles Using Intrinsic Two-Photon-Induced Photoluminescence. *Lasers in Surgery and Medicine* *42*, 630-639.
- Jain, R. K., and Stylianopoulos, T. (2010). Delivering nanomedicine to solid tumors. *Nat Rev Clin Oncol* *7*, 653-664.
- Jang, E. S., Shin, J. H., Ren, G., Park, M. J., Cheng, K., Chen, X., Wu, J. C., Sunwoo, J. B., and Cheng, Z. (2012). The manipulation of natural killer cells to target tumor sites using magnetic nanoparticles. *Biomaterials* *33*, 5584-5592.
- Jenssen, H., Hamill, P., and Hancock, R. E. (2006). Peptide antimicrobial agents. *Clin Microbiol Rev* *19*, 491-511.
- Jiang, X., Qu, W., Pan, D., Ren, Y., Williford, J. M., Cui, H., Luijten, E., and Mao, H. Q. (2012). Plasmid-Templated Shape Control of Condensed DNA-Block Copolymer Nanoparticles. *Adv Mater*.
- Jung, G.-Y., Li, Z., Wu, W., Chen, Y., Olynick, D. L., Wang, S.-Y., Tong, W. M., and Williams, R. S. (2005). Vapor-Phase Self-Assembled Monolayer for Improved Mold Release in Nanoimprint Lithography. *Langmuir* *21*, 1158-1161.
- Kang, Y. H., Tan, L. A., Carroll, M. V., Gentle, M. E., and Sim, R. B. (2009). Target pattern recognition by complement proteins of the classical and alternative pathways. *Adv Exp Med Biol* *653*, 117-128.
- Kim, B., Han, G., Toley, B. J., Kim, C. K., Rotello, V. M., and Forbes, N. S. (2010). Tuning payload delivery in tumour cylindroids using gold nanoparticles. *Nat Nanotechnol* *5*, 465-472.
- Kim, H. R., Andrieux, K., Gil, S., Taverna, M., Chacun, H., Desmaële, D., Taran, F., Georgin, D., and Couvreur, P. (2007). Translocation of Poly(ethylene glycol-co-hexadecyl)cyanoacrylate Nanoparticles into Rat Brain Endothelial Cells: Role of Apolipoproteins in Receptor-Mediated Endocytosis. *Biomacromolecules* *8*, 793-799.
- Kim, K.-D., Kwon, H.-J., Choi, D.-g., Jeong, J.-H., and Lee, E.-s. (2008). Resist Flow Behavior in Ultraviolet Nanoimprint Lithography as a Function of Contact Angle with Stamp and Substrate. *Japanese Journal of Applied Physics* *47*, 8648-8651.

- Kim, K. J., and Malik, A. B. (2003). Protein transport across the lung epithelial barrier. *Am J Physiol Lung Cell Mol Physiol* *284*, L247-259.
- Klein, J. (2007). Probing the interactions of proteins and nanoparticles. *Proc Natl Acad Sci U S A* *104*, 2029-2030.
- Korfee, S., Gauler, T., Hepp, R., Pottgen, C., and Eberhardt, W. (2004). New targeted treatments in lung cancer--overview of clinical trials. *Lung Cancer* *45 Suppl 2*, S199-208.
- Korn, E. D., and Weisman, R. A. (1967). Phagocytosis of latex beads by *Acanthamoeba*. II. Electron microscopic study of the initial events. *J Cell Biol* *34*, 219-227.
- L. C. Glangchai, M. Caldorera-Moore, L. Shi, and Roy, K. (2008). Nanoimprint lithography based fabrication of shape-specific, enzymatically-triggered smart nanoparticles. *J Control Release* *125*, 263-272.
- Lee, K. J., Yoon, J., Rahmani, S., Hwang, S., Bhaskar, S., Mitragotri, S., and Lahann, J. (2012). Spontaneous shape reconfigurations in multicompartmental microcylinders. *Proc Natl Acad Sci U S A* *109*, 16057-16062.
- Lesniak, A., Salvati, A., Santos-Martinez, M. J., Radomski, M. W., Dawson, K. A., and Aberg, C. (2013). Nanoparticle adhesion to the cell membrane and its effect on nanoparticle uptake efficiency. *J Am Chem Soc* *135*, 1438-1444.
- Li, Y., Chen, X., and Gu, N. (2008). Computational investigation of interaction between nanoparticles and membranes: hydrophobic/hydrophilic effect. *J Phys Chem B* *112*, 16647-16653.
- Liao, H., Nehl, C. L., and Hafner, J. H. (2006). Biomedical applications of plasmon resonant metal nanoparticles. *Nanomedicine (Lond)* *1*, 201-208.
- Lin, C., and Engbersen, J. F. (2008). Effect of chemical functionalities in poly(amido amine)s for non-viral gene transfection. *J Control Release* *132*, 267-272.
- Linder, V., Gates, B. D., Ryan, D., Parviz, B. A., and Whitesides, G. M. (2005). Water-soluble sacrificial layers for surface micromachining. *Small* *1*, 730-736.
- Lison, D., Thomassen, L. C., Rabolli, V., Gonzalez, L., Napierska, D., Seo, J. W., Kirsch-Volders, M., Hoet, P., Kirschhock, C. E., and Martens, J. A. (2008). Nominal and effective dosimetry of silica nanoparticles in cytotoxicity assays. *Toxicol Sci* *104*, 155-162.
- Liu, Y., Tan, J., Thomas, A., Ou-Yang, D., and Muzykantov, V. R. (2012). The shape of things to come: importance of design in nanotechnology for drug delivery. *Ther Deliv* *3*, 181-194.
- Loerke, D., Mettlen, M., Schmid, S. L., and Danuser, G. (2011). Measuring the hierarchy of molecular events during clathrin-mediated endocytosis. *Traffic* *12*, 815-825.

- Longmire, M., Choyke, P. L., and Kobayashi, H. (2008). Clearance properties of nano-sized particles and molecules as imaging agents: considerations and caveats. *Nanomedicine (Lond)* 3, 703-717.
- Lu, F., Wu, S. H., Hung, Y., and Mou, C. Y. (2009). Size effect on cell uptake in well-suspended, uniform mesoporous silica nanoparticles. *Small* 5, 1408-1413.
- Lynch, I., and Dawson, K. A. (2008). Protein-nanoparticle interactions. *Nano Today* 3, 40-47.
- Lynch, I., Salvati, A., and Dawson, K. A. (2009). Protein-nanoparticle interactions: What does the cell see? *Nat Nanotechnol* 4, 546-547.
- Ma, W. W., and Adjei, A. A. (2009). Novel agents on the horizon for cancer therapy. *CA Cancer J Clin* 59, 111-137.
- Malik, N., Wiwattanapatapee, R., Klopsch, R., Lorenz, K., Frey, H., Weener, J. W., Meijer, E. W., Paulus, W., and Duncan, R. (2000). Dendrimers:: Relationship between structure and biocompatibility in vitro, and preliminary studies on the biodistribution of 125I-labelled polyamidoamine dendrimers in vivo. *Journal of Controlled Release* 65, 133-148.
- Masson, C., Garinot, M., Mignet, N., Wetzer, B., Mailhe, P., Scherman, D., and Bessodes, M. (2004). pH-sensitive PEG lipids containing orthoester linkers: new potential tools for nonviral gene delivery. *J Control Release* 99, 423-434.
- Mayor, S., and Pagano, R. E. (2007). Pathways of clathrin-independent endocytosis. *Nat Rev Mol Cell Biol* 8, 603-612.
- Merkel, T. J., Chen, K., Jones, S. W., Pandya, A. A., Tian, S., Napier, M. E., Zamboni, W. E., and Desimone, J. M. (2012). The effect of particle size on the biodistribution of low-modulus hydrogel PRINT particles. *J Control Release*.
- Merkel, T. J., Jones, S. W., Herlihy, K. P., Kersey, F. R., Shields, A. R., Napier, M., Luft, J. C., Wu, H., Zamboni, W. C., Wang, A. Z., *et al.* (2011). Using mechanobiological mimicry of red blood cells to extend circulation times of hydrogel microparticles. *Proc Natl Acad Sci U S A* 108, 586-591.
- Mettlen, M., Loerke, D., Yarar, D., Danuser, G., and Schmid, S. L. (2010). Cargo- and adaptor-specific mechanisms regulate clathrin-mediated endocytosis. *J Cell Biol* 188, 919-933.
- Michaelis, K., Hoffmann, M. M., Dreis, S., Herbert, E., Alyautdin, R. N., Michaelis, M., Kreuter, J., and Langer, K. (2006). Covalent linkage of apolipoprotein e to albumin nanoparticles strongly enhances drug transport into the brain. *J Pharmacol Exp Ther* 317, 1246-1253.
- Mitragotri, S. (2009). In drug delivery, shape does matter. *Pharm Res* 26, 232-234.

- Moghimi, S. M. (1995). Mechanisms of splenic clearance of blood cells and particles: towards development of new splenotropic agents. *Advanced Drug Delivery Reviews* 17, 103-115.
- Mosqueira, V. C., Legrand, P., Morgat, J. L., Vert, M., Mysiakine, E., Gref, R., Devissaguet, J. P., and Barratt, G. (2001). Biodistribution of long-circulating PEG-grafted nanocapsules in mice: effects of PEG chain length and density. *Pharm Res* 18, 1411-1419.
- Mueller-Klieser, W. (1987). Multicellular spheroids. A review on cellular aggregates in cancer research. *J Cancer Res Clin Oncol* 113, 101-122.
- Mundy, D. I., Li, W. P., Luby-Phelps, K., and Anderson, R. G. (2012). Caveolin targeting to late endosome/lysosomal membranes is induced by perturbations of lysosomal pH and cholesterol content. *Mol Biol Cell* 23, 864-880.
- Nel, A., Xia, T., Madler, L., and Li, N. (2006). Toxic potential of materials at the nanolevel. *Science* 311, 622-627.
- Oh, E., Delehanty, J. B., Sapsford, K. E., Susumu, K., Goswami, R., Blanco-Canosa, J. B., Dawson, P. E., Granek, J., Shoff, M., Zhang, Q., *et al.* (2011). Cellular uptake and fate of PEGylated gold nanoparticles is dependent on both cell-penetration peptides and particle size. *ACS Nano* 5, 6434-6448.
- Oldenborg, P. A., Gresham, H. D., Chen, Y., Izui, S., and Lindberg, F. P. (2002). Lethal autoimmune hemolytic anemia in CD47-deficient nonobese diabetic (NOD) mice. *Blood* 99, 3500-3504.
- Osaki, F., Kanamori, T., Sando, S., Sera, T., and Aoyama, Y. (2004). A quantum dot conjugated sugar ball and its cellular uptake. On the size effects of endocytosis in the subviral region. *J Am Chem Soc* 126, 6520-6521.
- Panyam, J., and Labhasetwar, V. (2003). Biodegradable nanoparticles for drug and gene delivery to cells and tissue. *Advanced Drug Delivery Reviews* 55, 329-347.
- Parton, R. G., and Simons, K. (2007). The multiple faces of caveolae. *Nat Rev Mol Cell Biol* 8, 185-194.
- Peer, D., Karp, J. M., Hong, S., Farokhzad, O. C., Margalit, R., and Langer, R. (2007). Nanocarriers as an emerging platform for cancer therapy. *Nat Nano* 2, 751-760.
- Peiris, P. M., Bauer, L., Toy, R., Tran, E., Pansky, J., Doolittle, E., Schmidt, E., Hayden, E., Mayer, A., Keri, R. A., *et al.* (2012). Enhanced delivery of chemotherapy to tumors using a multicomponent nanochain with radio-frequency-tunable drug release. *ACS Nano* 6, 4157-4168.
- Peppas, N. A. (2004). Intelligent therapeutics: biomimetic systems and nanotechnology in drug delivery. *Advanced Drug Delivery Reviews* 56, 1529-1531.

- Perrault, S. D., Walkey, C., Jennings, T., Fischer, H. C., and Chan, W. C. (2009). Mediating tumor targeting efficiency of nanoparticles through design. *Nano Lett* *9*, 1909-1915.
- Perumal, O. P., Inapagolla, R., Kannan, S., and Kannan, R. M. (2008). The effect of surface functionality on cellular trafficking of dendrimers. *Biomaterials* *29*, 3469-3476.
- Petros, R. A., and DeSimone, J. M. (2010). Strategies in the design of nanoparticles for therapeutic applications. *Nat Rev Drug Discov* *9*, 615-627.
- Rejman, J., Bragonzi, A., and Conese, M. (2005). Role of clathrin- and caveolae-mediated endocytosis in gene transfer mediated by lipo- and polyplexes. *Mol Ther* *12*, 468-474.
- Rejman, J., Conese, M., and Hoekstra, D. (2006). Gene transfer by means of lipo- and polyplexes: role of clathrin and caveolae-mediated endocytosis. *J Liposome Res* *16*, 237-247.
- Rejman, J., Oberle, V., Zuhorn, I. S., and Hoekstra, D. (2004a). Size-dependent internalization of particles via the pathways of clathrin- and caveolae-mediated endocytosis. *Biochem J* *377*, 159-169.
- Rejman, J., Oberle, V., Zuhorn, I. S., and Hoekstra, D. (2004b). Size-dependent internalization of particles via the pathways of clathrin- and caveolae-mediated endocytosis. *Biochem J* *377*, 159-169.
- Rolland, J. P., Maynor, B. W., Euliss, L. E., Exner, A. E., Denison, G. M., and DeSimone, J. M. (2005). Direct fabrication and harvesting of monodisperse, shape-specific nanobiomaterials. *J Am Chem Soc* *127*, 10096-10100.
- Roy, K., Shi, L., and Glangchai, L. C. (2007). Methods for fabricating nano and microparticles for drug delivery. In, (US).
- Rudolph, C., Plank, C., Lausier, J., Schillinger, U., Muller, R. H., and Rosenecker, J. (2003). Oligomers of the arginine-rich motif of the HIV-1 TAT protein are capable of transferring plasmid DNA into cells. *J Biol Chem* *278*, 11411-11418.
- Sahay, G., Alakhova, D. Y., and Kabanov, A. V. (2010a). Endocytosis of nanomedicines. *J Control Release* *145*, 182-195.
- Sahay, G., Kim, J. O., Kabanov, A. V., and Bronich, T. K. (2010b). The exploitation of differential endocytic pathways in normal and tumor cells in the selective targeting of nanoparticulate chemotherapeutic agents. *Biomaterials* *31*, 923-933.
- Sandgren, K. J., Wilkinson, J., Miranda-Saksena, M., McInerney, G. M., Byth-Wilson, K., Robinson, P. J., and Cunningham, A. L. (2010). A differential role for macropinocytosis in mediating entry of the two forms of vaccinia virus into dendritic cells. *PLoS Pathog* *6*, e1000866.

- Schädlich, A., Caysa, H., Mueller, T., Tenambergen, F., Rose, C., Göpferich, A., Kuntsche, J., and Mäder, K. (2011). Tumor Accumulation of NIR Fluorescent PEG–PLA Nanoparticles: Impact of Particle Size and Human Xenograft Tumor Model. *ACS Nano* *5*, 8710-8720.
- Schafer, V., von Briesen, H., Andreesen, R., Steffan, A. M., Royer, C., Troster, S., Kreuter, J., and Rubsamen-Waigmann, H. (1992). Phagocytosis of nanoparticles by human immunodeficiency virus (HIV)-infected macrophages: a possibility for antiviral drug targeting. *Pharm Res* *9*, 541-546.
- Schneider, M. C., Prosser, B. E., Caesar, J. J., Kugelberg, E., Li, S., Zhang, Q., Quoraishi, S., Lovett, J. E., Deane, J. E., Sim, R. B., *et al.* (2009). Neisseria meningitidis recruits factor H using protein mimicry of host carbohydrates. *Nature* *458*, 890-893.
- Schweins, R., and Huber, K. (2001). Collapse of sodium polyacrylate chains in calcium salt solutions. *The European Physical Journal E: Soft Matter and Biological Physics* *5*, 117-126.
- Shah, S., Liu, Y., Hu, W., and Gao, J. (2011). Modeling particle shape-dependent dynamics in nanomedicine. *J Nanosci Nanotechnol* *11*, 919-928.
- Shin, J., Shum, P., and Thompson, D. H. (2003). Acid-triggered release via dePEGylation of DOPE liposomes containing acid-labile vinyl ether PEG-lipids. *J Control Release* *91*, 187-200.
- Shuvaev, V. V., Tliba, S., Pick, J., Arguiri, E., Christofidou-Solomidou, M., Albelda, S. M., and Muzykantov, V. R. (2011). Modulation of endothelial targeting by size of antibody-antioxidant enzyme conjugates. *J Control Release* *149*, 236-241.
- Simone, E. A., Dziubla, T. D., and Muzykantov, V. R. (2008). Polymeric carriers: role of geometry in drug delivery. *Expert Opin Drug Deliv* *5*, 1283-1300.
- Smith, B. R., Kempen, P., Bouley, D., Xu, A., Liu, Z., Melosh, N., Dai, H., Sinclair, R., and Gambhir, S. S. (2012). Shape matters: intravital microscopy reveals surprising geometrical dependence for nanoparticles in tumor models of extravasation. *Nano Lett* *12*, 3369-3377.
- Sreenivasan, S. V., Choi, J., Schumaker, P., and Xu, F. (2010). Status of UV Lithography for Nanoscale Manufacturing. *Handbook of Nanofabration Edited by Wiederrecht, GP Chapter 5*, 149-182.
- Stylianopoulos, T., Soteriou, K., Fukumura, D., and Jain, R. K. (2013). Cationic nanoparticles have superior transvascular flux into solid tumors: insights from a mathematical model. *Ann Biomed Eng* *41*, 68-77.
- Tao, L., Hu, W., Liu, Y., Huang, G., Sumer, B. D., and Gao, J. Shape-specific polymeric nanomedicine: emerging opportunities and challenges. *Exp Biol Med (Maywood)* *236*, 20-29.

- Tasciotti, E., Liu, X., Bhavane, R., Plant, K., Leonard, A. D., Price, B. K., Cheng, M. M., Decuzzi, P., Tour, J. M., Robertson, F., and Ferrari, M. (2008). Mesoporous silicon particles as a multistage delivery system for imaging and therapeutic applications. *Nat Nanotechnol* 3, 151-157.
- Teeguarden, J. G., Hinderliter, P. M., Orr, G., Thrall, B. D., and Pounds, J. G. (2007). Particokinetics in vitro: dosimetry considerations for in vitro nanoparticle toxicity assessments. *Toxicol Sci* 95, 300-312.
- Thomsen, T., Schlosser, A., Holmskov, U., and Sorensen, G. L. (2011). Ficolins and FIBCD1: soluble and membrane bound pattern recognition molecules with acetyl group selectivity. *Mol Immunol* 48, 369-381.
- Thorek, D. L., and Tsourkas, A. (2008). Size, charge and concentration dependent uptake of iron oxide particles by non-phagocytic cells. *Biomaterials* 29, 3583-3590.
- Toy, R., Hayden, E., Shoup, C., Baskaran, H., and Karathanasis, E. (2011). The effects of particle size, density and shape on margination of nanoparticles in microcirculation. *Nanotechnology* 22, 115101.
- Tsai, R. K., and Discher, D. E. (2008). Inhibition of "self" engulfment through deactivation of myosin-II at the phagocytic synapse between human cells. *J Cell Biol* 180, 989-1003.
- Tseng, P., Judy, J. W., and Di Carlo, D. (2012). Magnetic nanoparticle-mediated massively parallel mechanical modulation of single-cell behavior. *Nat Methods* 9, 1113-1119.
- Unezaki, S., Maruyama, K., Hosoda, J.-I., Nagae, I., Koyanagi, Y., Nakata, M., Ishida, O., Iwatsuru, M., and Tsuchiya, S. (1996). Direct measurement of the extravasation of polyethyleneglycol-coated liposomes into solid tumor tissue by in vivo fluorescence microscopy. *International Journal of Pharmaceutics* 144, 11-17.
- Uster, P. S., Working, P. K., and Vaage, J. (1998). Pegylated liposomal doxorubicin (DOXIL®, CAELYX®) distribution in tumour models observed with confocal laser scanning microscopy. *International Journal of Pharmaceutics* 162, 77-86.
- van de Ven, A. L., Kim, P., Haley, O., Fakhoury, J. R., Adriani, G., Schmulen, J., Moloney, P., Hussain, F., Ferrari, M., Liu, X., *et al.* (2012). Rapid tumortropic accumulation of systemically injected plateloid particles and their biodistribution. *J Control Release* 158, 148-155.
- Vercauteren, D., Vandenbroucke, R. E., Jones, A. T., Rejman, J., Demeester, J., De Smedt, S. C., Sanders, N. N., and Braeckmans, K. (2010). The use of inhibitors to study endocytic pathways of gene carriers: optimization and pitfalls. *Mol Ther* 18, 561-569.

- Wallis, R., Mitchell, D. A., Schmid, R., Schwaeble, W. J., and Keeble, A. H. (2010). Paths reunited: Initiation of the classical and lectin pathways of complement activation. *Immunobiology* *215*, 1-11.
- Wang, B., Zhang, L., Bae, S. C., and Granick, S. (2008). Nanoparticle-induced surface reconstruction of phospholipid membranes. *Proc Natl Acad Sci U S A* *105*, 18171-18175.
- Wang, X., Ishida, T., and Kiwada, H. (2007). Anti-PEG IgM elicited by injection of liposomes is involved in the enhanced blood clearance of a subsequent dose of PEGylated liposomes. *J Control Release* *119*, 236-244.
- Wen, J., Kim, B. Y. S., Rutka, J. T., and Chan, W. C. W. (2008). Nanoparticle-mediated cellular response is size-dependent. *Nature Nanotechnology* *3*, 145-150.
- Wong, C., Stylianopoulos, T., Cui, J., Martin, J., Chauhan, V. P., Jiang, W., Popovic, Z., Jain, R. K., Bawendi, M. G., and Fukumura, D. (2011). Multistage nanoparticle delivery system for deep penetration into tumor tissue. *Proc Natl Acad Sci U S A* *108*, 2426-2431.
- Yang, K., and Ma, Y. Q. (2010). Computer simulation of the translocation of nanoparticles with different shapes across a lipid bilayer. *Nat Nanotechnol* *5*, 579-583.
- Yi, X., Shi, X., and Gao, H. (2011). Cellular uptake of elastic nanoparticles. *Phys Rev Lett* *107*, 098101.
- Yoo, J. W., Chambers, E., and Mitragotri, S. (2010). Factors that control the circulation time of nanoparticles in blood: challenges, solutions and future prospects. *Curr Pharm Des* *16*, 2298-2307.
- Yoo, J. W., Doshi, N., and Mitragotri, S. (2011a). Adaptive micro and nanoparticles: temporal control over carrier properties to facilitate drug delivery. *Adv Drug Deliv Rev* *63*, 1247-1256.
- Yoo, J. W., Irvine, D. J., Discher, D. E., and Mitragotri, S. (2011b). Bio-inspired, bioengineered and biomimetic drug delivery carriers. *Nat Rev Drug Discov* *10*, 521-535.
- Yoo, J. W., and Mitragotri, S. (2010). Polymer particles that switch shape in response to a stimulus. *Proc Natl Acad Sci U S A* *107*, 11205-11210.
- Yuan, F., Dellian, M., Fukumura, D., Leunig, M., Berk, D. A., Torchilin, V. P., and Jain, R. K. (1995). Vascular permeability in a human tumor xenograft: molecular size dependence and cutoff size. *Cancer Res* *55*, 3752-3756.
- Yuhas, J. M., Li, A. P., Martinez, A. O., and Ladman, A. J. (1977). A simplified method for production and growth of multicellular tumor spheroids. *Cancer Res* *37*, 3639-3643.

- Zhang, L. W., and Monteiro-Riviere, N. A. (2009). Mechanisms of quantum dot nanoparticle cellular uptake. *Toxicol Sci* *110*, 138-155.
- Zhu, L., Kate, P., and Torchilin, V. P. (2012). Matrix metalloprotease 2-responsive multifunctional liposomal nanocarrier for enhanced tumor targeting. *ACS Nano* *6*, 3491-3498.

Vita

Rachit Agarwal is the son of Dr. Satish Kumar Agarwal and Chitra Agarwal. He was born in Bareilly, India on February 6th 1985 and has two elder brothers, Shobhit Agarwal and Ankit Agarwal. He completed his schooling in India from BBL Public School and pursued engineering at Indian Institute of Technology, Kharagpur, India. Rachit graduated with honors with a dual degree, Bachelor of Technology in Biotechnology and Master of Technology in Biochemical Engineering in 2009.

During this period, he worked on characterization of Antheraea Mylitta Cytoplasmic Polyhedrosis Virus (AMCPV) gene segments. For his doctoral studies at The University of Texas at Austin, Rachit worked on shape-specific particles for drug delivery applications. The results of his work were presented in many international conferences. He wrote 1 first-author publications and was a contributor to a few other articles. He was a recipient of the STAR award from Society for Biomaterials, 2013, for excellence in research.

Permanent address: 200 Prem Nagar, Bareilly – 243005, India

Email: rachitbly@gmail.com

This dissertation was typed by Rachit Agarwal